PHOTOCATALYTIC DEGRADATION OF PROFENOFOS BY ELECTROSPUN TITANIUM (IV) DIOXIDE NANOFIBERS WITH UV AND VUV IRRADIATION

Miss Pacharaporn Wangwinyoo

A Thesis Submitted in Partial Fulfillment of the Requirements

for the Degree of Master of Science Program in Environmental Management

(Interdisciplinary Program)

Graduate School

Chulalongkorn University

Academic Year 2014

การย่อยสลายโพรฟีโนฟอสด้วยวิธีโฟโตแคตาไลติคโดยใช้ไททาเนียมได ออกไซด์นาโนไฟเบอร์
ร่วมกับการฉายรังสียูวีและวียูวี

นางสาวพชรพร หวังวิญญ

วิทยานิพนธ์นี้เป็นส่วนหนึ่งของการศึกษาตามหลักสูตรปริญญาวิทยาศาสตรมหาบัณฑิต
สาขาวิชาการจัดการสิ่งแวดล้อม (สหสาขาวิชา)
บัณฑิตวิทยาลัย จุฬาลงกรณ์มหาวิทยาลัย
ปีการศึกษา 2557

Thesis Title	PHOTOCATALYTIC DEGRADATION OF PROFENOFOS BY ELECTROSPUN TITANIUM (IV) DIOXIDE NANOFIBERS WITH UV AND VUV IRRADIATION
By	Miss Pacharaporn Wangwinyoo
Field of Study	Environmental Management
Thesis Advisor	Thunyalux Ratpukdi, Ph.D.
Thesis Co-Advisor	Associate Professor Varong Pavarajarn, Ph.D.

Accepted by the Graduate School, Chulalongkorn University in Partial Fulfillment of the Requirements for the Master's Degree

....Dean of the Graduate School
(Associate Professor Sunait Chutintaranond, Ph.D.)

THESIS COMMITTEE

....Chairman
(Assistant Professor Srilert Chotpantarat, Ph.D.)

....Thesis Advisor
(Thunyalux Ratpukdi, Ph.D.)

....Thesis Co-Advisor
(Associate Professor Varong Pavarajarn, Ph.D.)

....Examiner
(On-anong Larpparisudthi, Ph.D.)

....External Examiner
(Assistant Professor Bunyarit Panyapinyopol, Ph.D.)

พชรพร หวังวิญญ : การย่อยสลายโพรฟีโนฟอสด้วยวิธีโฟโตแคตาไลติคโดยใช้ไททาเนียมได ออกไซด์นาโนไฟเบอร์ร่วมกับการฉายรังสียูวีและวียูวี (PHOTOCATALYTIC DEGRADATION OF PROFENOFOS BY ELECTROSPUN TITANIUM (IV) DIOXIDE NANOFIBERS WITH UV AND VUV IRRADIATION) อ.ที่ปรึกษาวิทยานิพนธ์หลัก: อ. ดร. ธัญลักษณ์ ราษฎร์ ภักดี, อ.ที่ปรึกษาวิทยานิพนธ์ร่วม: รศ. ดร. วรงค์ ปวราจารย์, 175 หน้า.

การย่อยสลายสารโพรฟีโนฟอสซึ่งเป็นยาฆ่าแมลงที่อยู่ในกลุ่มออร์กาโนฟอตเฟตที่ปนเปื้อนในน้ำด้วย กระบวนการโฟโตไลติคและโฟโตคะตาไลติคภายใต้ระบบยูวี วียูวี ยูวีกับไททาเนียมไดออกไซด์ และวียูวีกับไท ทาเนียมไดออกไซด์ทั้ง Deguss-P25 และเส้นใยคอมโพสิทขนาดนาโนไฟเบอร์ของไททาเนียมไดออกไซด์กับ พอลีไวนิลไพโรลิโดได้ถูกนำมาศึกษาในงานวิจัยนี้ สภาวะที่ดีที่สุดสำหรับปฏิกิริยาโฟโตคะลาไลติค คือ ความ เข้มข้นโพรฟีโนฟอส 10 มิลลิกรัมต่อลิตร พีเอช 7 ที่อุณหภูมิห้อง (25 ℃ ± 3) และระยะเวลาในการทำปฏิกิริยา 30 นาที กระบวนการย่อยสลายสารเป้าหมายด้วยแสงประกอบด้วยประสิทธิภาพการกำจัด อัตราจลนศาสตร์และ อัตราการกลายเป็นธาตุสามารถจัดอันดับความสามารถของการบวนการต่างๆ ได้ดังนี้ VUV/TiO$_2$ > VUV > UV/TiO$_2$ > UV ซึ่งกระบวนการของ VUV/TiO$_2$ ด้วย P25 และเส้นใยขนาดนาโนไฟเบอร์ให้ประสิทธิภาพใน การกำจัดโพรฟีโนฟอสได้ดีที่สุด คือ 98% และ 97% ตามลำดับ จากผลการศึกษาทำให้ทราบว่าการเพิ่มตัวเร่ง ปฏิกิริยาในระบบสามารถช่วยให้ประสิทธิภาพการกำจัด ดังนั้นการย่อยสลายสารด้วยกระบวนการและโฟโตคะ ตาไลติคจึงให้ผลดีกว่าโฟโตไลติค นอกจากนี้การเพิ่มความเข้มข้องของตัวเร่งปฏิกิริยาจาก 0 ถึง 0.20 กรัมต่อลิตร สามารถเพิ่มประสิทธิภาพการกำจัด อัตราจลนศาสตร์และอัตราการกลายเป็นธาตุในระบบให้ดีขึ้นเพิ่มตามไปด้วย เนื่องจากมีพื้นที่สำหรับการเกิดปฏิกิริยาโฟโตคะตาไลติคมากขึ้น อัตราจลนศาสตร์ของการย่อยสลายโพรฟีโน ฟอสด้วยกระบวนการโฟโตไลติคเป็นไปตามปฏิกิริยาอันดับที่หนึ่ง และอัตราจลนศาสตร์ของการย่อยสลายโพรฟี โนฟอสด้วยกระบวนการโฟโตคะคาไลติคเป็นไปตามปฏิกิริยาปฏิกิริยาอันดับที่หนึ่งเทียม ส่วนผลการศึกษาการ ย่อยสลายพบว่ากระบวนการโฟโตคะตาไลติคด้วยเส้นใยขนาดนาโนไฟเบอร์ของไททาเนียมไดออกไซด์ให้ผล ใกล้เคียงกับ Deguss-P25 นอกจากนี้งานวิจัยนี้ได้ศึกษาการนำตัวเร่งปฏิกิริยามากลับใช้ซ้ำ โดยพบว่าเส้นใยขนาด นาโนไฟเบอร์สามารถนำมาใช้ใหม่ได้ดีกว่า Deguss-P25 เนื่องจากเส้นใยนาโนไฟเบอร์ให้ผลที่ดีกว่าและ สามารถกำจัดออกจากระบบได้ง่ายกว่า ดังนั้นตัวเร่งปฏิกิริยาชนิดนี้จึงมีความเหมาะสมที่จะนำมากำจัดสารยาฆ่า แมลงที่อยู่ในกลุ่มออร์กาโนฟอตเฟตในน้ำได้ อีกทั้งยังเป็นกระบวนการที่สามารถนำไปปฏิบัติได้จริง

สาขาวิชา   การจัดการสิ่งแวดล้อม   ลายมือชื่อนิสิต _____

ปีการศึกษา 2557   ลายมือชื่อ อ.ที่ปรึกษาหลัก _____

                                                          ลายมือชื่อ อ.ที่ปรึกษาร่วม _____

5687558220 : MAJOR ENVIRONMENTAL MANAGEMENT

KEYWORDS: VUV / PHOTOCATALYSIS / PROFENOFOS / ORGANOPHOSPHATE PESTICIDES / NANOFIBERS / TITANIUM DIOXIDE

PACHARAPORN WANGWINYOO: PHOTOCATALYTIC DEGRADATION OF PROFENOFOS BY ELECTROSPUN TITANIUM (IV) DIOXIDE NANOFIBERS WITH UV AND VUV IRRADIATION. ADVISOR: THUNYALUX RATPUKDI, Ph.D., CO-ADVISOR: ASSOC. PROF. VARONG PAVARAJARN, Ph.D., 175 pp.

The photolytic and photocatalytic degradation of profenofos, an organophosphate pesticide, in aqueous solutions under UV, VUV, UV/TiO_2, and VUV/TiO_2 systems in both Deguss-P25 nanoparticles and synthesized electrospun TiO_2/PVP composite nanofibers were investigated. The experiments were performed at 10 mg/L of profenofos, pH 7 (unbuffered), room temperature (25 ℃ ± 3), 30 min of reaction time and dose of TiO_2 of 0, 0.05, 0.1, and 0.2 g/L. Photodegradation performances of profenofos including removal efficiency, kinetic rate and mineralization were in the order: VUV/TiO_2 > VUV > UV/TiO_2 > UV. Particularly, the VUV/TiO_2 system in both P25 and nanofibers showed the highest removal efficiency for 98% and 97%, respectively, indicating that the presence of titania photocatalyst could significantly improve the removal of profenofos in aqueous solution. Increasing of titania (both Deguss-P25 and nanofibers) significantly enhanced removal efficiency, kinetic rate and mineralization of profenofos under UV and VUV radiation due to more active sites on titania surface area, where the photocatalysis reaction occurred, and more formation hydroxyl radicals in the system. The kinetic rate results indicated that the degradation kinetic of profenofos by photolytic process followed first kinetic model and kinetic of profenofos by photolytic process followed pseudo-first kinetic model, and the results showed that photocatalytic degradation with Deguss-P25 had similarly resulted to TiO_2 nanofibers. Reusability of TiO_2 had been investigated for ten consecutive cycles, and the results revealed that TiO_2 nanofibers had more reusability than P25. Due to easy separation, readily easy reusable, eco – friendly solid photocatalyst, high activity, long-term stability, and insignificant loss in adsorption performance, TiO_2 nanofibers present appropriate properties to be a catalyst for photocatalytic purification of organophosphate pesticides in water sources and would be attractive to develop a real scale application.

Field of Study:	Environmental Management	Student's Signature ....
Academic Year:	2014	Advisor's Signature ....
		Co-Advisor's Signature ....

ACKNOWLEDGEMENTS

CONTENTS

LIST OF TABLE

LIST OF FIGURE

CHAPTER I

INTRODUCTION

1.1 Research Rationale

Thailand is one of the countries in Southeast Asia that widely uses variety of pesticides such as organochlorine, organophosphate, carbamate and pyrethrum. Especially, organophosphate pesticides are mainly used for pest management such as cotton, chili, and sugarcane and tobacco field (Srisawangwong et al., 2009). Nowadays, organophosphate pesticides (OP) exhibit greater than one-third of world pesticides consumption and considerably increasing used instead of organochlorine compounds, which are the much more persistent compounds in the environment, and expected to be bioaccumulated in water sources (Zamy et al., 2004; Badawy et al., 2006). Most of profenofos contamination generally occurs from agricultural drainage from application sites, production sites and the effluent from industrial manufacturer. Furthermore, OPs have been regularly detected as if a dominant appearing water contaminant in water media, especially in developing countries (Moussavi et al., 2014).

Profenofos (PF) is one of the organophosphate insecticides that was used in high quantity in Thailand. It is able to contaminated in surface water with a maximum concentration of 20 mg/L, and the Maximum Residue Limit (MRL) of profenofos is 5

mg/L dependent on weather and other conditions (National Bureau of Agricultural Commodity and Food Standards (AEFS), 2008). Profenofos can reduced acetylycholine esterase enzyme formation that resulted in decreased egg, Lutenizing hormone (LH) and progesterone production, and as well as obstructing acetylcholine neurotransmitter affected to the central nervous system in human causing to the transmission signal on postsynaptic cholinergic receptors (Buonasera et al., 2009). According to the report from US. EPA, profenofos has been growing contaminated in a wide range of the aquatic and terrestrial ecosystems (U.S.EPA, 2000). Consequently, human health must be protected from contaminated water and industrial effluent that may associate with drinking water sources impurity by eliminating this harmful pollutant before consumption.

There have been numerous processes including physical, chemical and biological processes having the potential to remove of profenofos (Ahmed et al., 2011). Among them, degradation processes induced by ultraviolet based advanced oxidation processes (UV-AOPs) have been taken into an account as a key for wastewater treatment and shown a large number of successful aqueous treatments. UV-AOPs consist of various processes such as UV/catalyst, UV/H_2O_2, UV/O_3, vacuum-UV (VUV), and photocatalysis (Imoberdorf and Mohseni, 2011; Wols et al., 2015). Upon the emerging AOPs, photocatalysis is one of the most successful processes to remove the contaminants in the air, water, and wastewater streams. It has capability to generate extremely reactive species, particularly hydroxyl radicals (•OH) which given energy photon at E = 2.8 eV (Xing et al., 2015). Recently, vacuum ultraviolet (VUV) photooxidation has become interesting for wastewater treatment

choice since it has ability to generate high energy photon at E = 6.7 eV causing the formation of excited state of atomic oxygen (O (^{1}D)) and •OH directly from oxygen and water molecule under light irradiation. Moreover, VUV process has revealed many advantages such as being an additive free process, making commercially viable and environmentally-sustainable treatment alternative (Kang et al., 2011). Huang et al. (2013) confirmed that VUV (254 and 185 nm) irradiation was more effective than UV (254 nm) irradiation due to more degradation efficiency and mineralization rate of organic compound.

However, photolysis (VUV or UV alone) has a limited capacity of •OH formation resulting in restricted oxidation and mineralization rate. To obtain greater oxidation potential and removal efficiency of the micropollutants, the combination of photochemical oxidation (VUV or UV) and strong oxidant catalyst are influential considered to boost the *in situ* reaction system. The examples of photocatalyst are ozone (Pingfeng et al., 2011), hydrogen peroxide (Imoberdorf and Mohseni, 2011), sodium persulfate (Wang and Liang, 2014), chlorate (Eskandarloo et al., 2014) and periodate (Guo et al., 2014). From all above photocatalyst mention, titanium (IV) dioxide (TiO_2) is currently more interested in photocatalytic experiment due to high hydroxyl radical production, high adsorption ability onto organic contaminants, inexpensive, and non-toxic treatment process (Andersen et al., 2013). Typically, one-dimensional TiO_2 photocatalyst has been fabricated numerous forms including nanoparticles, nanofibers and nanotubes. To obtain highly catalytic activity in photocatalytic reactor, a chosen catalytic form should having a large specific surface area. Nanoparticles display a large surface, small and uniform particle size.

Nevertheless, they are extremely difficult to be removed from aqueous solution, and causing agglomeration in the reactor working, leading to re-polluted in the treated water again (Xu et al., 2013). Among the reported TiO_2 nanostructures, nanofibers are outstanding interest in photocatalyst of pollutants in aqueous solutions owing to high photocatalytic activity, high surface area to volume ratio, lower electron – hole recombination rate, no agglomeration in the reaction system, and no waste time to precipitate particles (Liu et al., 2014).

Titania nanofibers can be fabricated by a combination of sol - gel and electrospinning techniques, which are being used to produce a lot of ultra thin nanofibers from a wide range of polymer materials (Nirmala et al., 2012). TiO_2 nanofibers is more attractive than typical TiO_2 powder based on the reason of high surface area to volume ratio, which enables to reduce the electron-hole recombination rate, (2) high interfacial charge carrier transfer rate being favorable for photocatalytic reactions (Nakata and Fujishima, 2012), (3) small diameter and high porosity (Kaewsaenee et al., 2010). Currently, the application of UV or VUV with TiO_2 nanofibers for removal of organophosphate pesticide has never been investigated.

The aim of this research is to investigate the removal efficiency and mineralization of profenofos by UV and VUV photocatalysis combining with the electrospun titania nanofibers. Experiments of UV/VUV with powder TiO_2 (P25) were also performed for comparison purpose. Titanium dioxide dosage was the studied variable of the processes. The performances of the process were compared with those of UV, and VUV, UV/TiO_2 and VUV/TiO_2. The •OH radical concentration

under specific experimental conditions were measured using a probe compound (methylene blue, MB). Correlation the quantified •OH radical concentrations with the photolysis and photocatalytic activities of profenofos was determined.

1.2 Objective of the research

1) To compare the performance of the processes in both titanium (IV) dioxide nanoparticles (P25) and titanium (IV) dioxide nanofibers with those of UV (254 nm), VUV (185 and 254 nm), UV/TiO_2 and VUV/TiO_2 on the degradation and mineralization of profenofos in aqueous solutions.

2) To determine the role of hydroxyl radicals (•OH) related to the degradation of profenofos by photolysis (UV and VUV) and photocatalysis (UV/TiO_2 and VUV/TiO_2).

1.3 Hypothesis

1) Photocatalytic processes (UV/TiO_2 and VUV/TiO_2) will enhance the degradation efficiency and mineralization of profenofos in aqueous solution rather than photolysis processes (UV and VUV).

2) Photocatalytic processes with titanium (IV) dioxide nanofibers have degradation efficiency and mineralization of profenofos in aqueous solution similar to photocatalytic processes with titanium (IV) dioxide nanoparticles (P25).

3) The formation of hydroxyl radicals (•OH) from VUV, UV, UV/TiO$_2$, and VUV/ TiO$_2$ processes will be associated with the degradation efficiencies and mineralization of profenofos.

1.4 Scope of the study

All experiments in this research were conducted in the laboratory scale. The scope of the research includes:

1) Synthetic profenofos solution will be used as the model of organophosphate pesticides.

2) The UV and VUV lamp used are low pressure mercury lamps. The wavelength emits from UV lamp is 254 nm while VUV lamp emits the wavelength of 185 and 254 nm.

3) Titania nanofibers synthesized by the combination of sol – gel method and electrospinning technique, and titania particle commercial grade (P25) were used as the photocatalyst.

4) All the experiments were conducted with 10 mg/L profenofos concentration, pH 7 (unbuffered, and not control pH) and room temperature (T = 25 ± 3 $^{\circ}$C).

1.5 Benefit of Research

This study provides beneficial information on the photocatalytic degradation activated by UV and VUV irradiation with the synthetic TiO_2 nanofibers, which might be enhance the removal of profenofos. The ultraviolet and vacuum-ultraviolet light stimulated TiO_2 is an effective photocatalyst, and can be developed to a practical environmental purification system such as wastewater treatment with lower operating cost and environmentally-sustainable treatment. Furthermore, the kinetic rate constants of profenofos photodegradation by TiO_2 with UV and VUV irradiation are also determined that can be applied to minister profenofos contaminated in water in the future.
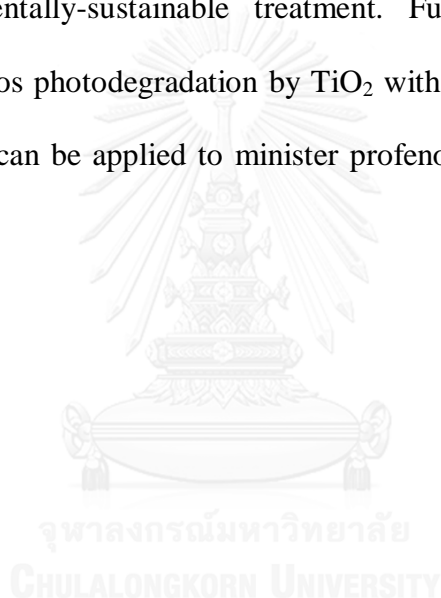
CHAPTER II

LITERATURE REVIEWS

2.1 Organophosphate Pesticides

Organophosphate pesticides are widely used to destroy many pesticides crop field until the present time. There have been produced more than forty types which are noted that they were utilized in household and agriculture (U.S.EPA, 1984). OPs are provided in the group of non-residual pesticides in the environment. Typically, they are completely degraded by the sun visible light within shortly weeks (Barr and Needham, 2002). The chemical structure of OPs has major form in phosphorus ester, which consists of oxygen atom, carbon atom, sulfur atom and nitrogen atom trapped with phosphorus atom, which has a lot of phosphorus molecule's name such as phosphate, phosphorothioate, phosphoro-dithioate, phosphonate and phosphoroamidate.

The chemical class of OPs is capable to classify in three groups into the following (Ramathibodi Poison Center, 2001) (Figure 2.1):

(1) Aliphatic organophosphate: it has the derivatives of aliphatic that consist of carbon chain in the chemical formula. The earliest aliphatic organophosphate substances aremalathion and others including trichlorfon, disulfoton, thiometon, acephate, and methamidophos etc.

*(2) Phenol organophosphat*e: it has the derivatives of phenol in the chemical formula replaced a hydrogen atom with a phosphorus atom in the part of benzene ring. The substances in this group may have been resistance in the environment more than aliphatic organophosphate. The examples of widely used phenol organophosphate are ethyl-parathion, which has much more toxic than others thus it is substituted with methyl-parathion, parathion, carbophenothion, phenthoatefenitrothion, isofenphos, triazophos, and profenofos.

(3) Heterocyclic organophosphate: the derivatives of hetero-cyclic compose with aromatic ring and organophosphate group, and carbon atom in heterocyclic carbon ring is replaced with oxygen, nitrogen, or sulphur atom. However, the heterocyclic carbon ring remains some carbon atoms (3, 5, or 6 atoms). It should be noted that the heterocyclic substances have the molecule's structure complexity rather than phenol and heterocyclic organophosphate. The examples of this group are such as azinphos-ethyl, chlorpyrifos, methidation, chlopyrifos-methyl dioxathion, and diazinon etc.
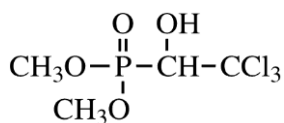
(a) Trichlorfon　　　　　　(b) Profenofos　　　　　　(c) Diazinon
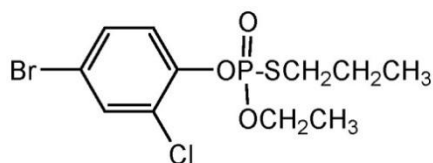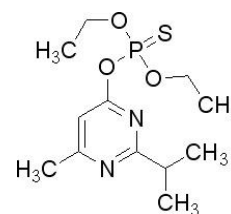
(Aliphatic organophosphate)　　　(Phenol organophosphate)　　(Heterocyclic organophosphate)

Figure 2.1 The chemical class organophosphate structure

2.2 Profenofos

Profenofos (PF) is an insecticide that was classified into the group of organophosphate pesticides. It was fabricated in the United States in 1982 which was normally used in order to manage the number of tobacco, budworm, cotton bollworm, armyworm, cotton aphid, whiteflies, spider mites, plant bugs, and flea hoppers (U.S. EPA, 2006). Moreover, it has been widely used instead the banning of organochlorine pesticides such as DDT due to high toxicity and long term resistance in the environment of DDT. There have many commercial names of profenofos such as supercron 50 EC, profenofos 50 EC and others. The chemical name is O-(4-bromo-2-chlorophenyl)-O-ethyl-S-propyl phosphorothioate, and the chemical structure and the properties of profenofos are shown in Figure 2.2 and Table 2.1
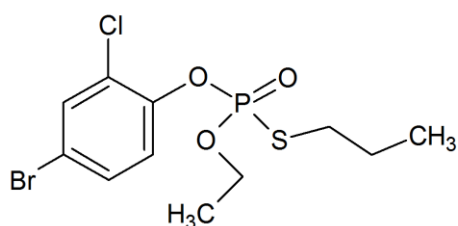
Figure 2.2 The chemical structure of profenofos

Table 2.1 The properties of profenofos

The physico-chemical properties	Information
Empirical formula	$C_{11}H_{15}BrClO_3PS$
Molecular weight	373.65
log K_{ow}	4.4
log K_{oc}	3.30
Boiling point	100 $^{\circ}$C
Density	1.46 g/cm^3 at 20 $^{\circ}$C
Water solubility	20 mg/l at 25 $^{\circ}$C
Solubility in organic solvents	Ethanol, acetone, toluene, n-octanol, and n-hexane at 25 $^{\circ}$C
Stability	neutral and weak acid
Instability	base
Henry law constant	0.034 Pa•m^3/mol
LD$_{50}$ (mice)	358 mg/kg
Hydrolysis	Depends on pH pH 5 t$^{1/2}$ = 93 days pH 7 t$^{1/2}$ = 14.6 days pH 9 t$^{1/2}$ = 5.7 days

Source: (Griffin, 1999; Sankom, 1999)

2.2.1 Toxicity of profenofos

Profenofos has been poisonous to insects, mammals, aquatic animals (estuarine and marine organisms), and birds, which can be inhibiting acetyl cholinesterase (Oppenlander et al.) activity (Oppenlander et al.). The reduced AChE has been associated with decreased egg, serum (Luteinizing Hormone) LH, and serum progesterone production. Moreover, AChE can significant damage the human fetal brain tissue and initially act by impairing the development of neurons, and later affect glia cells including astrocytes, oligodendrocites, and microglia, which are critical for brain development (Krieger, 2010). The effect from AChE inhibition involves in the outstanding of acetyl cholinesterase during synapsis, induced to myasthenia gravis, convulsion, sorrow, and be eventually lose consciousness. More recent experimental evidence suggests that subtoxic and other nonsympomatic developmental exposure to profenofos may pre dispose offspring to hypertension, obesity, and diabetes (Meyer et al., 2004). There has been some indication that profenofos may affect the menstrual cycle and cause an early menopause in humans. Nakazawa (1974) and Mattison et al. (1983) studied the reproductive effects from profenofos exposure among women in agriculture (Nakazawa, 1974; Mattisson et al., 1983). They found that these effects included abnormal menstruation such as hypermenorrhea, oligomenorrhes, amenorrhea, and early menopause. Furthermore, profenofos can be absorbed into human's body such as digestive system, dermal system, and respiration system, which has the obvious effect within 24 hours after exposure. The patients, who obtain high – dose exposure, can be shown the noticeable effect within 5 min. Profenofos has an acute effect to ingestion exposure (358 mg/kg) that is testing with the mice, and an

acute effect to dermal exposure (472 mg/kg) investigating with the rabbits. Summary of Toxicological endpoints for profenofos is shown in Table 2.2 (U.S.EPA, 2000).

Table 2.2 Summary of Toxicological endpoints for profenofos

Type of exposure (duration and route)	Endpoint and dose	Study
Acute Dietary (one day)	PAD[1] of 0.005 mg/kg/day [NOEL[2] 0.5 mg/kg/day inhibition of cholinesterase activities in plasma (males) and RBC's (females)] UF[3]:100	Non-guideline acute single-dose oral toxicity study in rats (MRID 43213302)
Chronic Dietary	PAD of 0.00005 mg/kg/day [NOEL 0.005 mg/kg/day/ inhibition of cholinesterasein plasma and RBC's] UF:100	Six-month dog study (MRID 00081687)
Short-Term Occupational (one to seven days) Intermediate-Term Occupational (one week to seven months)	NOEL of 1.0 mg/kg/day [NOEL for significant decreases in cholinesterase activities in RBC's, plasma, and brain]. UF:100	21-day dermal toxicity study in rabbit (MRID 41644501)
Inhalation (any duration)	LOEL[4] of 9.7 mg/kg/day. Dose calculated for route-to-route extrapolation based on the LOEL of 0.068 mg/L, which inhibited brain, RBC, and plasma cholinesterase activities]. UF: 300	21-day inhalation toxicity study in rat (MRID 00082079)

2.2.2 Contamination of profenofos

Contamination of profenofos in environmental waters is an extensive problem with widespread ecological consequences. The major sources of pollution are wastewater from agricultural industries and pesticide plants. Wastewater from those sources may contain profenofos at high level as several hundred mg/L. The main characteristics of this wastewater are its extreme toxicity, low volume and well-defined location.

2.2.2.1 Contamination of profenofos in surface water and ground water

Under some conditions profenofos can be generally contaminated in the surface water and ground water by runoff from treated land, for several days following application. These conditions include poorly draining or wet soils with readily visible slopes toward adjacent surface waters, frequently flooded areas, areas over-laying extremely shallow ground water, areas with in-field canals or ditches that drain to surface water, areas not separate from adjacent surface waters with vegetated filter strips, and highly erodible soils cultivated using poor agricultural practices such as conventional tillage, down the slope plowing and spray drift (U.S.EPA, 1996). Surface water and ground water were taken for primary sources of drinking water production. The measurement of profenofos in the risk area near agricultural field from various countries is shown in Table 2.3. Profenofos levels in summer and dry season are fluctuated from seasonal effect hence it can be detected throughout the year (Harnpicharnchai et al., 2013). This showed that profenofos concentrations in

these water sources were higher than the standard value from Australia Drinking Water Guideline for Pesticides (Halminton et al., 2003). The profenofos concentrations in dry season were less than in summer due to high photodegradation, which had a higher intensity of sunlight (Harnpicharnchai et al., 2013).

Table 2.3 Contamination of profenofos in surface water and ground water

Sources	Summer (mg/L)	Dry season (mg/L)	Reference
Agricultural area in Bueng Niam subdistrict, Khon Kaen, Thailand	0.9520	0.3186	(Harnpicharnchai et al., 2013)
The artesian well from agricultural area in Thailand	(1×10^{-6}) to (4.61×10^{-4})	(4×10^{-6}) to (1.323×10^{-3})	(Jaipieam, 2008)
Haraz river in Iran	(2×10^{-4}) to (5×10^{-4})	(1×10^{-4}) to (4×10^{-4})	(Nasrabadi et al., 2011)
Agricultural area in Jiangsu, China	-	3.854×10^{-3}	(He et al., 2010)

2.2.2.2 Contamination of profenofos in sediment

Profenofos can be generally contaminated in sediment from many areas as shown the example areas in Table 2.4. This showed that profenofos concentrations in these soil and sediment samples were highly contaminated. The seasonal fluctuation can influence profenofos level and even more frequently in summer. From

agricultural applications such as spray drift to the crops can be caused the remaining of this insecticide in soil and vegetable products (Harnpicharnchai et al., 2013).

Table 2.4 Contamination of profenofos in soil and sediment

Sources	Profenofos concentration (mg/kg)	Reference
Agricultural area in Bueng Niam subdistrict, Thailand	16.5956 (winter) – 41.8080 (summer)	(Harnpicharnchai et al., 2013)
Haraz river in Iran	0.38	(Nasrabadi et al., 2011)
Agricultural area in Benguest, Philippines	0.003	(Lu, 2010)
Agricultural area in Jiangsu, China	0.224	(He et al., 2010)

The standard value of profenofos in drinking water is 0.3 µg/l referring from Australia Drinking Water Guideline for Pesticides (Halminton et al., 2003). However, the drinking water standard of profenofos in Thailand has not been regulated.

2.2.2.3 Contamination of profenofos in fruits and vegetables

Profenofos can be generally contaminated in fruits and vegetables from many areas as shown the example areas in Table 2.5.

Table 2.5 Contamination of profenofos in fruits and vegetables

Sources	Profenofos concentration (mg/kg)	Maximum Residue Limits (MRLs, mg/kg)	Reference
Chili farm area in Ubonrachathani, Thailand	0.520 to 6.290	5	(Siriwong et al., 2011)
Frozen red pepper in imported station, Japan	0.13	0.05	(Hirahara et al., 2005)
Cabbage in upper northeast, Thailand	1.08	0.5	(Srisawangwong et al., 2009)
Orange in lower southern, Thailand	0.001-0.91	0.1	(Khemvong and Choungpim, 2010)

2.2.3 Production and Utilization of profenofos

Profenofos is an organophosphate pesticide which is widely utilize around the world, particularly in developing countries. It was early synthesized in the United State in 1982, with condensation reaction from O-ethyl-S-propyl chloride phosphate and 2-chloro-4-Bromophenol in the presence of acid-binding agent (Hangzhou weiku information & Technology Co., 2008). It was used to control tobacco budworm, cotton bollworm, armyworms (fall, beet), cotton aphid, spider mites, plant bugs, fleahoppers, and whiteflies. Approximately 85% of all profenofos is utilized for manage of lepidopteran species at varying rate, and about 30% is used for manifest the worm complex. The mid-South states of Arkansas, Georgia, Texas, Louisiana, and Mississippi utilize in cotton field approximately 80% of the yearly use of profenofos. (United States Environmental Protection Agency (U.S.EPA), 2000). In Thailand, profenofos was normally used in pest control in chili field and other vegetables for using rate 80 cc (40 %w/v concentration) mixing with 20 L-water or approximately 1.7 g/L. The list of profenofos imported to Thailand during 2007 – 2014 is presented in Table 2.6.

Table 2.6 List of profenofos imported to Thailand

Year	Imported Quantity (Kg)
2007	340,760.00
2008	246,918.00
2009	357,586.00
2010	210,484.40
2011	282,845.10
2012	380,862.00
2013	103,951.00
2014	261,146.00

Source: (Department of Agriculture [DOA], 2007-2014)

Thailand is one of developing countries that abundantly imported profenofos to Thailand in the range of 103,951 to 380,862 kg/year during 2007 – 2014. The maximum imported quantity is 380,862 in 2012 with the value of 65,976,966.87 Baht. Moreover, profenofos is the 6th highest insecticide imported to Thailand (Department of Agriculture [DOA], 2007-2014).

2.3 Ultraviolet (UV)

Ultraviolet is one of the electromagnetic wave having shorter wavelength than visible light. It can be normally found in the sunlight which can release various types of rays, however; these rays are absorbed, reflected, or refracted out of the atmosphere covering the earth causing 49% of total rays able to pass through the earth's surface. Among them, 9% of total rays are UV ray (Jaroensin, 2006).

2.3.1 Types of ultraviolet lamp

Ultraviolet can be classified into 10 types followed by ISO 21348 as shown in Table 2.7.

Table 2.7 Types of ultraviolet

Spectral Sub category	Name	Wavelength (nm)	Note
UV	Ultraviolet	100 - 400	
VUV	Vacuum Ultraviolet	10 - 200	• Cannot be found in the sunlight due to strongly absorbed by ozone in atmosphere
EUV	Extreme Ultraviolet	10 - 121	
H Lyman-α	Hydrogen Lyman-alpha	121 - 122	
FUV	Far Ultraviolet	122 – 200	
UVC	Ultraviolet C	100 – 280	• Cannot be found in the sunlight due to ozone in atmosphere absorption
MUV	Middle Ultraviolet	200 – 300	
UVB	Ultraviolet B	280 – 315	• Can be found in the sunlight • Medium wave • Largely absorbed by the atmospheric ozone
NUV	Near Ultraviolet	300 - 400	
UVA	Ultraviolet A	315 - 400	• Can be found in the sunlight

Source: (Space Environmental Technology, 2013)

2.3.2 Sources of ultraviolet

(1) Natural sources: The sunlight is the only one of natural sources that can be discoveredboth UV-A and UV-B in the sun shine through the earth's surface.

(2) Artificial sources(Parsons, 2004)

(2.1) *Low-pressure Hg lamp*

It operates in either hot cathode or cold cathode. The lamp is filled with a mixture of Hg and an inert gas, usually argon (Ar), at pressure of a few torr and 40 ^{0}C the optimum operating temperature conditions that should be warmed up. It emits mainly (85-90%) at 253.7 nm, and about 7-10% at 184.9 nm. Both radiations are important for the AOP applications, since they are part of the absorption spectra of most pollutants. The 184.9 nm radiation is filtered out by the ordinary quartz, but it is transmitted by the high quality quartz. Furthermore, it has life time up to 25,000 operating hours. The limiting factors of lamp are the lamp current, electrode failure and solarsation, which affect the initial radiant efficiency.

(2.2) *Medium – pressure Hg lamp*

In order to give a high conversion of the electrical energy into radiant energy, a Hg light source should have either high electron temperature or a high Hg atom temperature. In the medium – pressure Hg lamp, the gas pressure reaches ~ 10^2 - 10^4 torr, and a 'local thermal equilibrium' is established, where the temperatures of electrons, atoms and ions become almost identical – this is called a 'plasma pressure

lamp'. This lamp is polychromatic light sources, and the spectral distribution of the radiation emitted covers a wide wavelength range, from VUV to IR. The continuum radiation is significant in the UV region, and the spectral lines are fairly broad due to a number of factors such as pressure effect. The major emission lines from a standard medium – pressure Hg lamp of interest for the AOP applications are at 184.9, 222, 253.7, 265.2, 296.7, 302.8, 313.2 and 365 – 366 nm in the UV range, and visible range of spectrum.

(2.3) *Pulsed UV lamp*

The pulsed UV lamp is marketed now for both AOP and UV disinfection applications. These are Hg – free arc lamps, which operated in pulse mode by alternately storing electrical energy in a capacitor and releasing it through an inert gas such as Xe, Ar and Kr (or the mixture of them) by a specifically shaped electrical discharge pulse. Such high temperatures and shell geometry of the plasma produce UV radiation that spans the 185 – 3000 nm range, with temperature – specific maxima in the UV region (usually around 260 nm).

(2.4) *Excimer lamp*

It is relatively given narrow emission bands and regarded as quasi-monochromatic light sources. The radiation is produced either microwave or dielectric barrier discharge, and the emission wavelength depends on the nature of the filled gas. This lamp, like low-pressure Hg lamp, operates near room temperature and emits monochromic radiation. The generated excimer undergoes irradiative (VUV or UV radiation). Inert gases (Xe, Ar, Kr), halogen gases or their mixtures are used as

filled gases. The lamp is enveloped with high quality quartz, which exhibits high transmittance in the short wavelength ($\approx$ 70 -80% at λ = 172 nm; 92% at λ = 222 nm). Table 2.8 gives some examples of excimer and their emission wavelengths. Other features of this lamp such as lamp shape design, high power density, no warm up time (instant radiation), temperature independent, and Hg-free long life time make them suitable for commercial application for water remediation. It can generate high reactive species (•OH), no need for addition of oxidants, *in situ* generation of H_2O_2 and O_3, effective photomineralization of organic contaminants in water. This lamp is mostly used in short wavelength (in vacuity) that can degrade the organic substances with direct photolysis and hydroxyl radicals.

Table 2.8 Excimer and their emission wavelengths

Excimer	λ (nm)	Excimer	λ (nm)
Xe_2	172	Cl_2	259
ArF	193	Br_2	289
KrBr	207	XeCl	308
KrCl	222	I_2	342

Source: (Parsons, 2004)

2.3.3 Vacuum ultraviolet (VUV)

Vacuum ultraviolet (VUV) process is categorized in one of the advanced oxidation processes (AOPs). VUV region irradiates within the period of wavelength

100 – 200 nm as shown in Figure 2.3. The particular interest for VUV is that since the irradiation is absorbed by water, therefore generating highly reactive species including the primary radicals, hydrogen atoms, and hydroxyl radicals, according to reaction that further induce oxidative degradation of the dissolved organicpollutants(Padikkaparambil et al., 2013). Hydrated electrons are generated according to equation (2.1) – (2.2) on a smaller scale.

$$H_2O + h\nu \ (\lambda < 190 \ nm) \rightarrow H\bullet + \bullet OH \tag{2.1}$$

$$H_2O + h\nu \ (\lambda < 190 \ nm) \rightarrow H^+ + \bullet OH + e^- \tag{2.2}$$
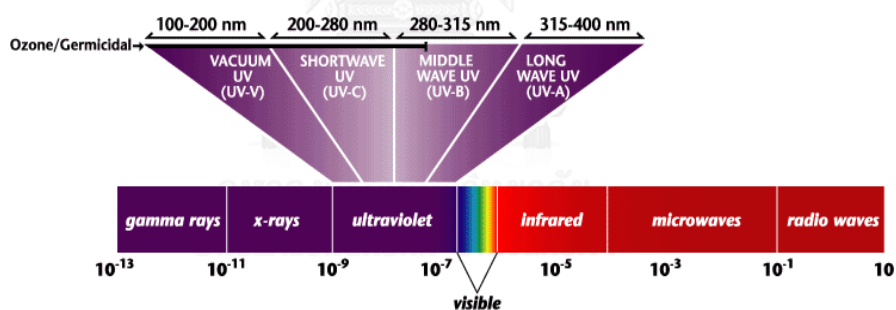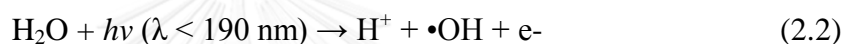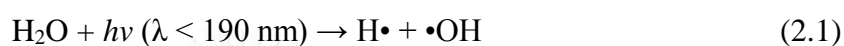
Figure 2.3 Ultraviolet visible light wavelength and vacuum ultraviolet region
(Water Treatment Guide, 2007)

Organic compounds also absorb in the VUV spectral range, but when dissolved in aqueous solution, water is the main absorber, as it is present at a concentration of about 55.5 M, which is typically a million times or more the

concentration of any contaminant present. Water is significantly important for •OH radical production that has the high quantum yield (E^0 = 0.33 eV), high oxidation potential (2.8 V) as shown in Table 2.9, greatly reactive, non-selectively with the organic pollutants at very high rates, and correspondingly short-lived (Heit et al., 1998; Parsons, 2004).

Table 2.9 Oxidation potential of any agents

Oxidizing agent	Oxidation potential (V)
Fluoride	3.06
Hydroxyl radical	2.80
Oxygen (atomic)	2.42
Ozone	2.08
Hydrogenperoxide	1.78
Hypochlorine	1.49
Chlorine	1.36
Chlorine dioxide	1.27
Oxygen (molecular)	1.23

Source: (Metcalf and Eddy, 2003)

2.4 Titanium (IV) dioxide (TiO$_2$)

2.4.1 Physical and chemical properties of titanium (IV) dioxide

There are major three crystalline forms of titanium (IV) dioxide existing including 1) anatase which attends to be more stable at low temperature, 2) rutile

which is generally encountered only in minerals and 3) brookite which is sometimes disclosure in the igneous rocks and normally stable at higher temperature. Among them, anatase form is the most effective catalyst, which is the major factor contributing to improve titanium (IV) dioxide activity resulting in enhancement the photocatalytic degradation as well (Watthanaarun et al., 2007). Titanium (IV) dioxide has been excellently prepared in three forms. Only rutile form is received in the form of the large single transparent crystal. The conclusion of the crystallographic properties of all forms is given inTable 2.10.

Table 2.10 Crystallographic properties of anatase, rutile, and brookite

	Anatase	**Brookite**	**Rutile**
Crystal structure	Tetragonal	Orthorombic	Tetragonal
Density, [g/cm^3]	3.9	4.0	4.23
Hardness, [Mohs scale]	5.5 - 6	5.5 - 6	7 -7.5
Unit cell	$D_4a^{19}.4TiO_2$	$D2h^{15}.8TiO_2$	$D4h^{12}.3TiO_2$
Lattice parameter, [nm]			
a	0.3758	0.9166	0.4584
b		0.5436	
c	0.9514	0.5135	2.953

Source:(Watthanaarun, 2004)

Both anatase and rutile are the important material forms of titanium (IV) dioxide, which have tetragonal crystal structure. Anatase is presented generally in

near-regular octahedral while slender prismatic crystals are found in rutile form. However, anatase and rutile are anisotropic. Refractive index is one of their physical properties associated with the crystal axes. Most applications found that the distinctions between crystallographic directions are lost due to the random orientation in a large number of small particles.

The rate transformation of crystalline forms for anatase to rutile is caused by temperature and the presence of other substances that could catalyze or inhibit the phase transformation, and may have obtained negative value of Gibb's free energy which are induced the non-reversible of anatase-to-rutile transformation.

Typically, titanium (IV) dioxide is steady at high temperature, which has the 1,855 ^{0}C of melting point and gets tremendous resistance to chemical attack. When it is heated up with vacuum irradiation resulted in the minor loss in oxygen atom, which may have a chance to reversal to TiO_2 composition. Nevertheless, it obtains the dark blue product; it is able to turn back to the original white color with heat in the air (Watthanaarun, 2004).

2.4.2 Titanium (IV) dioxide in industrial applications

Titanium (IV) dioxide, additionally known as titania, is the naturally happening the oxide of titania with the chemical formula as TiO_2. Most of TiO_2 is widely used with a white pigment in the industrial scale treatment since it has extremely high refractive index and brightness. Extensively utilizing of TiO_2 such as

plastics, coatings, paints, paper inks and other applications is caused from UV resistant properties onto this pigment surface, which can perform as a UV adsorber. Moreover, TiO_2 is also used in food equipment such as wrapping of salami, in medicines, in toothpaste, in cosmetics and skin care products including sunscreen, lipstick, body powder and soap (Putta, 2009a).

2.5 Sol – gel process

The sol-gel process associates with the formation of sol following by preparation in gel form. Sol is the suspension of solid particles with different diameter 1-10 nm in liquid obtained from hydrolysis and condensation of a precursor led to produce the gel. Gel is generated in the two phase material mixture between a large numbers of solids encapsulating in the solvent. Moreover, it can be carried out production by de-stabilized the preformed sol solution. Aquasol or aquagel is the gel using water as the solvent encapsulating the solids, and alcosol is the form of gel utilizing alcohol as the solvent. The encapsulated liquid can be removed from gel by either evaporative drying or drying with supercritical extraction or supercritical drying in short (Watthanaarun, 2004; Chantam, 2006).

There are major six advantages from the preparation of the sol-gel solution (or catalytic materials with sol-gel process into the following:

(a) the capability to keep up high purity due to the starting materials pureness;

(b) the capability to adjust the physical characteristics such as pore size distribution   and pore volume;

(c) the capability to diversify compositional homogeneity at a molecular level;

(d) the capability to provide samples at low temperatures;

(e) the capability to bring out several components in a single step;

(f) the capability to generate samples in different physical forms.

The conversion from a precursor, which is mostly used metal alkoxide due to its commercially available in high purity, to a catalytic material passed through the sol-gel process has six major steps that can be characterized as follows (Putta, 2009a):

Step 1: Formation of different stable solutions of the metal alkoxide or solvated metal precursor as the sol

Step 2: Gelation resulting from the formation of an oxide- or alcohol- bridged network as the gel by a polycondensation or polyesterification reaction that results in a significant increase in the viscosity of the solution.

Step 3: Aging the gel (Syneresis), during which the polycondensation reactions continue until the gel transforms into a solid mass, accompanied by contraction of the gel network and expulsion of solvent from gel pores. Phase transformations may occur concurrently with synergistic. The aging process of gels can exceed 7 days and is critical to the prevention of cracks in gels which have been cast.

Step 4: Drying of the gel, when water and other volatile liquids are removed from the gel network. This process is complicated due to fundamental changes in the structure of the gel.

Step 5: Dehydration, during which surface-bound R-OH groups are removed, there by stabilizing the gel against rehydration. This is normally achieved by calcining the monolith at temperature up to 800 ^{0}C.

Step 6: Densification and decomposition of the gels at high temperatures (T > 800 ^{0}C). The pores of the gel network are collapsed, and remaining organic species are volatilized.

Moreover, there are three main reactions for fabrication of titania polymers by sol-gel process including hydrolysis and condensations of the starting alkoxide. In this present work, we had chosen titanium isopropoxide namely (TTIP) to be the starting alkoxide. These reactions are shown according to reaction (2.3) – (2.5) (Kaliwoh et al., 2000).

Hydrolysis

$$Ti(OC_3H_7)_4 + H_2O \quad \rightarrow \quad Ti(OC_3H_7)_3OH + C_3H_7OH \qquad (2.3)$$

Condensation

$$Ti(OC_3H_7)_4 + Ti(OC_3H_7)_3OH \quad \rightarrow \quad Ti_2O(OC_3H_7)_6 + C_3H_7OH \qquad (2.4)$$

Water condensation

$$Ti(OC_3H_7)_3OH + Ti(OC_3H_7)_3OH \quad \rightarrow \quad Ti_2O(OC_3H_7)_6 + H_2O \qquad (2.5)$$
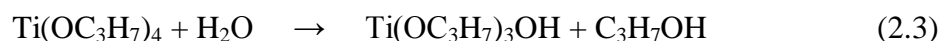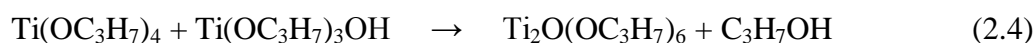
2.6 Electrospinning process

Electrospinning is a simple technique able to create both nanofibers and microfibers with the various diameter sizes. To make electrospinning working, electrical potential is applied between a collector and a droplet of the spinning solution (or sol-gel solution) order to overcome the surface tension force of polymer solution at the end-point of needle as a nozzle. When the applying electrical potential overcomes the surface tension force of polymer fluid, a droplet at the nozzle can elongate to form a conical shape called the Taylor cone, and then a charged jet of the polymer solution is spouted to form the Taylor cone. At the time a charged jet is travelling in the air toward a collector, some of solvent evaporates out of a charged jet, or the mixed polymer solution is solidified. Hence, the continuous fibers are led to form a non-woven on the collector(Chantam, 2006; Duriyasart, 2012).

2.7 Advanced oxidation processes (AOPs)

Advanced oxidation processes (AOPs) have been demonstrated as an effective means of water remediation as compared to the conventional technologies, such as adsorption on activated carbon, air stripping and biodegradation. There have been two main stages occurred in AOPs oxidation including the generation of strong oxidants (such as hydroxyl radicals), and the reaction between these strong oxidants and organic pollutants. These oxidants can react almost non-selectively with the organic pollutants at very high rates and can destroy a wide range of organic compounds. In general, the light-driven AOPs involve the production of hydroxyl radicals, which

react almost non-selectively with the organic pollutants at very high rates. The ultraviolet (UV) direct photolysis process is restricted to those pollutants that exhibit large molar absorption coefficient and quantum yields, and has limited applications. In most cases comparative studies revealed significant larger rates of pollutants removal through •OH radical-driven AOPs, such as UV/H_2O_2, UV/O_3, $UV/O_3/H_2O_2$, photo-Fenton or photocatalytic process than those of direct photolysis.

Hydroxyl radicals react with the organic compounds in short time, however; only the reaction of hydroxyl radicals cannot directly lead to the mineralization of pollutants. In contrast, this reaction might induce the production of organic oxidation by-products resulting in incomparably react with hydroxyl radicals. To improve the complete mineralization of organic compounds, adding more chemical dosage might be cost prohibitive in certain applications.

AOPs can be categorized into two groups (established and emerging technologies) based on the water treatment industry's experiencewith the technology, results from manufacturer, and engineering literature as shown in Table 2.11

Table 2.11 AOPstechnologies (Kommineni et al., 2000)

Establishedtechnologies	Emerging technologies
1. Hydrogen Peroxide/Ozone (H_2O_2/O_3) 2. Ozone/Ultraviolet Irradiation (O_3/UV) 3. Hydrogen Peroxide/Ultraviolet Irradiation (H_2O_2/UV)	1. High Energy Electron Beam Irradiation (E-beam) 2. Cavitation (Sonication &Hydrodynamic) 3. TiO_2 - catalyzed UV Oxidation 4. Fenton's Reaction

The advantages of AOPs are shown as follows:

    1. Can destroy and decompose many types of micropollutants

    2. Disinfection

    3. Can be used in the industrial scale

The disadvantages of AOPs are shown as follows:

    1. Difficult analysis of product combination potential

    2. Radical scavenging influences the decreasing of AOPs efficiency

Examples of AOPs related to ultraviolet (National Water Research Instituete (NWRI), 2013) as follows:

    1. O_3/UV

This process was done with the low-pressure lamp or medium-pressure lamp for hydroxyl radical generation from equation (2.6) – (2.7).

$$O_3 \;+\; H_2O \;\rightarrow\; O_2 \;+\; H_2O_2 \;(\lambda < 300 \text{ nm}) \qquad (2.6)$$

$$2O_3 \;+\; H_2O_2 \;\rightarrow\; 2OH\bullet \;+\; 3O_2 \qquad (2.7)$$
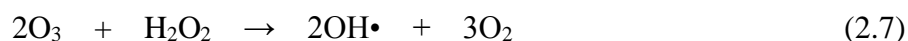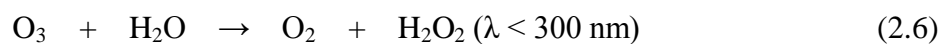
From equation (2.6), ozone has broken by the sunlight leading to generate hydrogen peroxide (H_2O_2), and then hydrogen has reacted with ozone causing production high quantity of hydroxyl radicals which are able to attack the micropollutants.

2. H_2O_2/UV

This process has been supplied with adding hydrogen peroxide for production high amount of hydroxyl radicals easily from direct photolysis of hydrogen peroxide and hydrogen peroxide decomposition as shown in equation (2.8) – (2.9).

$$H_2O_2 \;\rightarrow\; 2OH\bullet \;\;(\lambda < 300 \text{ nm}) \qquad (2.8)$$

$$OH\bullet \;+\; \text{organic compound} \;\rightarrow\; \text{Oxidation by – products} \qquad (2.9)$$
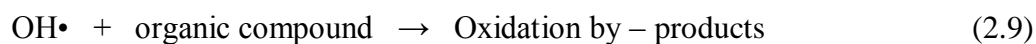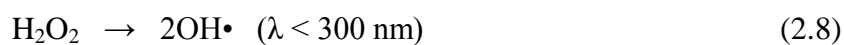
2.8 Photocatalytic process

Photocatalytic reactions have ability to convert solar energy into chemical energy passed through the absorption of light by photocatalyst in order to generate

highly reactive species that can oxidize or reduce materials. In semiconductor photocatalysis, the light-absorbing is a semiconducting material. The electronic structure of most semiconductor materials comprises a highest occupied band full of electron called valence band (VB), and a lowest unoccupied band called the conduction band (CB). These bands are separated by a region that is largely devoid of energy levels, and the different between two bands is called the band gap energy, E_{bg}. The band gap illumination produces electron-hole pairs, h^+ e^-, which can either recombine or separate ways to surface of the semiconductor materials such as metal oxides (TiO$_2$, ZnO, SrTiO$_3$, K$_4$NbO$_2$, Fe$_2$O$_3$ and SnO$_2$). Among these metal oxides, TiO$_2$ is most used in many treatment applications due to its long life for carriers. If the electron-hole pairs recombine either at surface or in the bulk, it may influence the photocatalytic efficiency to be low. No matter the light source irradiated a photon of energy bigger or equal to the band gap energy, it is certainly absorbed by a semiconductor particle, which contributes an electron at VB moving to CB with generation a hole (h^+) at the same time (Hoffmann et al., 1995; Parsons, 2004).

Photogenerated electrons which are able to make their way to the surface of semiconductor particle, which usually used TiO$_2$ due to having a large band gap ($E_{bg} \approx$ 3.2-3.0 eV) and having ability to absorb UV light (typically < 380 nm), can react either directly or indirectly through slightly less energetic trap surface states, with absorbed species. Thus, there is an electron donor, D, adsorbed on the surface of TiO$_2$, then the photogenerated holes can react with it (directly or indirectly) to generated an oxidized product, D$^+$. Similarly, if there is an electron acceptor present at the surface,

and then the photogenerated CB electrons can react with it to generated a reduced product, A^-.

Furthermore, positive potential of hydrogen ion (pH) dependant is one of the factors that can influence the adsorption of contaminants on the reactive sites of TiO_2 surface including the present of anions, cations, and neutral environmental condition. At low pH approximately 3 to 4, TiO_2 particles are significantly retarded due to anion adsorption onto the positively charged TiO_2 surface led to decrease the reaction rates. At high pH (more than 7), TiO_2 particles arenegatively charged and there was negligibleanion adsorption (Kommineni et al., 2000).

In this research study, we focus on the emerging technology called TiO_2 - catalyzed UV Oxidation. When TiO_2 is irradiated by UV light, valence band electrons are excited to the conduction band, resulting in the formation of holes. These holes react with water molecules to produce hydroxyl ant other radicals that can oxidize organic compounds. Moreover, the formation of H_2O_2 intermediate can also assist the overall oxidation process. Both advantages and disadvantages of TiO_2 - catalyzed UV Oxidation are presented as follow (Kommineni et al., 2000):

Advantages

- No potential for bromated formation
- Can be performed at higher wavelength (300 -380 nm) than other UV oxidation process
- No off – gas treatment required

- The TiO$_2$ oxidation process has been studied for many organic compounds under various types of water sample.

Disadvantages

- Currently, no full – scale applications exist for this emerging technologies

- In attached TiO$_2$ system, pre-treatment necessary to avoid fouling of the active TiO$_2$ sites and destructive inhibition of the TiO$_2$ catalyst.

- If TiO$_2$ is added as slurry, then a separation step is required to remove the solid TiO$_2$ from the treated water.

- There is a potential for rapid loss of TiO$_2$ photocatalytic activity, resulting in need for a large volume of replacement catalyst on-site storage or regeneration method.

- If DO concentrations in the source water are low such as in some groundwater, oxygen sparging may be required to increase the rate of contaminant degradation.

- Reaction efficiency is highly pH dependent, requiring close monitoring and control.

2.8.1 Mechanism of photocatalysis by TiO$_2$

Among the various types of advanced oxidation processes (AOPs), photocatalysis with TiO$_2$ is obviously dominant for removal and mineralization of organic contaminants in both water and air conditions than others, and are used in many applications due to its ability to produce strong oxidizing agents. The main

pathway of photomineralization (i.e., the breakdown of organic compounds) carried out in aerated solution may easily be summarized by this reaction.

$$\text{Organic compounds} \quad \rightarrow \quad CO_2 \ + \ H_2O \ + \text{mineral acids}$$

A schematic representation of this process in Fig. 2.4 (Naeem and Ouyang, 2013) shows major processes and their characteristic time for TiO_2 – sensitized photo-oxidative mineralization of organic compounds by dissolved oxygen in aqueous solutions. The radical ions formed after the interfacial charge transfer reactions can participate in several pathways of the degradation process:
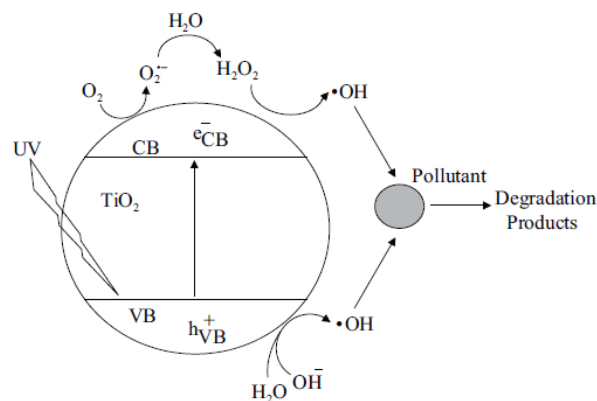
Fig. 2.4 The processes occurring on bare TiO_2 particles after UV excitation (Naeem and Ouyang, 2013)

(1) They may react chemically with themselves or with surface-adsorbed compounds.

(2) They may recombine via back electron-transfer reactions, especially when they are trapped near the surface, due to either the slowed-down outward diffusion or hydrophobicity.

(3) They may diffuse from the semiconductor surface and participate in chemical reactions in the bulk solution.

The mechanisms of photocatalysis by TiO_2 are shown according to reaction (2.6) − (2.13) (Houas et al., 2001; Watthanaarun, 2004). The examples of TiO_2-sensitized photomineralization of organic substance are presented in Table 2.12

(i) Absorption of efficient photons ($hv > E_{bg}$ − 3.2 eV) by TiO_2 particle

$$TiO_2 + hv \rightarrow e^-_{CB} + h^+_{VB} \qquad (2.6)$$

(ii) Oxygen ionosorption (first step of oxygen reduction; oxygen's oxidation degree passes from 0 to 0.05)

$$O_2 + e^-_{CB} \rightarrow O_2^{\bullet-} \qquad (2.7)$$

(iii) Neutralization of OH- groups by photoholes which produces OH· radicals

$$H_2O \leftrightarrow H^+ + OH^- + h^+_{VB} \rightarrow H^+ + \bullet OH \qquad (2.8)$$
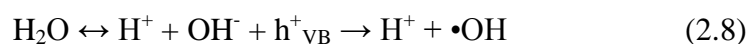
(iv) Neutralization of $O_2^{•-}$ by protons

$$O_2^{•-} + H^+ \rightarrow HO_2^{•} \qquad (2.9)$$

(v) Transient hydrogen peroxide formation and dismutation of oxygen

$$2HO_2^{•-} \rightarrow H_2O_2 + O_2 \qquad (2.10)$$

(vi) Decomposition of H_2O_2 and second reduction of oxygen

$$H_2O_2 + e^- \rightarrow OH• + OH^- \qquad (2.11)$$

(vii) Oxidation of the organic reactant via successive attacks by •OH radicals

$$R \text{ (pollutant)} + •OH \rightarrow R^{•} + H_2O \qquad (2.12)$$
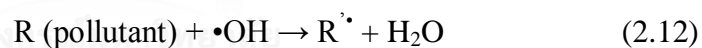
(viii) Direct oxidation by reaction with holes

$$R + h+ \rightarrow R^{+•} \rightarrow \text{degradation products} \qquad (2.13)$$

Table 2.12 Some examples of TiO_2-sensitized photomineralization of organic substances(Parsons, 2004)

Organic substances	Examples
Alkanes	Methane, *iso*-butane, pentane, heptanes, cyclohexane and paraffin
Haloalkanes	Mono-, di-, tri- and tetrachlomethane, tribromoethane and 1,1,1-trifluoro-2,2,2-trichloroethane
Aliphatic alcohols	Methanol, ethanol, *iso*-propyl alcohol, glucose and sucrose
Aliphatic carboxylic acids	Formic, ethanoic, dimethyethanoic, propanoic and oxalic acids
Alkenes	Propenem and cyclohexane
Haloalkenes	Perchloroethane, dichlorobenzene and 1,1,2-trichloroethane
Aromatics	Benzene and naphthalene
Nitrohaloaromatis	Chlorobenzene, 1,2-dichlorobenzene and bromobenzene
Phenols	3,4-Dichloronitrobenzene and dichloronitrobenzene
Halophenols	2-, 3-, 4-CP, pentachlorophenol, 4-fluorophenol and 3,4-difluorophenol
Aromatic carboxylic acids	Benzoic, 4-aminobenzoic, pthalic, salicylic, m- and *p*-hydroxy benzoic and chlorohydroxybenzoic acids
Polymers	Polyethylene and polyvinylchloride
Surfactants	SDS, polyethylene glycol, sodium dodecyl benzene sulphonate, trimethyl phosphate and tetrabutyl ammonium phosphate
Herbicides	Methyl viologen, atrazine, simazine, prometron, propetryne and bentazon

Organic substances	Examples
Pesticides	DDT, parathion and lindane
Dyes	Methylene blue, rhodamine B, methyl orange, fluorescein and reactive black 5

2.8.2 pH effect for the photolytic and photocatalytic activity

The pH condition has been reported to affect the photolytic rate and photocatalytic rate in aqueous solution. The example of photolytic oxidation, methyl orange, under VUV irradiation and aeration show the results in Table 2.13 (Tasaki et al., 2009). The results indicated that the removal efficiency of methyl orange had significant decreased (20%) under strong acidic and strong basic conditions compared to neutral condition.

Table 2.13 pH effectto the removal efficiency of methyl orange

pH	Removal efficiency of methyl orange
6.9	90%
8.7	80%
2.9 and 10.8	20%

Kutschera and coworkers (2009) had investigated the degradation of geosmin and 2-methylisomorneol (2-MIB) in aqueous solution under VUV irradiation. They found that the degradation rate at pH 3, 7, and 11 were 1.25, 1.75 x 10^{-3}, and 0.75 m^2/J, respectively. At pH 3, the degradation rate had considerably low because O_3 (from the reaction between O_2 and light as shown in equation 2.14 and 2.15) would react with H^+ and form $HO_3^{\bullet}$ under strong acidic conditions, $HO_2^{\bullet}$ and O_2^- under strong basic conditions resulting to O_3 insufficient react with the target compounds (as shown in equation 2.16). Moreover, hydroxyl radicals would be highly decomposed under strong basic conditions (as shown in equation 2.17) brought about decreasing the formation of these radicals (Kutschera et al., 2009).

$$3/2\ O_2\ +\ hv\,(185\ nm)\ \rightarrow\ O_3 \qquad (2.14)$$

$$O_3\ +\ H^+\ \rightarrow\ HO_3^{\bullet} \qquad (2.15)$$

$$O_3\ +\ OH^-\ \rightarrow\ HO_2^{\bullet}\ +\ O_2^- \qquad (2.16)$$

$$\bullet OH\ \rightarrow\ O^{\bullet-}\ +\ H^{\bullet+} \qquad (2.17)$$
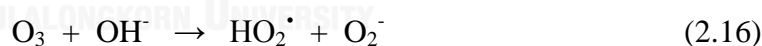
The example of photocatalytic oxidation, pyrimidine base, the reaction rate is also influenced by the condition of pH. Pyrimidine bases such as thymine, 6-methyl uracil, and cytosine show lower reaction rates at higher pH values (Dhananjeyan et al., 2000). The band edge positions of TiO_2 shift to more negatives values with increasing pH, resulting in a decrease of oxidation potentials. Conduction and valence

band edges increase at the rate of -60 mV per unit increase in pH under strongly basic conditions (Takeda et al., 1998). The dissociation of TiOH to TiO$^-$ and H$^+$ in basic solution can cause low concentration of surface hydroxyl groups that produce active hydroxyl radicals. Also the pyrimidine bases become negatively charged under basic conditions, and there is a decrease in the extent of adsorbility that leads to a decrease in the reaction rate. The pK$_a$ value of the reaction represented as in •O$_2^-$ + H$^+$ → •HO$_2$ is reported to be about 4.88 (Wang et al., 1999). As a result, the electron scavenging by oxygen decreases under strongly basic condition.

Inosine 5'-monophosphate (IMP), which is a totally mineralized via ring-opening by photocatalytic oxidation, also show reaction rate-dependency on the pH condition (Lee et al., 2003). Under strongly acidic conditions, non-bonding electrons can accept protons easily, and IMP exists as positively charged protonated species. On the other hand, dissociation of a proton from the IMP hydroxyl group happens readily under strongly basic conditions. The deprotonated IMP molecules exist as negatively charged species. The surface charge state of TiO$_2$ also depends on the pH condition. The isoelectric point of TiO$_2$ is located at about 6.5 of pH and the surface hydroxyl of TiO$_2$ exists as TiOH$_2^+$ and TiO$^-$ forms, causing electrostatic repulsion between IMP and TiO$_2$ under strongly acidic and basic conditions, respectively. Therefore, the overall degradation rate constants under acidic mildly acidic, and mildly basic conditions were higher than those under strongly acidic and basic conditions (see Table 2.14).

Table 2.14 Overall degradation rate constants of IMP by TiO_2 at different initial pH
conditions (Lee et al., 2003)

Catalyst	Initial pH					
	2		3		10	
	k (min^{-1})	R^2	k (min^{-1})	R^2	k (min^{-1})	R^2
TiO_2 (P25)	0.0127	0.9885	0.0223	0.9979	0.0073	0.9915
TiO_2 prepared by sol-gel method	0.0180	0.9898	0.0206	0.9906	0.0079	0.9901

The pH dependent behavior of photocatalytic oxidation is explained as
follows:

1. Nernstian shift of band edge position

2. Change in surface hydroxyl group concentration

3. Change in electron scavenging rate by O_2

4. Change in surface charge state of TiO_2 and ionic state of reactant

2.8.3 Photocatalytic kinetics of organic substance

The photocatalytic oxidation of various types of organic substances has been
determined in term of the Langmuir–Hinshelwood kinetic model, which has been
effectively used for heterogeneousphotocatalytic degradation to analyze the
relationship between initial degradation rate and initial concentration of organic
substance (Khezrianjoo and Revanasiddappa, 2012). Hydroxyl radicals and organic

substance can adsorb on the photocatalyst surface. Tsai et al. (2009) revealed that photocatalytic oxidation with the dependence of TiO_2 as photocatalyst is followed the Langmuir–Hinshelwood kinetic model as shown in equation (2.18) (Tsai et al., 2009).

$$r = -\frac{dc}{dt} = \frac{k_r \cdot K \cdot C}{1 + K \cdot C} \tag{2.18}$$

where r (mM.min^{-}1) is the rate of reaction, C (mM) is the concentration of organic substance, K (mM^{-1}) represents the Langmuir adsorption constant for adsorption of the substance onto catalyst, and k_r(mM.min^{-1})is limiting rate constant of reaction at maximum coverage under the given experimental conditions. This equation is a linear line when fitted the graph between inverse initial rate and inverse concentration as shown in equation (2.19). Slope (1/k_rK) and interception (1/k_r) are given positive.

$$\frac{1}{r} = \frac{1}{k_r} + \frac{1}{k_r K}\frac{1}{C} \tag{2.19}$$

The constants, k_r and K, can be obtained from the intercept and slope of the line formed when "1/r" is plotted against "1/C". The integrated form of equation (2.18) is shown in equation (2.19):

$$t = \frac{1}{k_r K} \ln\left(\frac{C}{C_0}\right) + \frac{1}{k_r}(C_0 - C_t) \tag{2.20}$$

Plotting between "$t_{1/2}*$, the half-life" and initial concentration of organic pollutant should be a linear line as in the following equation (2.21)

$$t_{1/2} = \frac{0.5C_0}{k_r} + \frac{ln2}{k_r\,K} \tag{2.21}$$

Moreover, the rate of reaction (r)is corresponding to organic concentration at low solute concentrations (mg/L). k_{obs} is the observed kinetic rate or apparent first-order rate constant.

$$r = k_r \cdot K \cdot C = k_{obs} \cdot C \tag{2.22}$$

Besides, the photocatalytic reaction equation can be formed as an apparent first-order rate:

$$r = k_{obs} \cdot C = -\frac{dc}{dt} \tag{2.23}$$

The integral form of the pseudo-first-order rate equation is generally expressed as follows:

$$ln\frac{C_t}{C_0} = -k_{obs} \cdot t \tag{2.24}$$

where C_o is the initial concentration of organic substance, and C_t is the residual concentration of organic substance at time t.

The pseudo-first-order rate equation was used as a model to analyze the photodegradation of many organic solutes. Lee et al. (2004), Wang et al. (2007), and (Watanabe et al., 2003; Chin et al., 2004) also agreement with the experimental data for photocatalytic activity, which was given more than 0.95 correlation coefficient for all the photocatalytic experiments. Besides, Tsai et al. (2009) suggested that initial organic concentration, TiO_2 dosage, initial pH, and temperature affected to the rate constants (k_{obs}) (Tsai et al., 2009).

2.9 Removal of organophosphate pesticides

2.9.1 Advanced oxidation processes (AOPs)

Badawy and coworkers (2006) investigated the removal of organophosphate pesticides by using Fenton and Photo-Fenton process. The results showed that the removal efficiency of profenofos from Fenton process was 50.3% within 90 min irradiation while Photo-Fenton process obtained 89.7% within 30 min irradiation. All experiments were controlled these variables to receive the optimum condition including pH = 3, COD: H2O2 = 1 : 2.2, Fe^{2+} : H_2O_2 = 1 : 100. Therefore, the removal efficiency from Photo-Fenton process had higher and taken short irradiation time than Fenton process. Photo-Fenton process was capable to enhance profenofos

degradation because it had UV light to accelerate the reaction for changing from ferric to ferrous form, and increased $\cdot$OH radical production from hydrogen peroxide and ferrous in aqueous solution (Badawy et al., 2006).

Beltran et al. (1996) compared the efficiencies of various AOPs (UV alone, O_3, O_3/H_2O_2, UV/ H_2O_2 and UV/O_3) for phenanthrene and acenaphthene ($\approx 10^{-6}$ M) removal from surface waters with relatively high content of natural organic matter (NOM) (18 – 30 mg C L^{-1}). A low-pressure Hg lamp was used as a UV light source. About 90% degradation of these compounds was achieved in less than 15 min for phenanthrene, and 30 min for FLU and acenaphthene. In organic free water, 90% removal of FLU was observed after about 7.5 min or irradaiation time. The other AOPs indicated up to 7 – 8 fold higher removal rates than UV photolysis. Among the PAHs studied, FLU exhibited the lowest oxidation rates, irrespective of type of AOP applied (Beltran et al., 1996).

Guittonneau et al. (1998) studied the kinetics of nitrobenzene, chloro-4-nitrobenzene and 4-nitrophenol (10^{-4} M) photo-oxidation in a closed batch reactor equipped with a 40-W low-pressure Hg lamp, at 16 ^{0}C and pH 7.5, in the absence and presence of H_2O_2. Only 10% removal was observed in all cases after 60 min of irradiation time without H_2O_2, whereas 90% decrease from the initial concentrations was measured after 36-,30-, and 18-min irradiation of nitrobenzene, chloro-4-nitrobenzene and 4-nitrophenol, respectively, in the presence of 10^{-3} M H_2O_2. No change in the organic carbon or nitrogen was observed under UV photolysis over 60-

min irradiation, but approximate 8% and 2% NO_3^- were quantified at 90% reduction of nitrobenzene and 4-nitrophenol in the presence of H_2O_2 (Guittonneau et al., 1988).

Doong and Chang (1998) studied the photo-induced degradation of diazion in aqueous solution by UV direct photolysis, UV/H_2O_2, $UV/Fe(II)/H_2O_2$ and $UV/Fe(0)/H_2O_2$ processes. The experiments were performed in a 1.2 l hollow cylindrical 100-W medium pressure Hg lamp (253 – 578 nm range) photoreactor equipped with a water jacket. The initial concentrations of diazion, H_2O_2 and Fe(0) or Fe(II) were 10, 20 and 2.8 mg/L, respectively. The photodegradation followed pseudo-first-order kinetics, with rate constants o 0.0025, 0.011, 0.011, and 0.009 min$^-$^{1} for direct photolysis, UV/H_2O_2, $UV/Fe(II)/H_2O_2$ and $UV/Fe(0)/H_2O_2$, respectively (Doong and Chang, 1998).

2.9.2 Vacuum ultraviolet (VUV) and ultraviolet (UV) direct photolysis

Xing et al. (2015) had evaluated the removal of the raw coking wastewaters that were collected from a coking factory in Hebei Province, northern China under ultraviolet (UV) and vacuum ultraviolet (VUV) photolysis along with the biodegradation by the acclimated activated sludge. They found that the water samples were removed 15.9% - 35.4% of total organic carbon removal efficiency within 24 h irradiation as TOC decreased when the irradiation time increased, and VUV had removal efficiency of chemical oxygen greater than UV. Due to VUV (λ = 185 nm) carries more energy than UV (λ = 254 nm), it might induce the much more oxidizing the organic compound in wastewaters. VUV can attack the organic compound bonds

since it has ability to produce lots of hydroxyl radicals led to react with O_2 to form O_3 efficiently. Furthermore, UV and VUV can eliminate the NH_4^+- N, NO_2^-- N, and TN in the coking wastewaters, and can form a large amount of NO_3^- - N (Xing et al., 2015).

Torrents et al. (1997) reported a thorough mechanistic investigation of the UV photolysis, emphasizing the role of DOC on the rate of removal. A Xe lamp and special glass filters ($\lambda > 290$ nm), with an average irradiance of 40 W m^{-2}, were used in all experiments. Direct photolysis of atrazine was slow (235 removal over 60 h) yielding to hydroxyatrazine (4-ethylamino-2-hydroxy-6-isopropylamino-S-triazine, 14%), chloride-alkylated and chloroalkyloxidized derivatives (9%). The efficiency of direct photolysis decreased by 15% with increasing DOC. Generation of hydroxyl radicals can significantly increase the rate of removal for both atrazine and its degradation by-products (Torrents et al., 1997).

Jing et al. (2007) had investigated the study of perfluorooctanoic acid (PFOA) degradation in aqueous solution by using a low-pressure Hg lamp with 185 nm – VUV irradiation. The results displayed that decomposition rate of PFOA followed by pseudo – first order model. Degradation rate using under VUV irradiation was given greater decomposition rate than 254 nm - UV irradiation, and VUV process could reach the decomposition efficiency to 61.7% within 2 h with 0.0075 min^{-1} of kinetic rate. In contrast, using UV radiation caused the long time approximately to 72 h for obtaining 89.5% of decomposition efficiency. Study of PFOA degradation mechanism revealed that PFOA could be absorbed by VUV irradiation light led to be stimulated

to the excited state formed to many radicals reacting with water caused the generation of products and hydroxyl radicals that could be completely degrade under VUV irradiation light (Jing et al., 2007).

Yoon et al. (2008) had examined the study of Arsenic (As (III)) photodegradation under 185 nm - VUV irradiation light with 10 W comparing to other types of oxidation processes including UV-C irradiation supplied with hydrogen peroxide (UV-C/H_2O_2), Photo Fenton (UV-A / Fe (III) / H_2O_2), and UV-A / TiO_2. The resulted disclosed that a VUV process was given higher efficiency than other oxidation processes, and had ability to absolutely degrade 100 µg/L of As (III) in synthetic aqueous solution and natural solution within 10 min. This was resulted from the production of hydroxyl radicals from photolytic reaction that was able to oxidize with As at alkaline condition led to forming hydrogen peroxide during VUV oxidation (Yoon et al., 2008).

2.9.3 Photocatalytic process (VUV/TiO_2 and UV/TiO_2)

Mingma et al. (2011) compared the mechanism of TiO_2 degradation of Diuron (3-(3,4-dichlophenyl)-1, 1-dimethyurea) in aqueous solution compared with direct UV photodegradation. The radical anions, phenylurea•$^-$, generated by one – electron reduction, have $pK_a \approx 5$. From the rate constants of one – electron reduction, it can be deduced that the generation of phenylurea•$^-$ and O_2•$^-$ on the surface of photocatalysts may be competitive. Hydroxyl radicals react with phenylurea via addition to the aromatic ring and/or hydrogen abstraction from a saturated carbon atom (98%), rather

than one – electron oxidation (2%). Adsorption studies on TiO_2 show that photocatalysis is independent the specific are of the catalyst. A variety of compounds have been observed upon photocatalytic degradation of Diuron, while only two hydroxychloro derivatives were generated after direct 365 nm irradiation. The photocatalytic degradation proceeds by three main pathways 1. oxidation of the side chain methyl group, 2. hydroxylation of aromatic ring, and 3. dechlorination. Different photoproducts were found depending on the polymorphic from TiO_2 used. Correlation analysis showed that the reactivity of phenylurea upon TiO_2 heterogeneous photocatalysis is associated with polar effects of the substituents in aromatic ring. However, the aqueous photocatalytic degradation of Diuron has been found to follow Langmuir-Hinshelwood kinetics, thus leading to complete mineralization (MingMa et al., 2011).

Kang et al. (2011) investigated the degradation of oily wastewater from restaurant by using VUV and TiO_2 nanoparticles for the pretreatment. The optimum conditions include 10 min of irradiation time, 3981 mg/L of COD concentration, 150 mg/L of TiO_2 concentration, 40 L/h of air flow rate, and pH 7. The results illustrate that VUV/TiO_2 process has carried out of $63 \pm 3\%$ of COD, $43 \pm 2\%$ of BOD_5, and $70 \pm 3\%$ of oil removal efficiency. The removal efficiencies were apparently increased when the irradiation time was raised. Moreover, VUV/TiO_2 process also considerably promotes the biodegradability of the oily wastewaters concurrently. As the 185 nm VUV (6.7 eV) has higher most of chemical bond energy and can generate more hydroxyl radicals, it can enhance the degradation and removal efficiency. Adding appropriate TiO_2 concentration improved adsorption of organic compounds on

TiO$_2$surface that would enlarge the removal efficiency by photocatalytic process (Kang et al., 2011).

Huang et al. (2013) had evaluated the destruction of methylene blue under UV, VUV, UV/TiO$_2$, and VUV/TiO$_2$ conditions. The optimum conditions include 20 mg/l of 400 ml for methylene blue concentration, low-pressure mercury lamps (7 W), 0.2 L/min of aeration flow rate, 90 min of irradiation time, and 0.5 g/L of TiO$_2$ powder condition. TiO$_2$ powder was stirred 30 min in the dark for adsorption of this contaminant on TiO$_2$ surface. They found that the initial concentrations of methylene blue were slightly dropped from 20 mg/L after adsorption equilibrium indicated that TiO$_2$ was not considerably adsorbed. The rate constants of methylene blue degradation were in ordered VUV/TiO$_2$ (0.0793 min^{-1}) > VUV (0.0468 min^{-1}) > UV/TiO$_2$ (0.0205 min^{-1}) > UV (0 min^{-1}). Combination of TiO$_2$ can be enhanced the degradation rate due to the synergistic effect, which improve the generation of hydroxyl radicals. The overall reactions were pseudo-first-order kinetic (Huang et al., 2013).

Ochiai et al. (2013) compared the purification of phenol in water media under light irradiation synergized with TiO$_2$ coated titanium mesh filter into the following the excimer VUV/TiO$_2$, UV-C/TiO$_2$, BLB/TiO$_2$, and excimer VUV alone processes. The optimum conditions include 2.5 mM/L of phenol concentration, excimer lamps (172 nm wavelength), 1 L/min of aeration flow rate, and 3 h of irradiation time. They found that the removal rates were in ordered VUV/TiO$_2$ (0.19 h^{-1}) > UV-C/TiO$_2$ (0.11 h^{-1}) > excimer VUV alone (0.01 h^{-1}) > BLB/TiO$_2$ (0.02 h^{-1}). The excimer

VUV/TiO$_2$presented the more removal efficiency of phenol than other processes because it can generate more hydroxyl radicals and strongly reactive oxidants such as hydroperoxyl radicals, superoxide and oxide radical anions from photolysis of water and photocatalysis under VUV irradiation. All these reactive species can directly attack with the organic pollutants (Ochiai et al., 2013).

Tsai et al. (2009) investigated the photocatalytic behavior of endocrine disrupting chemical called bisphenol-A (BPA), succeeded in a batch TiO$_2$ suspension reactor. The conditions could be 0.5 g/L of TiO$_2$ dosage (100 mg/200 cm^3), 25 ^{0}C of temperature, pH 7, UV, 60 min irradiation time, and five concentration of BPA (1, 5, 10, 20, 50 mg/L). The results revealed that the destruction-removal efficiency of BPA in the photodegradation system had decreased when increasing the concentration. The reaction rate constants are in ordered 1 mg/L (0.396 ± 0.246 min^{-1}) > 5 mg/L (0.150 ± 0.036 min^{-1}) > 10 mg/L (0.096 ± 0.002 min^{-1}) > 20 mg/L (0.075± 0.002 min^{-1}) > 50 mg/L (0.019± 0.000 min^{-1}). All these kinetic rates are described pseudo-first order reaction. The degradation efficiencies carried out due to electrophilic hydroxyl radicals (•OH) generated from the oxidation of water molecules and sintered by TiO$_2$. The photocatalytic degradation of BPA with TiO$_2$ suspension can quickly remove the concentration of the endocrine disrupting compound in water to lower level (Tsai et al., 2009).

Watthanaarun et al.(2007) studied the photocatalytic activity of methylene blue in aqueous solutions under UV/TiO$_2$ nanofibers process. TiO$_2$ nanofibers were fabricated by sol-gel and electrospinning technique. The optimum conditions include

10 ppm of methylene blue concentration, 0.14 g/L of TiO_2 concentration, 35 ± 1 ^0C temperature, and 6 h of irradiation time. The results showed the comparison of kinetic rate constants from titania fibers, titania fibers doped with 1 wt% TEOS, and titania fibers doped with 2 wt% TEOS were 0.221 h^{-1}, 0.301 h^{-1}, and 0.349 h^{-1} indicated that the presence of TiO_2 nanofibers would improve the degradation of methylene blue. Due to TiO_2 nanofibers can generate electron-hole pairs upon illumination under UV light on fibers, which they enhance to subsequently scavenge such as H_2O or OH^- led to high hydroxyl radical formation as a key for photocatalysis. In addition to dope with TEOS can prolong the electron-hole recombination associated with higher photocatalytic activity and significantly increase generation of hydroxyl radical (Watthanaarun et al., 2007).

2.9.4 Effect of TiO_2 dosage

Tsai et al. (2009) had proved the photocatalytic degradation of bisphenol-A (BPA), succeeded in a batch TiO_2 suspension reactor. The conditions were 20 mg/L of BPA concentration, 25 ^0C of temperature, pH 7, UV, 60 min irradiation time, and six TiO_2 dosages (5, 10, 30, 50, 100, 200 mg/L). They found that the destruction-removal efficiency in the slurry reaction system increased parallel to adding more TiO_2 dosage. The kinetic rate constants were into the following 200 mg/L (0.098 $\pm$ 0.006 min^{-1}) > 100 mg/L (0.081 $\pm$ 0.009 min^{-1}) > 50 mg/L (0.065 $\pm$ 0.009 min^{-1}) > 30 mg/L (0.043 $\pm$ 0.004 min^{-1}) > 10 mg/L (0.028 $\pm$ 0.001 min^{-1}) > 5 mg/L (0.021 $\pm$ 0.001 min^{-1}). Due to rising of active sites for photocatalytic reaction as increasing of photocatalyst could induce the degradation rate of BPA (Tsai et al., 2009).

Huang et al. (2013) had compared the degradation of methylene blue under UV and VUV irradiation. Numerous TiO_2 dosages (0.5, 1, 1.5, and 2 g/L) were used in photocatalytic degradation processes. The results showed that under 60 min UV/TiO_2 irradiation, removal efficiency of 0.5 g/L TiO_2 dosage was 79.6% and 98.5% from 1 g/L TiO_2 dosage. Adding more photocatalyst led to supply more active centers for photocatalytic activity of methylene blue and improve the removal efficiency. The highest removal efficiency was received from 1.5 g/L TiO_2, however; the overall degradation efficiency of 2 g/L TiO_2 dosage was not increased as prediction. It showed insignificant decline of removal efficiency since additional increase of catalyst influenced the light intensity in aqueous solution during irradiation resulting to light absorption and scattering effects. Besides, addition of TiO_2 dosage in VUV/TiO_2 was insignificant improved the photocatalytic activity compared to VUV photolysis (Huang et al., 2013).

Yixin et al. (2014) studied the degradation of atrazine under catalyzed ozonation process enhanced with TiO_2. Various TiO_2 dosage (0.1, 0.5, and 1 g/L) was determined to the effect of removal. They found that the rate constant was raised from 0.0015 to 0.0027 s-1 when extend the TiO_2 dosage from 0.1 to 1 g/L. The maximum removal rate of atrazine was 1 g/L TiO_2 dosage compared to other dosages. The removal efficiencies were more than 90% and mineralization efficiencies were rather than 50 %. The existence of TiO_2 catalyst can clearly improve the efficiency of ozonation process and accelerate the decomposition of dissolved ozone to form hydroxyls radicals (Yixin et al., 2014).

2.9.5 Removal of organic compounds by biological treatment

Malghani et al. (2009) had examined the degradation of profenofos by using biological treatment under aerobic condition with *Pseudomonas aeruginosa* OW. The results showed that this method was able to enhance profenofos degradation, which had 86.81 percent of removal efficiency within 48 h. It indicated that bacteria had ability to degrade profenofos because profenofos acting as their food (carbon source) to increase their growth and cell mass production (Malghani et al., 2009a).

Martinez et al. (1992) evaluatedthe degradation of profenofos using biological treatment with microflora microfloraincluding bacteria population, fungipopulation, dinitrogen fixer, denitrifying bacteria, and nitrifying bacteria on agricultural soilunder aerobic condition. The concentrations of profenofos (10, 50, 100, 200 and 300 μg per gram of soil were investigated to the growth of microflora, and the total soil microflora populations were count by soil dilution technique. The results showed that the total viable count of soil bacteriahad considerably increased from 596 ± 52 to 1,022 ± 55 numbers of bacteria in thousand per gram of soil at concentration 10 to 300 μg/g after 7 days that associated with microbial activity utilized profenofos as carbon source (Martínez-Toledo et al., 1992).

2.9.6 Physical treatments

Gupta et al. (2011) investigated the removal of organophosphate pesticides (methoxychlor, methyl parathion and atrazine) from wastewater in column experiment by using adsorption process that used a cabonaceous adsorbent having higher

mesopore and macropore with high surface area and suitable surface chemistry. The optimum conditions include 60 min of contact time, pH 2, 25 ^{0}C, 0.14 g/L of adsorbent dose, and 12 mg/L of initial pesticides concentration. The results revealed that the maximum removal of the methoxychlor, methyl parathion and atrazine were 91%, 71%, and 82%, respectively, and the maximum adsorption of methoxychlor, methyl parathion and atrazine were 112.0 mg g^{-1}, 88.9 mg g^{-1}and 104.9 mg g^{-1}, respectively indicated the adsorbent had ability to enhance the adsorption of pesticides (Gupta et al., 2011).

Akhtar et al. (2007) evaluated the removal of organophosphate pesticides (methyl parathion) from surface in agricultural area of Taluka Hyderabadusing adsorption process with various sorption materials. The optimum conditions include 90 min of agitation time, pH 6, 303 K, 0.14 g/L of adsorbent dose, and 10 mg/L of initial pesticides concentration. The results showed that the removal efficiencies of contaminated water sample with adsorbent from surface water were 99% ± 0.4, 99% ± 0.3, 98% ± 0.5, and 97 ± 0.5 % in rice bran (Nasrabadi et al.), bagasse fly ash (BFA), *Moringa oleifera* pods (MOP), and rice husk (RH) adsorbent, respectively. Due to high surface area and pore volume of sorbent, the removal efficiencies were also raising, indicated the sorbents had ability to perform in water contamination from industrial effluent and agricultural wastewater (Akhtar et al., 2007).

CHAPTER III

METHODOLOGY

3.1 Chemicals and Materials

Profenofos was purchased as commercial grade in form of a 50% w/v from Nonkasate Co., Ltd, Thailand, and was prepared in 18 mΩ de-ionized distilled water without further purification for photolytic and photocatalytic experiments. Methylene blue (MB) from Sigma Aldrich, Germany was used as the probe compound for hydroxyl radical measurement in the experiments. Tert-butanol (t-BuOH, TBA) was used as the •OH radical scavenger and adding at the beginning of the experiments, hence the direct photolysis of MB can be distinguished (Kutschera et al., 2009). In addition to ensure that the major degradation of MB is actually oxidized by hydroxyl radicals, produced during UV irradiation. Titanium tetraisopropoxide (TTIP, 97%)from Sigma Aldrich, Germany was used as the titanium starting material, and was used as received. Before using, it must preserve in dry for prevent moisture adsorption. Polyvinylpyrolidone (PVP, Mw ≈ 1,300,000 Da)from Sigma Aldrich, Germany was used as the polymer for titanium precursor. TiO_2 powder (Degussa, P25, nanopowder) was purchased as commercial grade from Sigma Aldrich, Germany with the BET surface of 55 m^2/g and average particle diameter of 25 nm, and was

used as received. It was used as the reference nanoparticles catalyst for photocatalytic degradation comparison. Gracial acetic acid (99.99%) from Sigma Aldrich, Germany was used as as a solvent for prepare sol-gel solution or spinning solution. Ethanol (99.99%) from Carlo Erba, France was used as a solvent for prepare sol-gel solution.

3.2 Fabrication of electrospun TiO$_2$ nanofibers

3.2.1 Spinning solution preparation

TiO$_2$ nanofibers were fabricated according to the method proposed by (Watthanaarun et al., 2007) from spinning solution by sol – gel process. To prepare spinning solution, 1.6 mL of TTIP, 3 mL of glacial acetic acid, and 3 mL of ethanol were well mixed with the magnetic stirrer. After that resting for 10 min, this mixing solution was added with 7.5 mL solution of 13 % wt of PVP in ethanol and continuously stirred in the dark for 30 min. Then, the prepared sol – gel solution was obtained, and ready to use in spinning process to produce TiO$_2$ nanofiber.

3.2.2 Spinning of TiO$_2$ nanofibers

The experimental set up for electrospun TiO$_2$ nanofibers synthesis is shown in Figure 3.1. The prepared spinning solution was subjected to electrospinning process, immediately loaded into a 10 mL plastic syringe, to which a 20 – gauge stainless steel needle (a nozzle), was attached with the syringe. A positive electrode (anode) from a Gamma High Voltage Research ES30P power supply, which can generate DC voltage

in the range of $0 - 30$ kV, was connected to a nozzle, and a negative electrode (cathode) was attached to a stationery collector plate covered by a piece of aluminum sheet. The solution was briefly electrospun at 11.25 kV and 7–cm working distance (the distance between the tip of needle and the collector). A continuous stream of charged liquid was ejected from the tip of nozzle to the collector plate, and then the solvent on the plate gradually evaporated, remaining only the ultrathin fibers on the collector plate, where nanofibers were formed. The formed nanofibers mat was left exposed to moisture in ambient condition for approximately 5 h to ensure complete hydrolysis of TTIP.
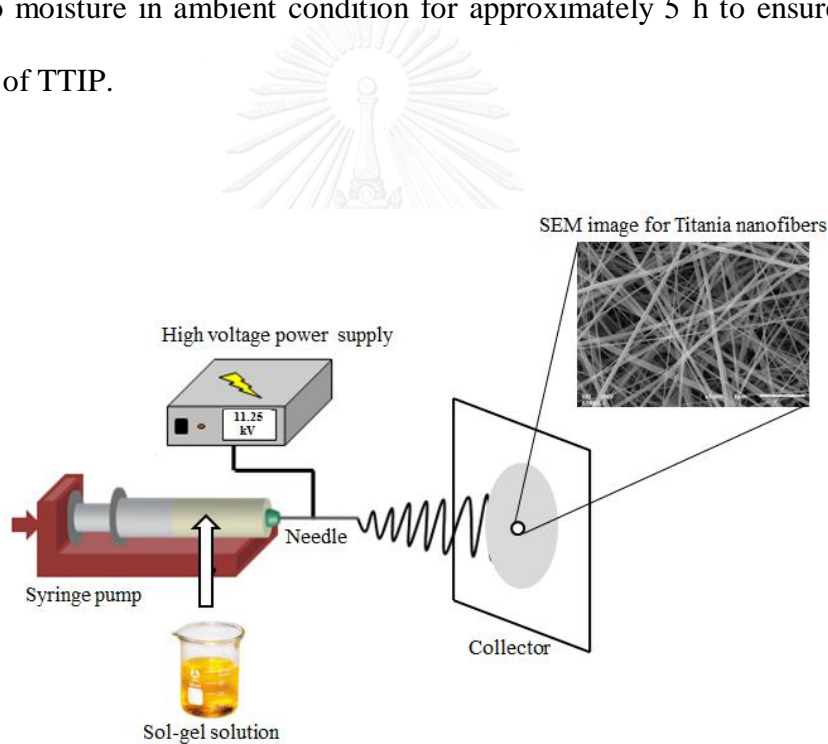
Figure 3.1 The experimental set up for electrospun TiO_2 nanofibers synthesis

3.2.3 Calcination of TiO_2 nanofibers

The obtained electrospun nanofibers were put in the step of heat treatment (calcination) at a high temperature (500 °C) for 3 h with heating rate of 10 °C/min using the box furnace to eliminate PVP residuals. After calcination, the obtained titania nanofibers were kept in an amber glass to prevent light reaction.

3.3 Reactor Set-up

The schematic diagram of the experimental system and photo of the setup for UV/VUV process are shown in Figure 3.2 and 3.3 respectively. The batch photo-reactor was a cylindrical vessel made of glass with a diameter of 50.8 mm, a length of 337 mm, and effective volume of 500 mL. For VUV photolytic experiment (no catalyst) a VUV lamp (30W/lamp, 5.22 x 10^{-4} einstein/min (light intensity), model GPH383T5/VH/HO, Universal Light Source, Inc.) was placed at the center of the photo-reactor, and immersed in the solution. The solution was mixed using magnetic stirrer (SP131320-33, Barnstead International) at 600 rpm. The light intensity of 254 nm and 185 nm from the lamp was determined by potassium ferrioxalate actinometry (Hatchard and Parker, 1956). For UV photolytic process was setup in similar like VUV process except that a UV lamp (30W/lamp, 5.15 x 10^{-4} einstein/min (light intensity), model GPH383T5/L/HO Universal Light Source, Inc.) was replaced instead. It should be noted that two types of low-pressure mercury lamp used in this work was a VUV lamp emitting at both wavelength of 185 (10%) and 254 nm (90%),

and a UV lamp that able to irradiate at wavelength of 254 nm. The reactor was covered with aluminum foil box to prevent eye exposure from irradiation.

1.Magnetic stirrer
2.Magnetic bar
3.Photo-reactor (graduated cylinder) with 500 ml of volume
4.A low pressure-Hg UV or VUV lamp
5.Sampling glass tube
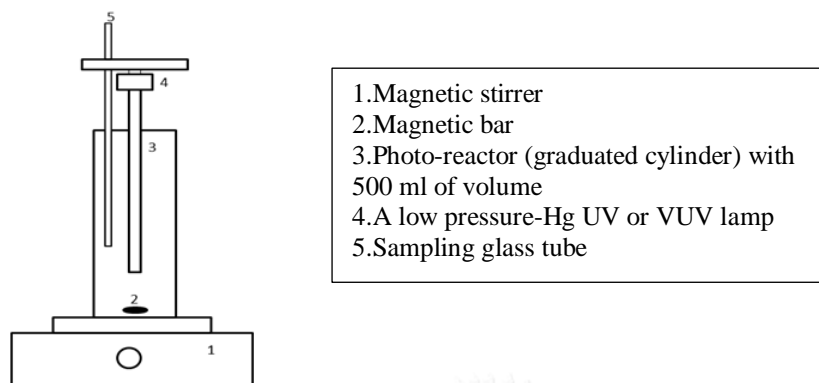
Figure 3.2 The schematic diagram of the experimental system for UV/VUV process
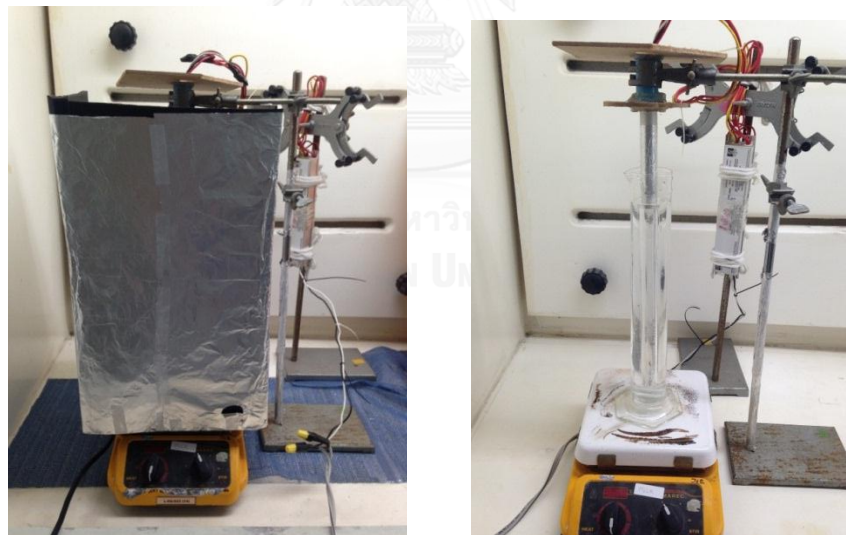
(a) Outside   (b) Inside

Figure 3.3 The experimental setup for UV/VUV process

3.4 Profenofos Degradation Experimental Procedures

The experimental procedures were divided into two parts including determination on profenofos photodegradation by UV or VUV with/without catalyst and determination on hydroxyl radical exposure on MB photodegradation.

3.4.1Photolytic and photocatalytic degradation of profenofos in aqueous solution

3.4.1.1 Profenofos solution preparation

A stock solution of profenofos was prepared by dissolving 1 mL 50% w/v profenofos into hexane with 10 mL final volume that was given 50,000 mg/L of solution, and then dilute into 18 mΩ de-ionized distilled water without further purification that was obtained 5,000 mg/L of profenofos concentration. This aqueous solution was stored in an amber glass vial at 4 °C in the dark for prevent photo-degradation. The working solutions were prepared daily from a stock solution which were diluted with DI water to obtain approximately 10 mg/L of profenofos.

3.4.1.2 Photolytic and Photocatalytic experiments

The photooxidation activities of all samples were evaluated by the degradation and mineralization of profenofos (PF) in an aqueous solution. The four different processes including UV, VUV, UV/TiO$_2$, and VUV/TiO$_2$ were studied in this work.

Before the experiment, the initial concentration of profenofos in each solution was 10 mg/L, and was adjusted pH (unbuffered) at 7 with 0.1 N HCL and 0.1 N NaOH using a pH meter (Sension2, Envi Science Co., Thailand). The profenofos solution was unbuffered owing to study the photodegradation of this target compound without other reactions with the scavengers such as bicarbonate, nitrate, natural organic matter (NOM), and so on. For each experimental run, 500 mL of profenofos solution was treated in the photoreactor. Photolytic experiment included UV and VUV processes while photocatalytic experiment refers as UV/TiO$_2$, and VUV/TiO$_2$ processes.

The photocatalytic experiment was carried out similar like photolytic process except that the system was maintained and well spread by a magnetic stirrer in the dark for 30 min to ensure that the adsorption-desorption equilibrium of profenofos on titania surface before the irradiation was completed, so that the decreased concentration of profenofos with irradiation time could fully reflect the photocatalytic activity of the catalysts. The experiments were performed by vary in electrospun TiO$_2$ nanofibers and TiO$_2$ nanoparticles (P25) concentration (0.05, 0.1, and 0.2 g/L). Reusability of the photocatalyst is determined in both photocatalytic with TiO$_2$ nanofibers and TiO$_2$ powder (P25) under the selected reaction conditions (VUV irradiation with 0.2 g/l of TiO$_2$). The catalysts were easily separated from the reaction solution by filtration throughout a sintered funnel with Nylon filter membrane (diameter = 47 mm, pore size = 0.45 μm, Pall Corporation, USA), washing with DI water, overnight drying at room temperature, and then reused without any calcination treatment (Haghighi and Nikoofar, 2014a; Gomez et al., 2015). The reusable

experiments were rerun for 10 times under room temperature and ambient atmosphere.

3.5 Determination of Hydroxyl Radical Exposure

The hydroxyl radicals involve in the reaction was measured indirectly by the determining the degradation of probe compound in which the rate constant with •OH is known. In this research, methylene blue (MB) was used as a probe compound in this study because of its high reactivity with •OH (2×10^{10} L/mol s) (Buxton et al., 1988). MB working solution was prepared with modification according to the method proposed by (Keen et al., 2012). The 0.0032 g solids of probe compound were dissolved in 1,000 mL of DI water to obtain the concentration of 10 mM. This solution was prepared fresh daily. The hydroxyl radical exposure is calculated as shown in equation (3.1) (Ratpukdi et al., 2010).

$$\int_0^t [\bullet OH] dt \ = \ \frac{(k_{obs} - k_d)t}{k_{\bullet OH,MB}} \tag{3.1}$$

Where t is the reaction time (s), $k_{\bullet OH, MB}$ is a second order reaction rate constant of MB with •OH (2×10^{10} L/(Mol s)), k_{obs} is an observed pseudo-first order removal rate of MB (s^{-1}), k_d is a pseudo-first order rate constant of MB destruction by direct photolysis (s^{-1}).

To account for the influence of direct photolysis, hydroxyl radicals must be scavenged during the experiments. The rate constant between t-BuOH and •OH is shown in equation (3.2). The MB solution was spiked by adding 20 mM of t-BuOH before the experiment.

$$\text{t-BuOH} \quad + \quad \text{•OH} \quad \rightarrow \quad \text{products} \quad k_{\text{t-BuOH}} \quad = \quad 6.0 \times 10^8 \quad \text{L/Mol} \cdot \text{s} \tag{3.2}$$

To determine MB degradation, the irradiation experiments of the four different processes including UV and VUV experiments with using various dosage of TiO_2 nanoparticles (P25) and TiO_2 nanofibers (0, 0.05, 0.1, and 0.2 g/L) were conducted in similar fashion as profenofos degradation. Five milliliter of samples was withdrawn from the reactor for MB analysisat the same time intervals as for DOC measurement (0, 2, 5, 10, 15, 20, 25 and 30 min). The aliquots were filtered through a 0.2-µm Nylon filter and kept in the amber glass at 4 °C before analysis. All the experiments were duplicated, and performed at an ambient temperature (25 ± 3 ^{0}C) and atmospheric pressure.

3.6 Analytical Methods

3.6.1. Characterization of electrospun TiO_2 nanofibers

The surface morphology and size of the as-prepared TiO_2 nanofibers were observe by a JEOL JSM scanning electron microscope (SEM). Crystalline phase of the nanofibers was identified at ambient condition by a Siemens D5000 X-Ray

diffractometer with a Cu Kα radiation that operated at a scanning rate of 0.02º/s in the 2θ range of 20 – 80 degree at the scan step of 0.04 degree, and a Raman scattering microscope (BRUKER EQUINOX 55 FRA 106/5). After that the fraction of anatase and rutile in the product were calculated (Xianzhi et al., 1996).

3.6.2 Measurement of profenofos concentrations and total organic carbon

To determine the degradation of profenofos in aqueous solution, 5 mL of aliquots were withdrawn from reactor at specific time interval of 0, 2, 5, 10, 15, 20, 25 and 30 min, and were analyzed by using gas chromatography – electron capture detection (GC – ECD, 6890N, Agilent Technologies, USA) with a column (HP-5, 19091J-413, 0.25 μm film, 0.32 mm × 30 m, Agilent Technologies, USA), as shown more detail in Appendix A. To examine the concentration of profenofos, the calibration curve should be provided by dilution to various concentrations as described in detail in Appendix A. The recovery percentage of profenofos solution extraction was 90%.

Mineralization of profenofos refers as the transformation from organic carbon to inorganic. The mineralization was measured at total organic carbon (TOC). The experiments were carried out similar to degradation of profenofos except that the specific time interval for sample withdrawal at 0, 30, 60, 90, and 120 min. The samples were analyzed in term of dissolved organic carbon (DOC) by a TOC analyzer with non-purgeable organic carbon (NPOC) (TOC-Vcph, Shimadsu, Japan). All the

experiments were duplicated, and performed at an ambient temperature ($25 \pm 3 \; ^{0}C$) and atmospheric pressure.

In this study, the removal of profenofos (PF) was calculated according to equation (3.3), and mineralization of PF was calculated with equation (3.4).

$$\text{Removal of PF} \;=\; \frac{[PF]_{initial} - [PF]_{t}}{[PF]_{initial}} \times 100\% \tag{3.3}$$

$$\text{Mineralization of PF} \;=\; \frac{TOC_{initial} - TOC_{t}}{TOC_{initial}} \times 100\% \tag{3.4}$$

Where $[PF]_{initial}$ and $[PF]_{t}$ represents the initial concentration of PF and those at time t, respectively. $TOC_{initial}$ and TOC_{t} represent the initial concentration of TOC and those at time t, respectively.

3.6.3 Measurement of MB degradation

To determine hydroxyl radicals exposure in each experimental conditions, these were done with modification according to the method proposed by (Keen et al., 2012). Aliquots of MB at specific time interval were systematically analyzed by measuring the absorbance of the solution using a UV-Visible scanning spectrophotometer (BioMate3, Thermo Electron Corporation, United States) at 664 nm wavelength. MB calibration curve was used for MB analysis in aqueous solution

in the reactor. The standard curve of MB was prepared by serial dilution to various concentrations as exactly shown in Appendix B.

CHAPTER IV

RESULTS AND DISCUSSION

4.1 Physical Properties of the As-spun Titanium Dioxide Nanofibers

The as-spun titanium dioxide nanofibers were prepared from electrospinning technique and sol-gel process. The spinning solution was ejected as the jet and the ultrathin fibers deposited as a non-woven mat on the collector plate by 11.25 kV of power supply electric field strengths. Upon exposure to the ambient moisture, hydrolysis and condensation of TTIP within the fibers took place, resulting in the formation of TiO_2/PVP composite fibers. The obtained fibers were calcined at 500 ℃ within 3 h for change the crystalline phase of titania nanofibers into anatase phase, and without calcination, the crystallinity and titania content of nanofibers could not be transformed from orthorhombic phase to amorphous phase. The nanofiber was characterized for morphology and crystal structure as described in section 4.1.1 and 4.1.2, respectively.

4.1.1 Surface morphology analysis

The surface morphology of the nanofibers was observed by a JEOL JSM 5800 Scanning Electron Microscope (SEM). It should be noted that the diameter size of the nanofibers were calculated by the SEM digital image analysis software (JEOL SemAfore 5.21). Figure 4.1 shows SEM images of Degussa-P25 and the TiO_2/PVP composite nanofibers before and after calcination at 500 ℃. The commercial titania nanoparticles, Degussa-P25 was also presented for comparison. Apparently, the Degussa-P25 had greater uniformity than the obtained nanofibers, which displayed the nanogranular on their surface, as displayed in Figure 4.1 (a). It is seen from Figure 4.1 (b) that the surface of the as-spun nanofibers was smooth surface continuous, and beads-free. In contrast, the morphology of the as-calcined TiO_2/PVP composite nanofibers had more surface roughness, more distorted and composed of connected crystalline TiO_2 nanoparticles, as shown in Figure 4.1(c). The size distributions of diameter of the TiO_2/PVP composite nanofibers before and after calcination at 500 ℃ are shown in Figure 4.2 (a) and (b).The average diameter of the obtained fibers was calculated from 55 fibers randomly selected from several locations in a sample. The resulted exhibited that diameter of the as-spun nanofibers were in the range from 100 to 550 nm (approximate diameters = 233 nm), and diameter of the as-calcined nanofibers were in the range from 40 to 350 nm (approximate diameters = 141 nm) with narrower distribution. It revealed that the as-calcined fibers' diameter had smaller that the as-spun fibers. Due to the shrinkage caused mainly by the complete removal of PVP matrix, organic content, residual solvent, and development of titania crystalline during calcination process, it was resulted to reduction in average diameter

size of fibers (Xia, 2003; Watthanaarun et al., 2007). Furthermore, the as-calcined nanofibers had maintained the surface of fibers with polymorphic structures, and the particle morphology had readjusted to a fiber, which was interconnected with crystallites or particles. The raw data of the TiO_2/PVP composite nanofibers diameters are presented in Appendix H.
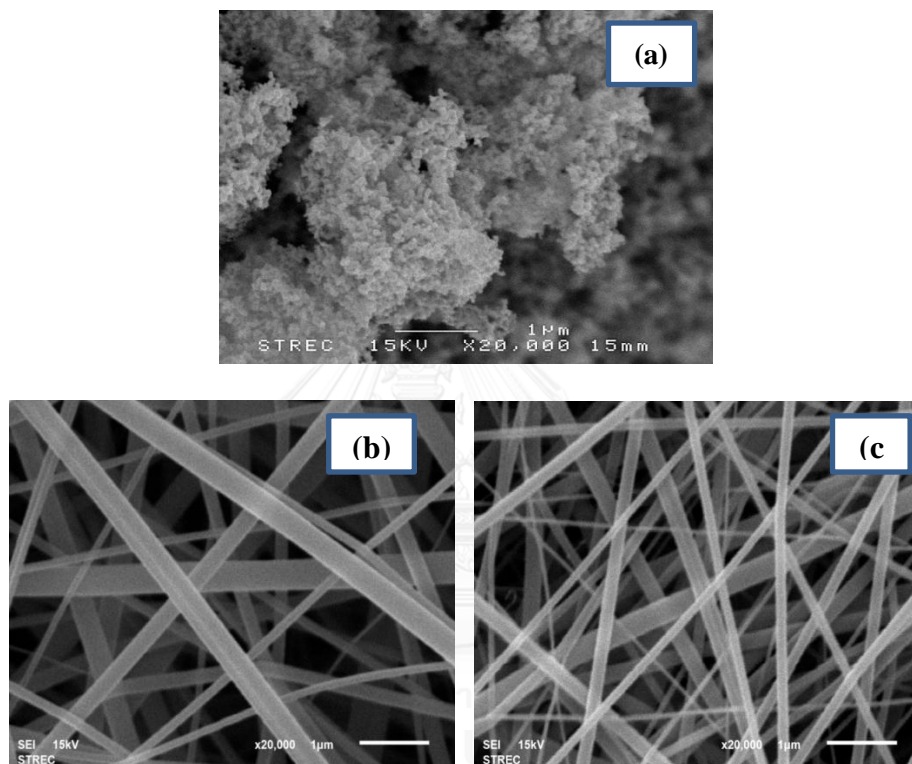
Figure 4.1 SEM images of the TiO_2/PVP composite materials (a) the commercial titania nanoparticles (P25) for comparison (b) as-spun fibers (c) as-calcined fibers at 500 ºC
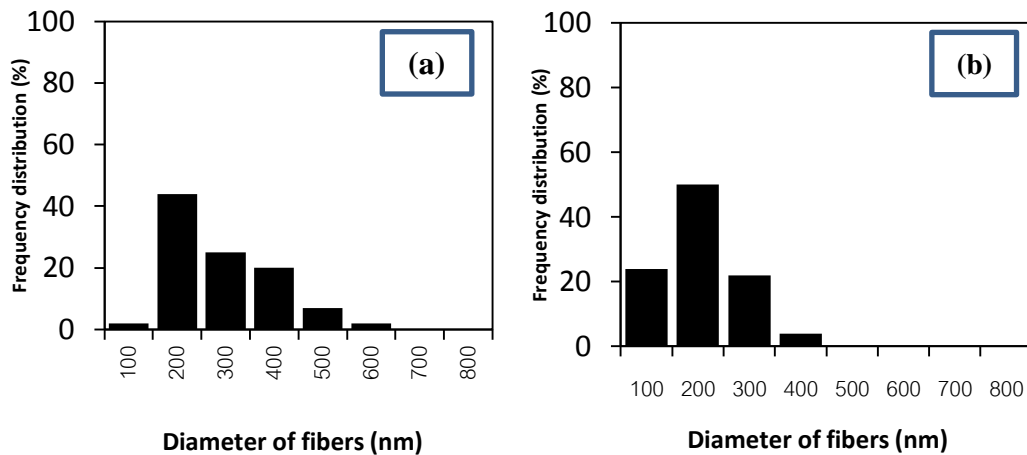
Figure 4.2 The distribution of diameter of the TiO$_2$/PVP composite nanofibers (a) as-spun fibers (b) as-calcined fibers at 500 ℃

4.1.2 Crystalline phase analysis

The chemical configuration and crystalline phase in the structure of titania had been characterized with the X-ray diffraction (XRD) analysis. The XRD patterns of the TiO$_2$/PVP composite nanofibers before and after calcination at 500 ℃ is presented in Figure 4.3. For comparison, the XRD pattern of the commercial titania nanoparticles, Degussa-P25 was also analyzed. The reflection peak at diffraction angles (2θ) of 25.28º and 27.41º perform as the crystal plane of anatase (1 0 1) and rutile (1 1 0). It should be note that the Scherrer formula as shown in equation (4.1) is used to calculated the crystalline size of anatase, rutile, and brookite crystal from the sharp peak of 2θ intensity (Scherrer, 1918).

$$D = \frac{K\lambda}{\beta cos\theta} \qquad (4.1)$$

Where D is the mean size of crystalline domains, λ is the X-radiation wavelength characteristic of the Cu Kα radiation ($\lambda = 0.154$ nm), β is the full width at half the maximum intensity of the crystalline peak (anatase, rutile, and brookite peak) that received from the XRD pattern (radians), K is the Scherrer constant (can be assumed to be 0.94, dimensionless), and θ is the reflecting angle (radians). Furthermore, the proportion of anatase and rutile can be quantified from equation (4.2) – (4.3) (Jung and Park, 2003), using the integrated intensities of the anatase (1 0 1), and rutile (1 1 0) peaks acquired from the XRD pattern in Figure 4.3.

$$W_A = \frac{K_A A_A}{K_A A_A + A_R + K_B A_B} \qquad (4.2)$$

$$W_R = \frac{A_R}{K_A A_A + A_R + K_B A_B} \qquad (4.3)$$

where W_A, W_R, W_B serve as the weight fractions of the anatase, rutile, and brookite peaks, respectively. A_A, A_R, A_B represents the integrated intensities of the anatase, rutile, and brookite peaks, respectively. K_A and K_B are the coefficient constants with value 0.886 and 2.721, respectively (Putta, 2009b). Thus, the crystalline sizes of the obtained titania nanofibers and the percentage of anatase and rutile in this study were summarized in Table 4.1.

Table 4.1 The crystalline size and percentage of crystal phase in TiO_2 nanofibers

Titania sample	Anatase		Rutile	
	%Anatase	Crystalline size (nm)	% Rutile	Crystalline size (nm)
As-calcined nanofibers at 500 ℃	64.32	56.8	35.68	57.7
Degussa-P25	82.52	42.8	17.48	48.3

Figure 4.3 shows the comparison of the XRD patterns from the as-calcined TiO_2/PVP nanofibers after heated up to high temperature for 3 h and the commercial TiO_2 nanoparticles, Degussa-P25. As shown in Figure 4.3 (a), it was found that the anatase peak intensity of Degussa-P25 had sharper and narrower peak at 2θ of 25.28° than the post-calcined obtained fibers, and was composed of a mixture of rutile and anatase phase with having crystalline size of 48.3 nm and 42.8 nm, respectively. As shown in Figure 4.3 (b), the XRD pattern of the as-calcined TiO_2/PVP nanofibers after heated up to high temperature for 3 h had a dominant reflection peak at 2θ of 25.28° with the crystalline size of 56.8 nm, and lesser rutile reflection peak at 2θ of 27.41° (57.7 nm). It was revealed that anatase peak intensity of these nanofibers had lower than anatase peak of Degussa-P25, and also apparently obtained the main anatase crystalline phase with the less amount grain of rutile phase. This is due to the hydrothermal process (calcination) which easily motivates the transformation of crystalline phase from the low orthorhombic crystal system and almost entirely amorphous to anatase phase in the titania nanofibers with high crystallinity and

orthorhombic crystalline system (Lai et al., 2008; Mahata and Kundu, 2009). Furthermore, hydrothermal treatment also induced the increment of anatase crystalline size, indicating that the nanocrystallines on the surface of titania fibers could be agglomerated to the larger grains, related to surface properties adjustment, particle morphology distortion and raise the crystallinity(Watthanaarun, 2004; Putta, 2009b). Surprisingly, the as-calcined fibers also restrained 64.32% of anatase phase proportion, which was rather than the as-spun fibers due to the same reasons, and also had no significant broadening and shift in anatase peak position were noticed after calcination.
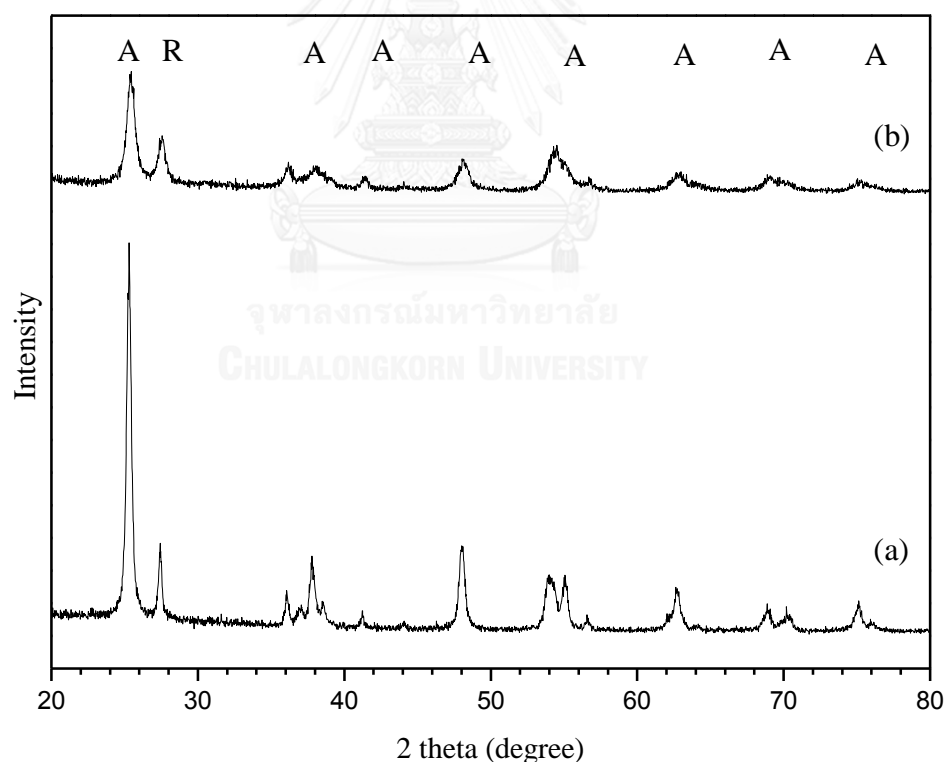
Figure 4.3 XRD spectra of the TiO_2/PVP (a) the commercial TiO_2nanoparticles,

Degussa-P25, (b) the as-calcined nanofibers .A and R represents the crystal plane of

anatase and rutile, respectively.

4.2 Profenofos degradation by UV, UV-TiO_2, VUV, and VUV-TiO_2

4.2.1 UV and VUV processes

The photodegradation of profenofos ($[PF]_0 = 10$ mg/L) was examined in unbuffed aqueous solution (pH = 7, T = 25 ºC $\pm$ 3, deionized water) under UV or VUV irradiation within 30 min is shown in Figure 4.4.
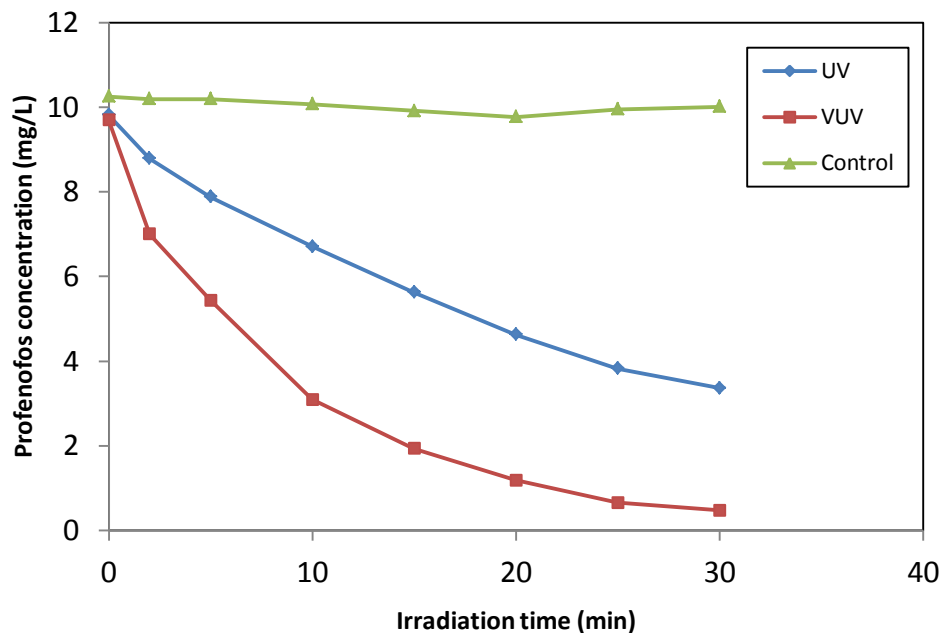
Figure 4.4 Profenofos degradation by UV and VUV

Both UV and VUV conditions showed the similar trend in that profenofos concentration was decreased with increase the course of irradiation time. Profenofos concentration gradually decreased from 10 mg/L to 0.47 mg/L (almost degraded) within 30 min by VUV process while the concentration of profenofos found in a UV process had steadily declined to 3.36 mg/L (incomplete degraded) within the same period of irradiation time. The removal efficiency of profenofos by the VUV system had gradually increased as increasing reaction time and reached to the highest removal efficiency approximately 95% while the UV system had steadily increased and obtained maximum of removal efficiency to nearly 66%. Similar results from Huang and coworkers (2013) were reported that the highest degradation efficiency of methylene blue (approximately 90%) was done by a VUV system, and the UV trend did not change higher than 10% within 30 light illumination, showing that UV photolysis can be ignored. Although both methylene blue and profenofos had differed adsorption coefficiency at 254 nm wavelength that were approximately 18,000 M^{-1} cm^{-1} (methylene blue) and 460 ± 30 M^{-1} cm^{-1} at 254 nm (profenofos), UV seemed to be an important pathway for decomposition of pollutants in aqueous solution (Heit and Braun, 1997; Miloševic et al., 2013).

The control experiment of profenofos degradation was also investigated in this research study. The results found that it had a constant linear graph, indicating that no change in profenofos concentration with in the time scale of the experiments in the absence of light. It could be observed that profenofos hardly decomposed with other chemical reactions such as hydrolysis, and it was clearly that decreasing of this target pollutant in this study resulted from photooxidation from UV or VUV radiation.

The degradation rates of profenofos in aqueous solution using the UV and VUV processes, which were homogeneous reaction, were also investigated in this study. As the kinetic rate can predict the efficiency of photoreactor system, it is very useful to search the simple and user-friendly rate equation fitting to the experimental data. According to the chemical kinetic theory (Fu et al., 2006), the kinetic rates in photolytic and photocatalytic degradation of profenofos (r, mg/(L•min)) can be described by pseudo-first order kinetic model and given a positive relationship, as expressed in equation (4.4).

$$-\frac{d[PF]}{dt} = k_{obs}[PF] \Rightarrow \int_{PF_0}^{PF_t} \frac{1}{[PF]}\, d[PF]$$

$$= -k_{obs} \int_{t_0}^{t} dt \Rightarrow \ln\frac{[PF]}{[PF]_0} = -k_{obs}(t) \quad (4.4)$$

where k_{obs} was the observed pseudo-first order reaction kinetic rate constant of initial degradation (min^{-1}), $[PF]_0$ was the initial concentration of profenofos at time = 0 min (10 mg/L), $[PF]$ was the concentration of profenofos at time = t min, and t was the irradiation time (min). Thus, the rate constants can be obtained from slope of the graph plotted between $\ln(C_0/C_t)$ and irradiation time.

The observed kinetic rate constant of profenofos degradation by UV and VUV processes was determined by Figure 4.5. The fitting results showed that the kinetic rates of profenofos were followed first order kinetic model since these two trends

were giving a positive linear relationship between $\ln(C_0/C_t)$ and irradiation time during entire experiment. Thus, profenofos photodegradation could be described using this kinetic model. These finding were the same as demonstraed by Zamy and coworkers (2004) that confirmed the first order kinetic model photolysis of profenofous in aqueous solution. The VUV process had higher overall kinetic rate constant than that of UV process ((0.1049 min^{-1} versus 0.0374 min^{-1}). This result has similar trend as to Prasertwongchai (2011) that the kinetic rate constant by VUV and UV photolysis were 0.141 min^{-1} and 0.043 min^{-1}, respectively for removal 8.5 mg/L of profenofos in aqueous solution. It can be implyed that profenofos could be decomposed more slowly under UV irradiation, and the photon energy from UV light irradiation had influenzed to slow the rate reaction and efficiency of profenofos degradation. Moreover, Zoschke et al. (2014) also that VUV process has more degradation rate than UV process.
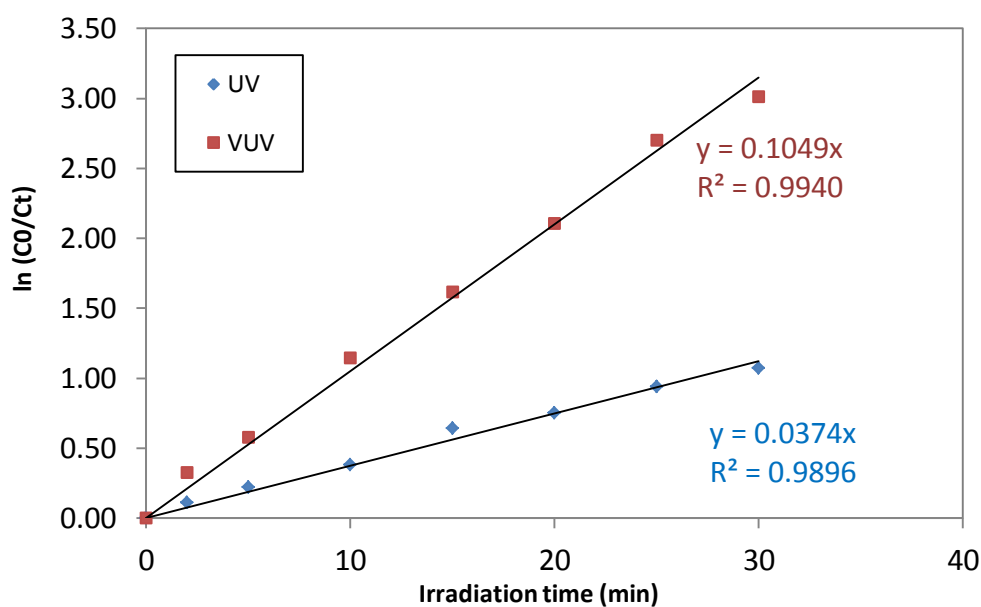
Figure 4.5 Plot of $\ln C_0/C_t$ of profenofos concentration by UV and VUV

The direct photolytic degradation of profenofos under UV – C was happened because UV – C can emitted at 254 nm wavelength that is the period of light wavelength to induce absorbtion spectra of profenofos in aqueous solution, causing the electrons in profenofos molecules going up to the excited state (not stable) bring about to easily breaking down its bond, as seen the reaction in equation (4.5):

$$\text{profenofos} \ + \ hv \ (\lambda \leq 254 \, \text{nm}) \ \rightarrow \ \text{profenofos} \bullet \qquad (4.5)$$
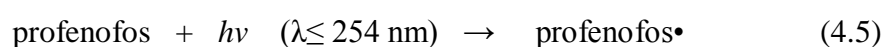
Since profenofos has high molar absorption coefficients ($460 \pm 30 \, \text{M}^{-1}\text{cm}^{-1}$) at 254 nm (Heit et al., 1998), it is capable to be decomposed in this period with appropriate energy photon. Thus, the UV light irradiation has ability to transform absorbing profenofos to profenofos radicals (product). This can be confirmed by the results from profenofos concentration and removal efficiency in this research study, having moderate efficiency. However, its photodegradation obviously exhibited less degradation efficiency compared to VUV process. This was resulted from VUV lamp can emit both 254 nm photons and the additional photons of 185 nm wavelengths.

The 185 nm photon light has significantly higher photon energy of irradiation at E = 6.7 eV than a UV light irradiation (254 nm) at E = 4.9 eV so that profenofos degradation might be excited by both UV and VUV photon energy. However the photolysis of the target pollutant is not mainly pathway for profenofos removal, only 5% of 185 nm wavelength can emit in VUV system. Kang and coworkers (2011) reported that VUV can break most of the chemical bonds of pollutants' structure since it has higher energy than the bond energy of the chemicals because the energy of VUV has

larger than the bond energy of absolute majority such as C – H except to C = O (7.6 eV), and C ≡ C (8.4 eV), and significantly transformed the hydrophobic fractions of pollutant into lower molecular weight hydrophilic charged and hydrophilic neutral fractions (Arany et al. (2013). Additionally, the water molecules can strongly absorb light at $\lambda<$ 190 nm, 90% of the initial VUV incident light within a few millimeter depth (ϵ = 0.03135 M-1 cm^{-1}) that led to increase water photolysis with a quantum yield = 0.33 eV to form the strong oxidant, especially hydroxyl radical more than happening from UV incident light (equation 4.6) (Kang et al., 2011; MingMa et al., 2011; Cordeiro et al., 2013).

$$H_2O \quad + hv \quad (\lambda< 190 \text{ nm}) \quad \rightarrow \quad H\bullet \ + \ \bullet OH \quad\quad (4.6)$$

These hydroxyl radicals can randomly (non-selective) oxidize with the contaminants during entire of experimental time causing the broken down of the target compound bonding that could get more degradable profenofos in the solution, as expressed in equation (4.7).

$$\bullet OH \quad + \quad \text{profenofos} \quad \rightarrow \quad \text{products} \quad\quad (4.7)$$

Therefore, the combined irradiations of these two wavelength (from 90% of 254 nm and 10 % from 185 nm) be more powerful than UV process (Arany et al., 2013), as shown the mechanism for organic decomposition using a VUV process in Figure 4.6.
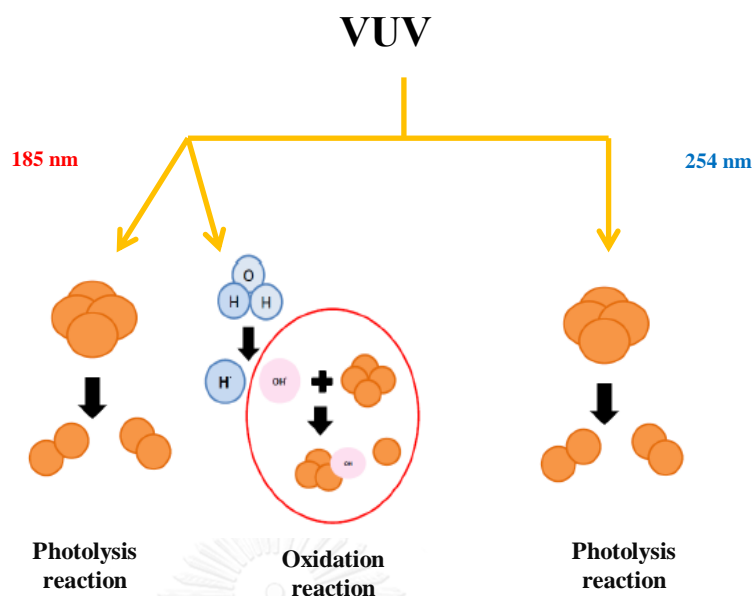
Figure 4.6 The mechanism for organic decomposition using a VUV process
(Chunhapimol, 2013)

Interestingly, it can be observed that pH of profenofos solution being irradiated gradually declined from pH 7 (neutral) to nearly 5 (weak acid) in both UV and VUV processes. Since pH of the solution including acidic and base condition would have to be taken into an account for reaction under photolysis of pure liquid water because hydrolysis of target compound might considerably influence to the kinetic rate reaction and mechanism of degradation (Farhataziz and Rodgers, 1987). Griffin (1999) had been reported that hydrolysis of profenofos followed first order kinetic model (as shown in equation (4.8) – (4.11)), dependent on pH and its half-life ($t_{1/2}$) in acid, base and neutral condition. At pH = 5 and 7, its half-life were 93 days (133,920 min) and 14.6 days (21,024 min), respectively. Hence, hydrolytic rate constant (k) at any pH can be easily calculated from equation (4.11) as follows.

$$[A] \; = \; \frac{1}{2}[A]_0 \tag{4.8}$$

$$\frac{[A]_{1/2}}{[A]_0} \; = \; \frac{1}{2} \; = \; e^{-k\,t1/2} \tag{4.9}$$

$$\ln 0.5 \; = \; -kt \tag{4.10}$$

$$t_{\frac{1}{2}} \; = \; \frac{ln2}{k} \; \sim \; \frac{0.693}{k} \tag{4.11}$$

The results show that hydrolytic kinetic rate constant of profenofos in pH 5 and 7 were 5.17×10^{-6} min^{-1} and 3.30×10^{-5} min^{-1}, respectively. And the first order kinetic rate constants of profenofos decomposition from UV and VUV processes were 0.0358 min^{-1} and 0.1010 min^{-1}, respectively. It can be observed that the degradation rate constant from hydrolysis was too small and could be neglected. Therefore, it could not affect to the overall oxidation reaction of the experiments. Similar results were found for dichorvos (an organophosphate pesticide), Suter (1981) declared that hydrolysis of this compound might be low under acidic and neutral condition, and mostly significantly increased when pH was at alkaline condition. Moreover, it was found that the solution's temperature from photolysis processes had gradually change from 25 ºC ± 3 to 35 ºC ± 3 during the course of experiment. In addition, the temperature is one of the factors can affect to the rate of reactions happening at around room temperature. Clark (2002) recommended that the rate of reaction might be speed up for every 10 ºC rise in temperature because this could

increase the collision frequency of particles in the solutions to move faster and more frequent. It could imply that rising of temperature was able to minimize the activation energy for the reaction. Although this study was performed at room temperature at the beginning of the experiment and the solution's temperature (resulted from a heating lamp) at the end of experiment had approximately increased to 10ºC, the period of this high temperature had considerably short period as we could observe that degradation of pollutants had slightly declined. In contrast, it could be seen that profenofos concentration had significantly dropped within the first period of light radiation that was affected to the overall kinetic rate reaction. Thus, the effect of temperature might influence to the kinetic rate in very less amount. This result was agreement with Leifer (1988) that temperature usually had less impact on photochemical processes in photolysis of chemicals and the rate constant slightly increased with raising temperature, and the molar absorption of the intermediates and their decays at various temperatures does not change the rate constants (Einschlag et al. (1997)).

4.2.2 UV/TiO$_2$ and VUV/TiO$_2$ processes

The photocatalysis of profenofos ([PF]$_0$ = 10 mg/L) was also investigated in an unbuffed aqueous solution (pH = 7, T = 25 ºC ± 3, DI water) by UV/TiO$_2$ or VUV/TiO$_2$ with the presence of 0.20 g/L of TiO$_2$ (both synthesized titania fibers and P25) in its raw form, as same condition as demonstrate in photolysis processes. P25 nanoparticles were used as received and TiO$_2$ nanofibers were utilized in flake form, which the mat of as-calcined titania fibers would be broken down into small pieces and suspended in the reactor for photocatalytic activity. The photocatalytic

degradation of profenofos using UV/TiO$_2$ and VUV/TiO$_2$ with nanoparticles (P25) and nanofibers was shown in Figure 4.7.
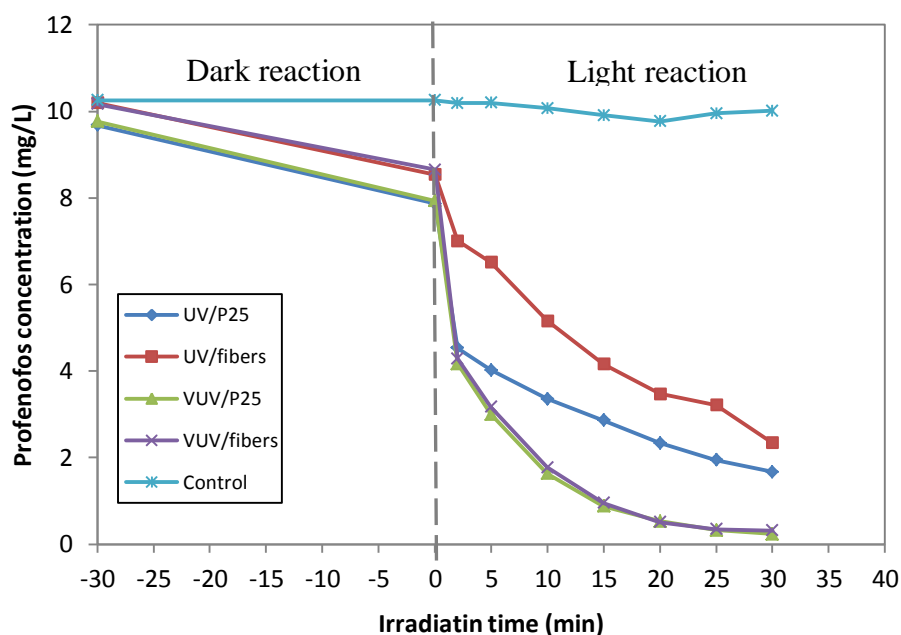
Figure 4.7 Photocatalytic degradation of profenofos using UV/TiO$_2$ and VUV/TiO$_2$ with nanoparticles (P25) and nanofibers

The results revealed that the initial concentration of profenofos has slightly declined from 10 mg/L to approximately 8.5 mg/L (for nanofibers) and around 8 mg/L (for P25) after impending completely adsorption equilibrium on the surface of 0.20 g/L photocatalyst in the dark within 30 min prior to irradiation in these four processes including UV/P25, UV/fibers, VUV/P25, and VUV/fibers. It revealed that the adsorbtion of profenofos with TiO$_2$ nanocatalyst (both P25 and fibers) could not be neglected, and adsorbtion - equilibration between solid surface area and aqueous phase (main absorber) could influence the degradation efficiency of profenofos. The adsorption of profenofos in

solution containing P25 and fibers were not equal. This was resulted from absorption ability onto titania surface area that the commercial P25 nanoparticles (with BET surface specific area $= 56$ m^2/g) had slightly greater absorption ability than the synthesized TiO_2 nanofibers (with BET surface specific area $= 50$ m^2/g, as demonstrated by previous study (Watthanaarun et al., 2007)). This results was consistent with the research of Yin and coworkers (2003), they found that photocatalytic of the target contaminant (ozone) with the synthesized titania had slightly less destruction capacity and absorption ability than P25. Xianzhi and coworkers (1996) recommended that more absorption on the active site of photocatalyst, where photocatalytic reaction can occur, could improve the photodegradation of the contaminants. The important factor which influenced its adsorption may be the hydrophobicity of profenofos on the hydrated TiO_2 nanocatalyst surface in aqueous solution due to the chemisorption of water molecules at the lattice titanium ion site on its surface causes the hydration of TiO_2 nanocatalyst (Yixin et al., 2014). For VUV/TiO2 photocatalytic process, profenofos degradation of both P25 and nanofibers had similar trend in that profenofos concentration dropped from 10 mg/L to 0.24 and 0.32 mg/L (almost complete degradation), respectively. However, the trends of profenofos removal in UV/TiO_2 photocatalysis had obviously differed between P25 and fibers. Profenofos concentration treated by UV/P25 had steadily fallen from 10 to 1.67 mg/L whereas the maximum to degrade in UV/fibers had significantly reached 2.34 mg/L. These results showed that the photocatalytic system with UV radiation using both Degussa-P25 and nanofibers could not decompose this target pollutant completely within 30 min light illumination because the quantum yield of hydroxyl radicals from UV/catalyst system was not enough for oxidizing and degrading all profenofos molecules. Preliminary evaluations for control experiment revealed that

inconsiderably changed of profenofos concentration in dark reaction (absence of UV light). The removal efficiency of profenofos using photocatalytic processes both P25 and nanofibers for 30 min UV and VUV irradiation showed that VUV/nanocatalyst (98%) obtained higher removal efficiency than UV/nanocatalyst (88%), and both P25 and nanofibers seemed to obtain similar result. This might be from the structures of nanofibers that has less surface area than P25 nanoparticles. Similar results found in the research of Huang and coworkers (2015), they exhibited that photocatalytic degradation of contaminant (benzene) using P25 nanoparticles was slightly greater than the synthesized titania due to its surface area.

The kinetic rates of photocatalytic degradation for various compounds typically followed the Langmuir-Hinshelwood kinetic model (heterogeneous reaction) that differs to the kinetic rate for photolytic degradation (homogeneous reaction) that is first-order reaction. The reaction rate of Langmuir-Hinshelwood kinetic model is proportional to the surface coverage (θ) and evolves into corresponding to the target compound concentration (Pruden and Ollis, 1983; Ollis, 1985). However, this model can be also simplified to pseudo-first order reaction at very low concentration (mg/L) according to equation (4.11) – (4.14).

$$r \ = \ \frac{dC}{dt} \ = k\theta \ = \ \frac{kKC}{1+KC} \tag{4.12}$$

At low concentration (mg/L) (KC << 1),

$$r = kKC \tag{4.13}$$

$$r = ln\frac{Co}{Ct} = k_{obs}C \tag{4.14}$$

where r is kinetic rate reaction, k_{obs} is the observed pseudo-first order reaction kinetic rate constant of initial degradation (min^{-1}), C_0 was the initial concentration offor adsorption onto the surace area of titania compound at time = 0 min, C_t was the concentration of compoundat time = t min, K is the equilibrium constant. Hence, $k_{obs}$for entire experiment could be determined from the slope of graph fitting between $ln(C_0/C_t)$ and irradiation time, as seen in Figure 4.8 and Table 4.2.
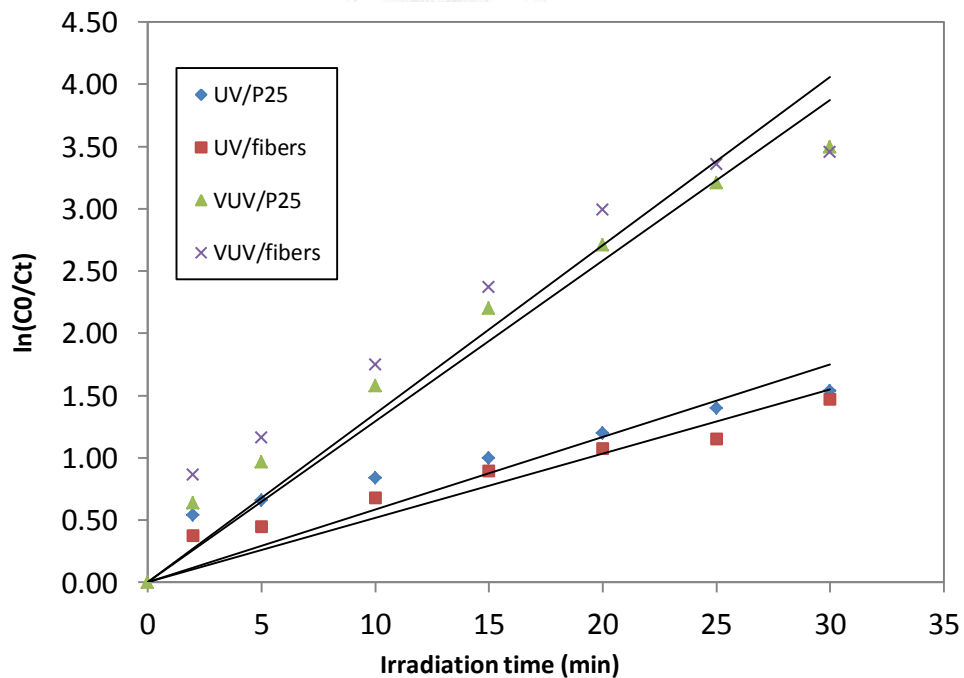
Figure 4.8 The kinetic rate of profenofos degradation from various photocatalysis processes

Table 4.2 Kinetic rate constants of profenofos degradation from each AOPs experimental condition

Type of AOPs	Kinetic rate constant (min^{-1})	R-square
UV/P25	0.0584	0.7473
UV/fibers	0.0517	0.8886
VUV/P25	0.1353	0.8825
VUV/fibers	0.1292	0.9499

Figure 4.8 shows that decomposition of profenofos by photocatalytic processes (heterogeneous reaction) both nanoparticles and nanofiber followed the pseudo-first order kinetic model (Petrick et al., 2013). The observed pseudo-first order kinetic rates for whole experimental time (30 min) were ordered as follows: VUV/P25 > VUV/fibers > UV/P25 > UV/fibers. The highest kinetic rate of profenofos removal was 0.1353 min^{-1} by the VUV/P25 process, whereas the maximum kinetic rate of the UV/fibers process was relatively 0.0517 min^{-1}. It should be noted that the obtained kinetic rates from P25 and electrospun nanofiber were not much different for both UV and VUV part. However, the titania nanofiber has more advantage over P25. The titania nanofibers in flake form was no trouble to manage and easily separated than using P25 nanoparticles. This results was consistent with Doh and coworkers (2008) who investigated the degradation of 10 mg/L of dye under 10W- UV illumination with using nanoparticles and electrospun nanofibers. They found that the photocatalytic degradation capability with nanoparticles was slightly greater than the fibers because these nanoparticles had inconsiderably titania surface area that had more pollutants absorbed on catalyst's surface (more photocatalysis reaction area) than fibers.

Profenofos degradation by photocatalytic process can be from the synergistic effect of the incident light irradiation and the photocatalyst initiated by photoexcitaion of the semiconductor (TiO_2). Since the photoexcitation of TiO_2 may bring about the production of a pair of conduction band electrons (e_{CB}^-) and valence band holes (h_{VB}^+) on the surface of semiconductor catalyst (Rongchang et al., 2009; Huang et al., 2013) from equation (4.15):

$$TiO_2 \; + \; h\nu \; \rightarrow \; TiO_2 \; + \; e_{CB}^- \; + h_{VB}^+ \qquad\qquad (4.15)$$

The high oxidation potential of the holes is responsible for oxidation of organic compound to degradation product as shown in equation (4.16):

$$h_{VB}^+ + \text{pollutant} \; \rightarrow \; \text{pollutant}^{\bullet+} \rightarrow \text{degradation of pollutant} \qquad (4.16)$$

Hydroxyl radical is the strong oxidant and non-selective that can allow the degradation and mineralization of the pollutant (Neshvar et al., 2004; Behnajady et al., 2006). During UV/TiO2 and VUV/TiO2 processes, hydroxyl radicals on the catalyst surface can be generated from photolysis of water or by the reaction with the holes interacting with OH^- as shown in equation (4.17) – (4.18):

$$h_{VB}^+ + H_2O \; \rightarrow \; \bullet OH \; + \; H^+ \qquad\qquad (4.17)$$

$$h_{VB}^+ + \; OH^- \rightarrow \bullet OH \qquad\qquad (4.18)$$
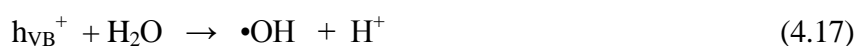
Furthermore, the conduction band electrons (e_{CB}^-) on catalyst surface are capable to reduce oxygen to form the superoxide anions, which can produce the hydroxyl radicals (Naeem and Ouyang, 2013), as displayed in equation (4.19) – (4.21):

$$e_{CB}^- + O_2 \rightarrow O_2^{\bullet -} \quad (4.19)$$

$$2O_2^{\bullet -} + 2\,H_2O \rightarrow 2\bullet OH + 2\,OH^- + O_2 \quad (4.20)$$

$$\bullet OH + \text{pollutant} \rightarrow \text{degradation products} \quad (4.21)$$
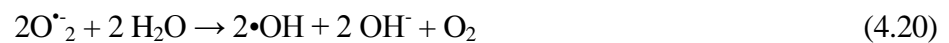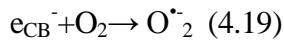
The overall mechanism of heterogeneous photocatalysis on the semiconductor catalyst surface after photo-excited by light illumination is shown in Figure 4.11.
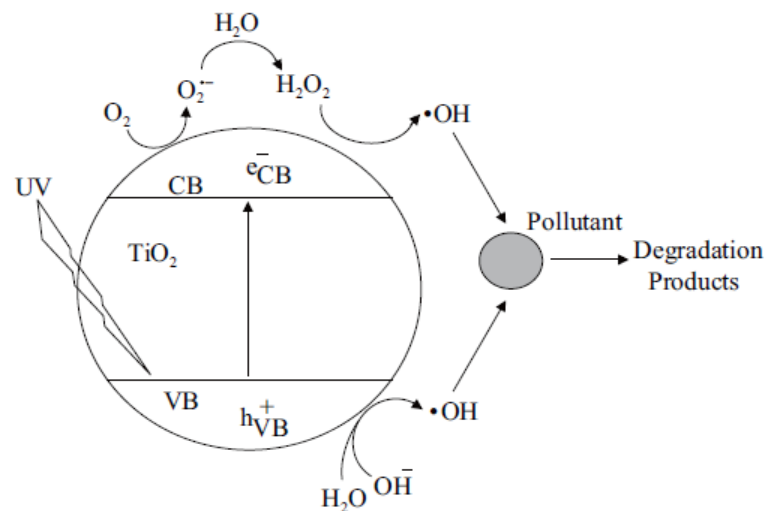
Figure 4.9 The processes occurring on bare TiO_2 particles after UV excitation
(Naeem and Ouyang, 2013)

4.3 Effect of TiO₂ Dosage to the Efficiency of Profenofos Degradation

As the catalyst concentration was an essential factor for photoreactor efficiency and operating cost. Thus, photodegradation of profenofos (10 mg/L) in aqueous solutions irradiated in 30 min in the presence (heterogeneous reaction) and absence (homogeneous reaction) of TiO_2 (both P25 and nanofibers) had been investigated under four different dosages including 0, 0.05, 0.10, and 0.20 g/L. It should be noted that the photocatalyst must be stirred in the absence of light 30 min before light illumination for absorption-desorption equilibrium onto its surface area, where the photocatalytic can be directly happened. The effects of TiO_2 nanocatalyst dosage on photodegradation of profenofos under VUV and UV radiation with P25 and synthesized nanofibers were illustrated in Figure 4.10 to Figure 4.13 (more details in Appendix C).
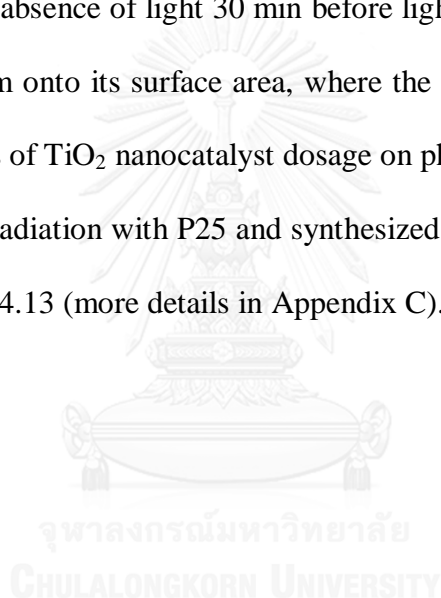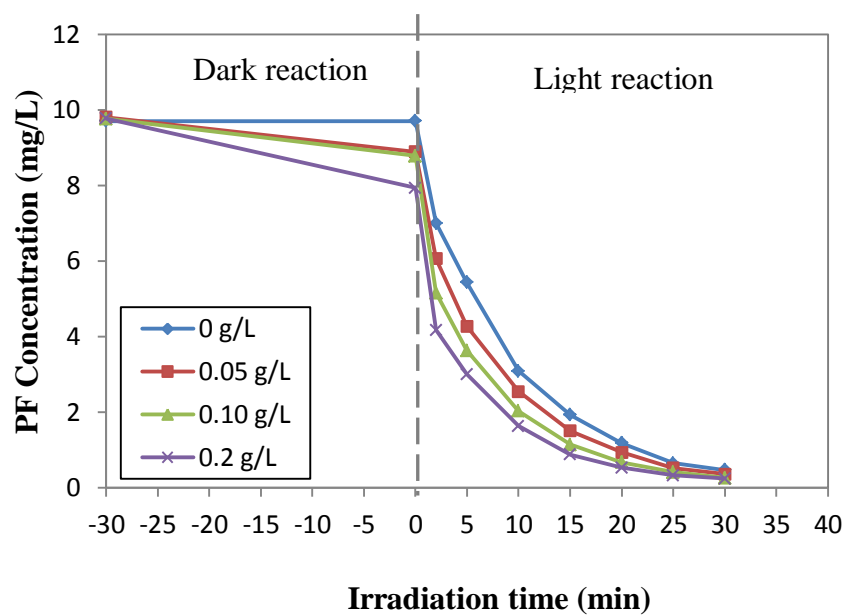
(a) P25 nanoparticles
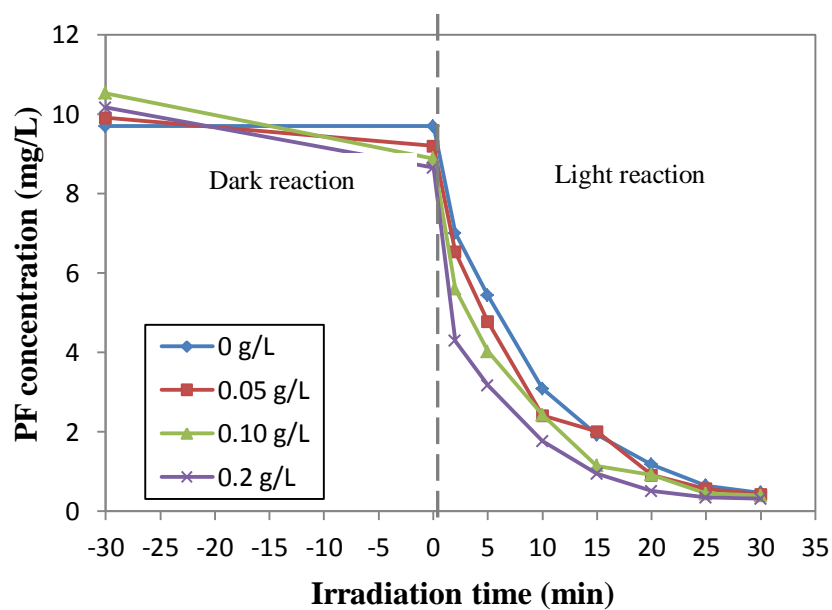
(b) Synthesized electrospun TiO₂ nanofibers

Figure 4.10 The effects of TiO_2 nanocatalyst dosage on photodegradation of profenofos under VUV radiation
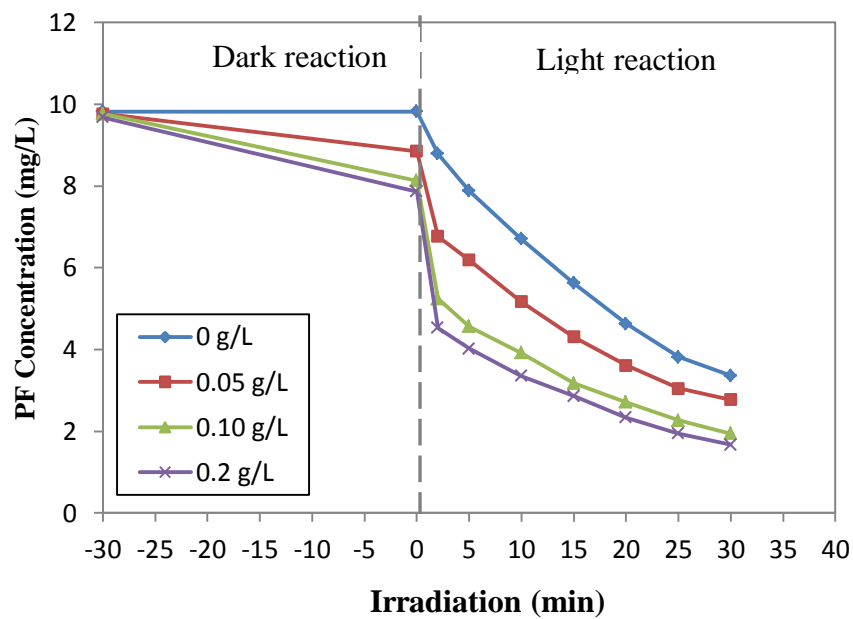
(a) P25 nanoparticles
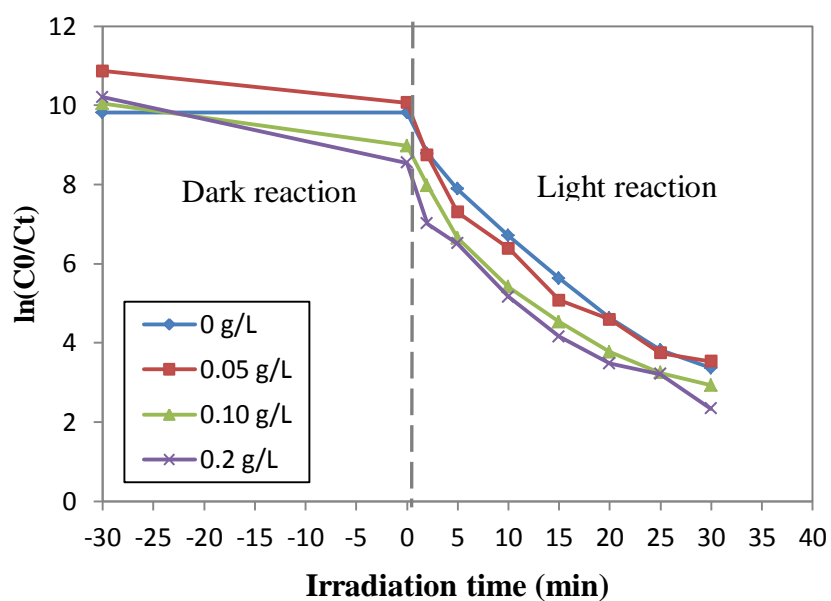
(b) Synthesized electrospun TiO₂ nanofibers

Figure 4.11 The effects of TiO$_2$ nanocatalyst dosage on photodegradation of profenofos under UV radiation

Figure 4.10 and Figure 4.11 exhibited the concentration of profenofos in aqueous solution as a function of light irradiation time with various nanocatalyst dosages. The results show that the decrease of profenofos in solution after stirred 30 min in the dark for absorption onto titania surface with 0.05, 0.10, and 0.20 mg/L dosage of P25 were approximately 9%, 16%, and 18%, respectively. This was consistent with the absorption ability when using TiO_2 nanofibers with 0.05, 0.10, and 0.20 mg/L were relatively 7%, 10%, and 16%, respectively. It could be observed that absorption ability of profenofos onto titania surface both P25 and fibers was similar. However, it appeared that nanofibers had absorption ability slightly less than the commercial titania. Moreover, it was very clear that the more addition of titania concentrations from 0 to 0.20 g/L in the solution, the greater absorption capacity onto their surface area where the photocatalytic could be directly occurred. This led to higher removal efficiency.

For the effect of VUV illumination, the results show that the VUV/P25 and VUV/fibers could achieve almost degradation of profenofos within 30 min light radiation (Figure 4.10 (a) and (b)). The final concentration of profenofos at 30 min with 0, 0.05, 0.10, and 0.20 mg/L P25 dosage were 0.47, 0.36, 0.26, and 0.24 mg/L, respectively whereas those of VUV/TiO_2 nanofibers were 0.47, 0.43, 0.40, and 0.33 mg/L, respectively. It could be seen that addition more titania concentration was capable to slightly degraded profenofos in aqueous solution, this was resulted from the target compound could be mainly decomposed by photolysis than photocatalysis reaction hence supplement more titania dosage could cause slightly increment of removal efficiency.

For UV/TiO_2 process, UV/P25 and UV/nanofiber did not completely decomposed profenofos within 30 min of experimental time. The profenofos concentrations were

gradually declined from 10 mg/L to 3.49, 2.78, 1.95, and 1.67 mg/L, respectively whereas UV/TiO$_2$ nanofibers process had gently fallen to 3.49, 3.54, 2.80, and 2.34 mg/L, respectively. These results were correspond to the removal efficiency of profenofos that the UV/P25 processes from 65% to 82% % as the photocatalyst dosage increased from 0 to 0.20 g/L, whereas the VUV/fibers processes had shoot up to 77%, as displayed in Appendix D. It could be observed that addition more titania concentration was capable to considerably degraded profenofos in aqueous solution, this was resulted from profenofos could be decomposed with both photolysis and photocatalysis reaction in similar quantity hence supplement more titania dosage could significant cause increment of removal efficiency (for UV/P25 processes). While UV/fibers trends had less efficiency than those of UV/P25, this might be caused from the flake form of elctrospun nanofibers led to decreasing light penetration to the reactor system and slow down photolysis and photocatalysis reaction.

The results from both P25 and fibers parts under UV and VUV irradiation had been revealed that increase of nanocatalyst dosage could increase profenofos removal efficiency because more titania concentration was meant to be more surface area (active sites) for continuous photocatalytic – oxidation reaction onto the heterogeneous photocatalyst with great amount of hydroxyl radicals (E. Rosenfeldt et al., 2006; Rongchang et al., 2009). Similar results were found for Putta (2009b), that investigated the effect of synthesized TiO$_2$ nanoparticles dosage (0.25, 0.50, and 1.0 g/L) with sol-gel process for photocatalytic activity of 2-chlorophenol under UV irradiation. The results showed that increasing of catalyst amount could increase the number of active sites on catalyst's surface hence it also caused a great number of hydroxyl radical formation. However, in this work, addition of more than 0.10 g/L

dosage of photocatalyst resulted to slight increase of the removal efficiency of profenofos. It was found that excess amount of the photocatalyst dosage led to the suffer loss of removal efficiency and degradation rate due to the agglomeration into larger size (more than nanosize) of the photocatalyst particles that restricted the existence of gradient light intensity into the photoreactor to the overall photo-oxidation reaction. In addition, a screening effect of the TiO_2 suspension may diminish the photolytic reaction and did not greatly change the degradation efficiency of pollutant (Han et al., 2004; Kang et al., 2011; Huang et al., 2013).

Figure 4.12, 4.13 and Table 4.3, it shows the effect of nanocatalyst dosages of degradation kinetic rate of profenofos under VUV/TiO_2 and UV/TiO_2, respectively. The results showed that the rate constant of profenofos degradation from the VUV/P25 processes had followed pseudo-first order kinetic model while the kinetic rate from the VUV/fibers processes had less followed pseudo-first order kinetic model (lesser linear line) because the kinetic rate from VUV/fibers systems had lesser correlation (R^2) between $\ln(C_0/C_t)$ and reaction time within 30min than VUV/P25 systems. This might resulted from KC values (in the Langmuir-Hinshelwood kinetic model) obtain from adsorption of nanofibers surface with profenofos molecule might be higher than 1, hence the Langmuir-Hinshelwood kinetic model for VUV/fibers (heterogeneous reaction) cannot be also simplified to pseudo-first order reaction at low concentration (mg/L). Moreover, the morphology of nanofibers had differed propertie to P25 nanoparticles in case of light absorption into the all part of photoreactor when they were stired with magenetic stirrer. P25 photocatalytic systems had the solution liked milky that meaned all particles in the reactor could regularly

absorb the incident light to excited the titania activity whereas the solution of TiO_2 nanofibers had unliked milky. Some fibers were on top of the solution but some were at the bottom of the reactor that influenze to the exposure light absorbtion onto the total titania nanofibers surface area affected to the photocatalytic reaction on titania surface. The rate constants from VUV/P25 systems had increased from 0.1049 min^{-1} to 0.1292 min^{-1} as the photocatalyst dosage increased from 0 to 0.20 g/L similar to those of VUV/fibers processes that increase from 0.104 min^{-1} to 0.1353 min^{-1}. For UV/TiO_2 (Figure 4.13), the results illustrated that the UV/P25 processes had increase from 0.0374 min^{-1} to 0.0584 min^{-1} as the photocatalyst dosage increased. Similarly, the same trend was found for UV/fibers process.Both UV/P25 qnd UV/fibers, they are propotional to the photocatalst dosage that the rates were increased as the addition of catalyst concentration since it can improve in the total surface area of catalyst. The increase of more active sites led to more reactive hydroxyl radicals generation (Rongchang et al., 2009). Both VUV/P25 and VUV/nanofibers with 0.20 g/L of catalyst had the profenofos degradation rate constant about 3 times compare to that of UV/P25 and UV/fiber, indicating that hydroxyl radicals from UV photocatalytic processes were not enough for complete degradation of profenofos in aqueous solution. Hence, VUV photocatalytic processes were also greater kinetic rate contants than the photolytic decomposition under UV and VUV process, indicating that the synergistic effect can improve degradation of pollutant and photoreactor removal efficiency. However, the observe rates can be slightly increased with increase of TiO_2 dosage in both UV and VUV processes due to limitation of light penetration in the system as increasing of catalyst concentration.
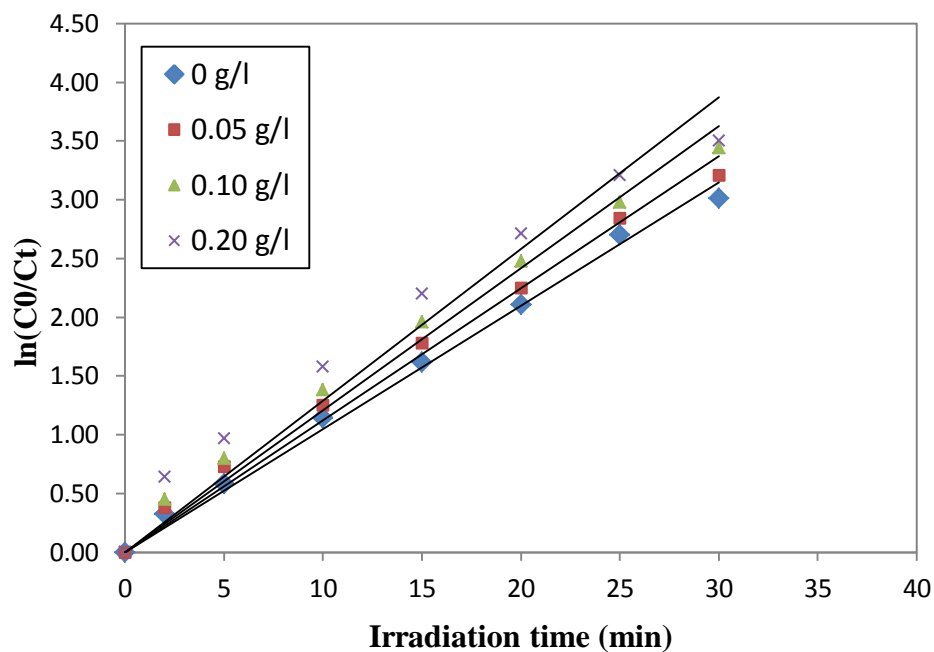
(a)P25 nanoparticles
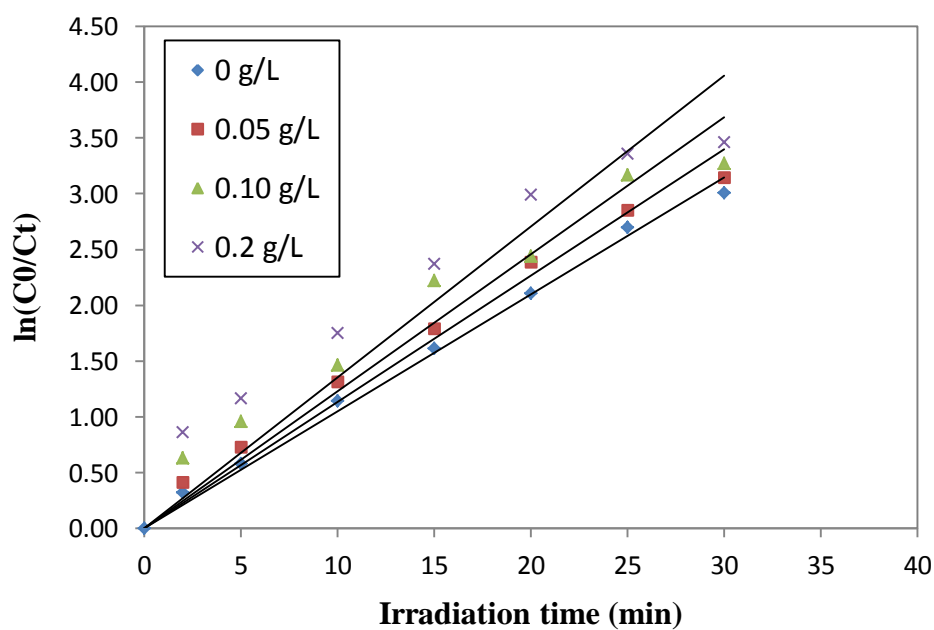
(b) Synthesized electrospun TiO₂ nanofibers

Figure 4.12 Plot of $\ln(C_0/C_t)$ versus time of profenofos under VUV with various TiO₂ nanocatalyst dosages
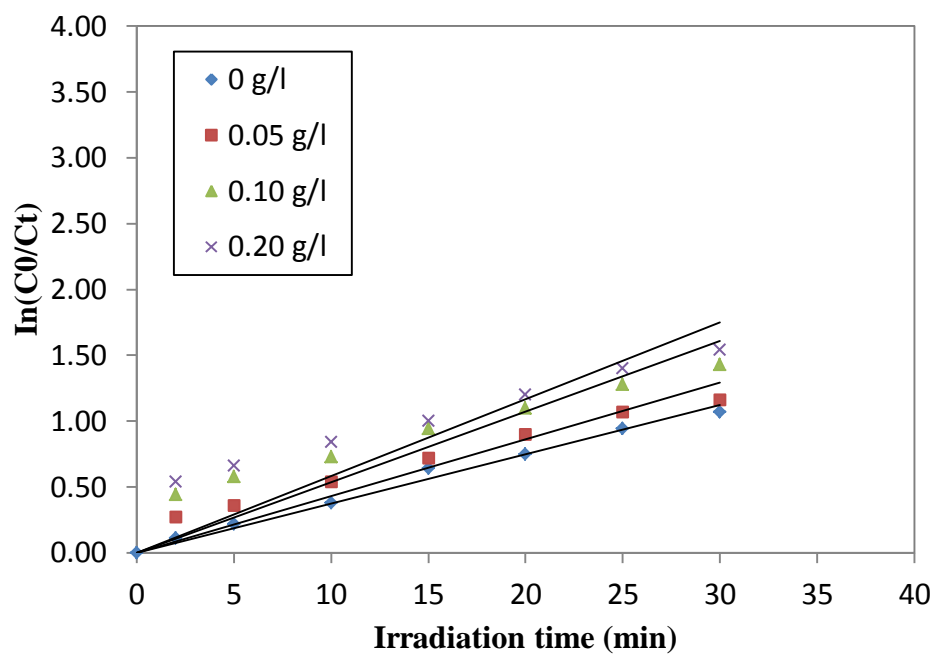
(a) P25 nanoparticles
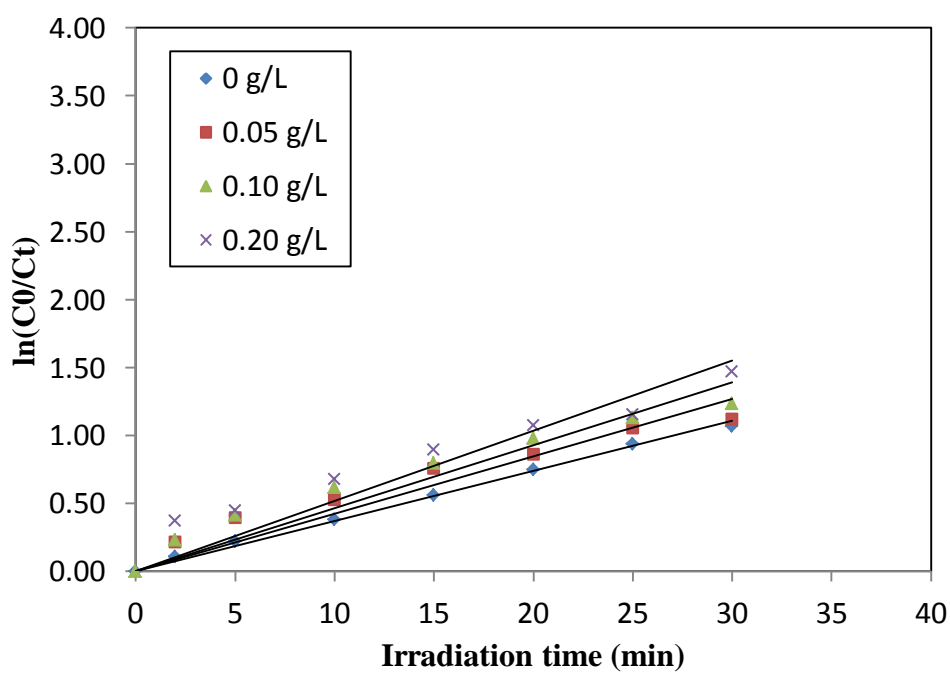
(b) Synthesized electrospun TiO₂ nanofibers

Figure 4.13 Plot of $\ln(C_0/C_t)$ versus time of profenofos under UV with various TiO$_2$ nanocatalyst dosages

Table 4.3 Kinetic rate constants of profenofos degradation from each AOPs experimental condition

Type of AOPs	TiO$_2$ dosage (g/L)	Kinetic rate constant (min^{-1})	R-square
UV/P25	0	0.0374	0.9896
	0.05	0.0430	0.9217
	0.10	0.0536	0.8074
	0.20	0.0584	0.7473
UV/fibers	0	0.0374	0.9896
	0.05	0.0423	0.9105
	0.10	0.0463	0.9148
	0.20	0.0517	0.9958
VUV/P25	0	0.1049	0.9940
	0.05	0.1123	0.9890
	0.10	0.1208	0.9839
	0.20	0.1292	0.9499
VUV/fibers	0	0.1049	0.9940
	0.05	0.1132	0.9802
	0.10	0.1229	0.9351
	0.20	0.1353	0.8825

4.4 Mineralization of profenofos

Mineralization rate of profenofos in aqueous solution was determined based on from dissolved organic carbon (DOC) measurement with this optimum condition ([PF]$_0$ = 10 mg/L, pH = 7, room temperature) using photolysis and photocatalysis processes under UV and VUV irradiation. The reduction of DOC by UV and VUV is shown in Figure 4.14.
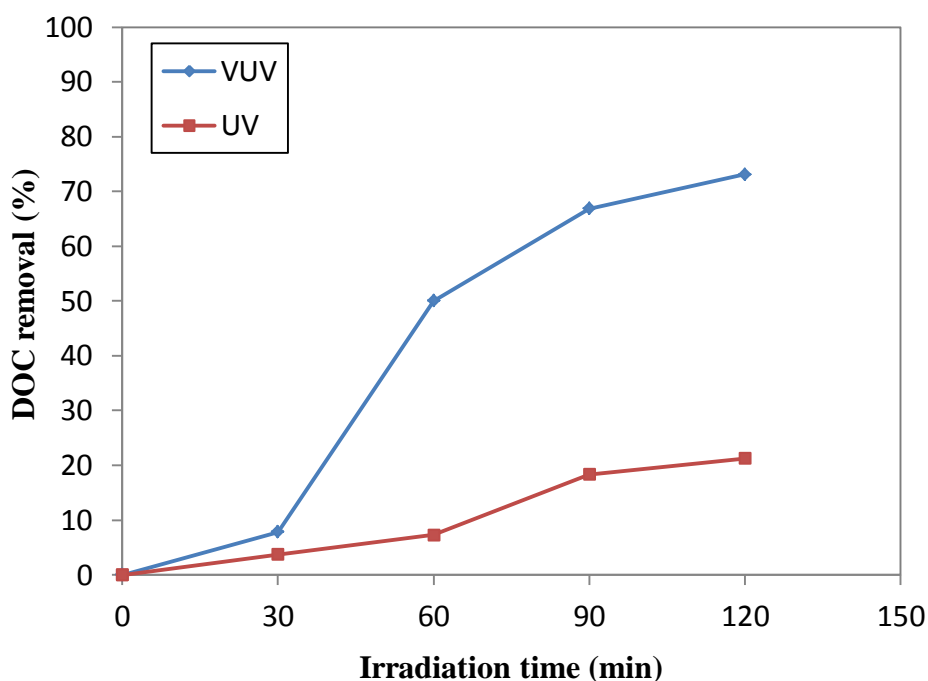
Figure 4.14 Mineralization of profenofos under UV and VUV photolysis processes

The results show that DOC reduction provided by VUV process slowly increased during the first 30 min after that it suddenly increased during the period of 30 to 90 min and began to level off thereafter. The mineralization profenofos by VUV was 73% (incomplete mineralization within 120 min). On the other hand, mineralization of profenofos by UV was only 21% at 120 min of irradiation. This finding were consistent with Prasertwongchai (2011) who investigate the removal of 8.5 g/L of profenofos solution under UV and VUV radiation. VUV outperformed UV for mineralization because the VUV process can emit UV light at wavelength of 185 nm that resulted in direct photolysis and formation of $^{\bullet}$OH. The degradation of profenofos with UV photolysis involved a long reaction time compared to the VUV

photolysis process resulted from 8% DOC mineralization of profenofos under VUV radiation required only 30 min nevertheless UV needed more time to obtain this point (60 min), indicating that UV radiation enhanced the activity photolysis system quite insignificantly and the photon energy from UV wavelength was found to have effect on mineralization rate. Thus, VUV photolytic process significantly obtained higher mineralization rate and more rapidly decomposition of profenofos than UV process. This was consistent with Prasertwongchai (2011), the results revealed that the VUV process could obtain much more amount of mineralization efficiency (77%) than UV photolytic process (8%). Mineralization of organic carbon refers as transformation of organic carbon to carbon dioxide. Organic carbon will be undergone series of oxidation steps to become the final product (CO_2). The presence of oxygen is one of important factor that lead to complete oxidation. During the oxidation, carbon-center radical from photodegradation profenofos in aerobic condition could be decomposed to peroxyl radicals and transformed to more amount of CO_2 in thesystem (Stefan, 2005), as seen the reaction in equation (4.22) – (4.24):

$$R \text{ (organic compound)} \ + \ \bullet OH \ \rightarrow \ R\bullet \text{ (carbon-center radical)} \ + \ H_2O \quad (4.22)$$

$$R\bullet \ + \ O_2 \ \rightarrow \ R\text{-}O_2\bullet \text{ (peroxyl radicals)} \quad (4.23)$$

$$R\bullet \ + \ nO_2 \ \rightarrow \ CO_2 \ + \ H_2O \ + \ \ldots\ldots \text{ (Mineralization)} \quad (4.24)$$
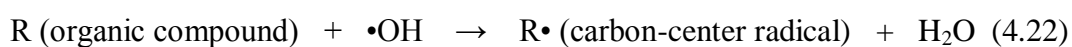
It was noticed that the mineralization of profenofos took longer time compared to the removal of profenofos itself which 90% removal occurred in the first 10 min of

reaction. This means there are intermediate products occurred during photolysis and photocatalytic oxidation. Zamy and coworkers (2004) investigated the role of hydroxyl radical oxidation and photolysis under 285 nm of 40 W-UV radiation that they reported the photodegradation by-products of profenofos from photolysis and hydroxyl radical oxidation including O-4-bromo-2-chlorophenyl, O-S-dihydrogen phosphorothioate, 4-bromo-2-chlorophenol, phenol, and thiono-thiolo isomerization. Chen and coworkers (2014) investigated the role of hydroxyl radical oxidation generated by UV/ferrate (VI) oxidation under 254 nm UV wavelength, they reported some of these photodegradation products of profenofos were corresponding to de-ethylation, de-propylation, de-bromination, cleavage of the O – Ethyl alkyl ester bond, and cleavage of P – S to P – O bond (Zamy et al., 2004; Chen et al., 2014).

The effect of TiO_2 dosages on profenofos mineralization by VUV/TiO_2 and UV/TiO_2 are shown in Figure 4.15, 4.16, respectively. The results show that the increasing of TiO_2 dosages increased the mineralization (based on DOC) for VUV/TiO_2 and UV/TiO_2. For example, in VUV/P25, the DOC mineralization at 0.05, 0.10, and 0.20 g/L of TiO_2 at 120 min were approximately 77%, 84% and 88%, respectively. This because the system with more TiO_2 dosage (more active site for photocatalytic degradation) would have considerably high quantum yield of hydroxyl radical production (Macedo et al., 2007). When comparing between types of TiO_2, it was found that the process with nanofiber TiO_2 provided little less than mineralization of profenofos by VUV/P25. Mineralization by VUV/fibers at 0.05, 0.10, and 0.20 g/L of TiO_2 were 71%, 78%, and 81%, respectively within 120 min. This was resulted from these nanofibers were utilized in flake form that it could be broken off into small

pieces in the solution led to decrease the incident light penetration to react with profenofos and water molecules (also decrease the mineralization efficiency) on titania surface area (Watthanaarun et al., 2007). For UV/P25 and UV/nanofiber, the mineralization of profenofos was approximately 30% less for the same TiO_2 dosage. For example, the TOC mineralization at 0.05, 0.10, and 0.20 g/L of TiO_2 for UV/P25 was approximately 32%, 47% and 57%, respectively. Furthermore, comparison of mineralization rate between photocatalysis and photolysis system showed that photocatalytic process had much more DOC removal rate and efficiency, indicating that the existence of titania photocatalyst could significantly enhance mineralization of pollutant in aqueous solution. Similar phenomena was found in Huang and coworkers (2013) for the decomposition of methylene blue using photocatalysis processes with different dosage from 0 to 2 g/L in aqueous solution. This was plausibly owing to the degraded intermediate molecules on the catalyst surface could be decomposed with the power of strong oxidation capability from hydroxyl radicals in photocatalysis processes.
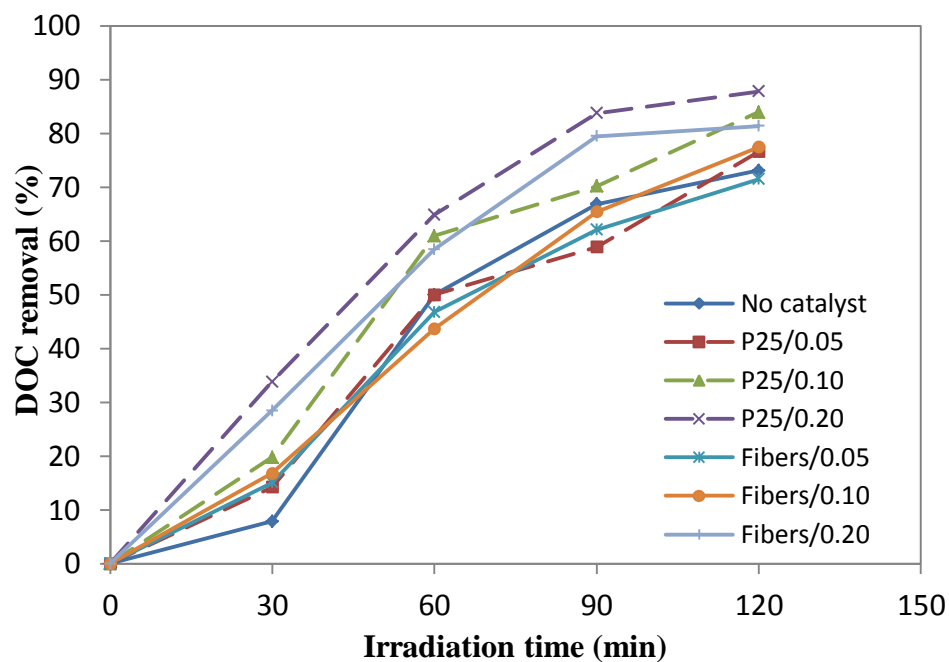
Figure 4.15 Mineralization of profenofos under VUV photocatalysis processes
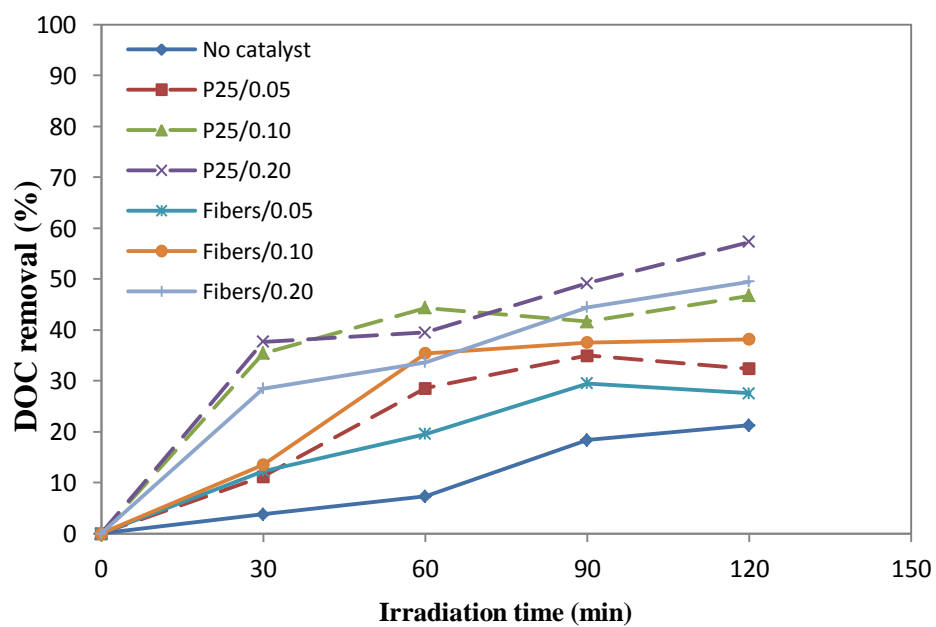
Figure 4.16 Mineralization of profenofos under UV photocatalysis processes

4.5 Hydroxyl radical formation

The potential of photodegradation of methylene blue, as a hydroxyl radical probe compound to predict a relationship between initial TiO_2 catalyst and hydroxyl radical exposure from photolytic and photocatalytic systems under UV and VUV irradiation was investigated in this research study with this condition ($[MB]_0 = 10$ µM, pH = 7, room temperature, with and without t-BuOH), as shown more detail in Appendix G. To measure hydroxyl radical exposure (•OH concentration x time) for the following conditions: UV/P25, UV/fibers, VUV/P25, VUV/fibers system with various dosages including 0, 0.05, 0.10, and 0.20 g/L f titania, the working solution into the reactor must be spiked by adding 20 mM of t-BuOH at the beginning of the experiments to scavenge •OH. The method for calculating •OH exposure from a probe compound was expresses by Rosenfeldt and Linden (2007), as shown in equation (4.25) – (4.28):

$$\frac{d[MB]}{dt} = -(k_d' + k_i')[MB] \tag{4.25}$$

Substitute $k_i' = k_{OH,MB}[OH•]$ in equation (4.25), obtained this equation

$$\frac{d[MB]}{dt} = -(k_d' + k_{OH,MB}[OH•])[MB] \tag{4.26}$$

Integration of equation (4.26), obtained this equation

$$ln\left\{\frac{[MB]_0}{[MB]_t}\right\} \ = \ k'_T = \ k'_d + k_{OH,MB} \int_0^t [OH\bullet]dt \qquad (4.27)$$

Hence, •OH exposure can be calculated from this equation

$$\bullet\ OH\ exposure\ (concentration\ x\ time) \ = \ \int_0^t [OH\bullet]dt \ = \ \frac{k'_T - k'_d}{k_{OH,MB}}\ (4.28)$$

Where t is the irradiation time in the experiment (s), k'_d is a pseudo-first order rate constant of MB destruction by direct photolysis (s^{-1}), k'_I is a pseudo-first order rate constant of MB destruction by •OH radical mechanism (s^{-1}), k_T is an observed pseudo-first order removal rate of MB (s^{-1}), and $k_{\bullet OH,MB}$ is a pseudo-first order reaction rate constant of MB degradation with OH• radical had been reported as 2.1× 10^{10} ($M^{-1}\ s^{-1}$) (Buxton et al., 1988). Both k_T (no adding t-BuOH) and k_d (adding t-BuOH) rate constants were obtained from plotting graph between $ln(C_0/C_t)$ and irradiation time.

As shown in Figure 4.17 – 4.19 and Table 4.4, the results displayed thatthe kinetic rates on photolytic and photocatalytic degradation of methylene blue under UV and VUV radiation were followed pseudo-first order kinetic model. The kinetic rate constants from each experimental conditions were obtained from plotting graph between $ln(C_0/C_t)$ and irradiation time within 10 min due to undetectable of MB after this period. Hydroxyl radical exposures using P25 and titania nanofibers under the UV/VUV radiation system were revealed in Table 4.2 (calculated from equation 4.28). It could observed that the kinetic rates had increased with the function of

increasing titania nanocatalyst dosage (both P25 and fibers) from 0 to 0.20 g/L, and •OH from photocatalytic systems also had much more •OH exposure than the photolytic processes. It was consistent with Keen and coworkers (2007) reported that the steady-state hydroxyl radical concentrations formation by UV/ H_2O_2 were significantly high when supple of H_2O_2 (catalyst) dosage from 0 to 10 mg/L, additional up to 10 mg/L will not enhance considerably to the •OH generation owing to the light filtration effect. Furthermore, it could be notice that the different kinetic rate value between k'_T (no addition of t-BuOH) and k'_d (addition of t-BuOH) under VUV illumination had significantly differed more than kinetic rates under UV radiation (k'_T rate constants was higher than k'_d), indicating that t-BuOH was greatly achieved to act as a hydroxyl radical scavenger in these AOPs systems that means photolysis of the probe compound under VUV radiation could not be neglected. Chunhapimol (2013) reported this familiar results that addition of t-BuOH into the UV reactor systems had not much different values between k'_T and k'_d, indicating that this system hardly generate •OH from photolysis of water hence the photolysis of water under UV radiation could be neglected. In contrast the VUV systems had significantly differed between both of them (mostly generate •OH from oxidation reaction) because t-BuOH was expected to scavenge the oxidation reaction of hydroxyl radicals, which might decrease the oxidation reaction with organic compound in aqueous solution (E. Rosenfeldt et al., 2006). Hence, the results as shown in Figure 4.20 that was the evidence for higher generate the quantum yield hydroxyl radical (•OH exposure) from UV/VUV photolysis systems and UV/VUV photocatalysis system when synergize with addition more titania nanocatalyst into the solution. We believed that most of methylene blue molecules were decomposed by

mainly •OH radicals more than other reactive species so that this could be assumed that non-selective •OH radicals for profenofos degradation was same to MB decomposition. Since the removal efficiencies and mineralization rates of profenofos in aqueous solution with the presence of titania nanocatalyst under UV and VUV irradiation were higher than the UV/VUV alone system and the profenofos degradation was increased when increased titania nanocatalyst dosage from 0 to 0.20 g/L. Likewise, the •OH exposure from UV/VUV system with TiO_2 photocatalyst were greater than only photolysis system, and it could be increased when supple more catalyst from 0 to 0.20 g/L. Hence, the •OH exposure from methylene blue degradation could agree with profenofos removal results.
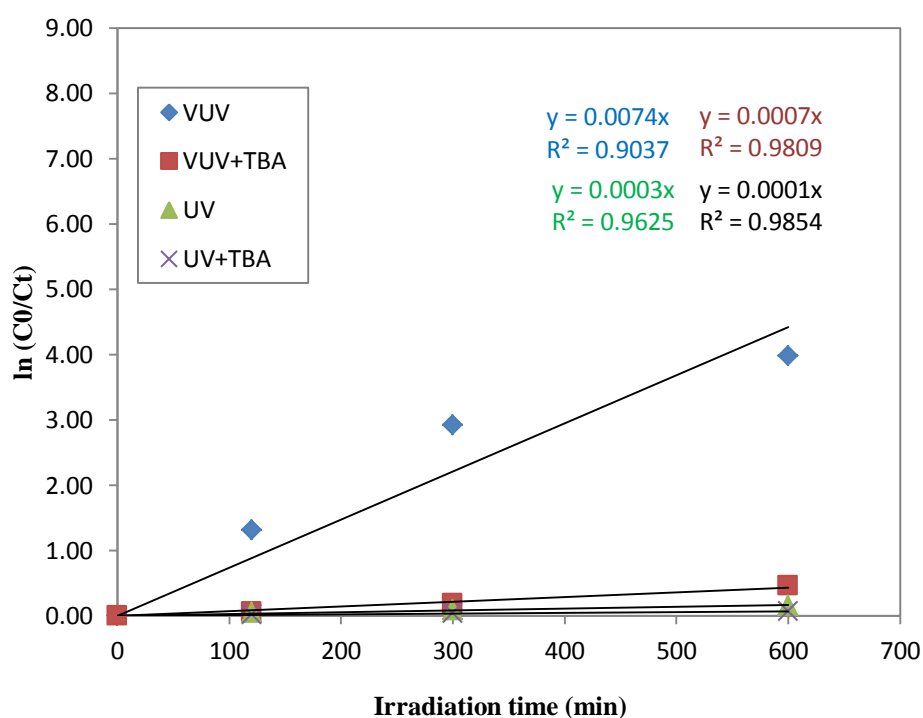
Figure 4.17 The kinetic rate on photolytic degradation of methylene blue under UV and VUV radiation
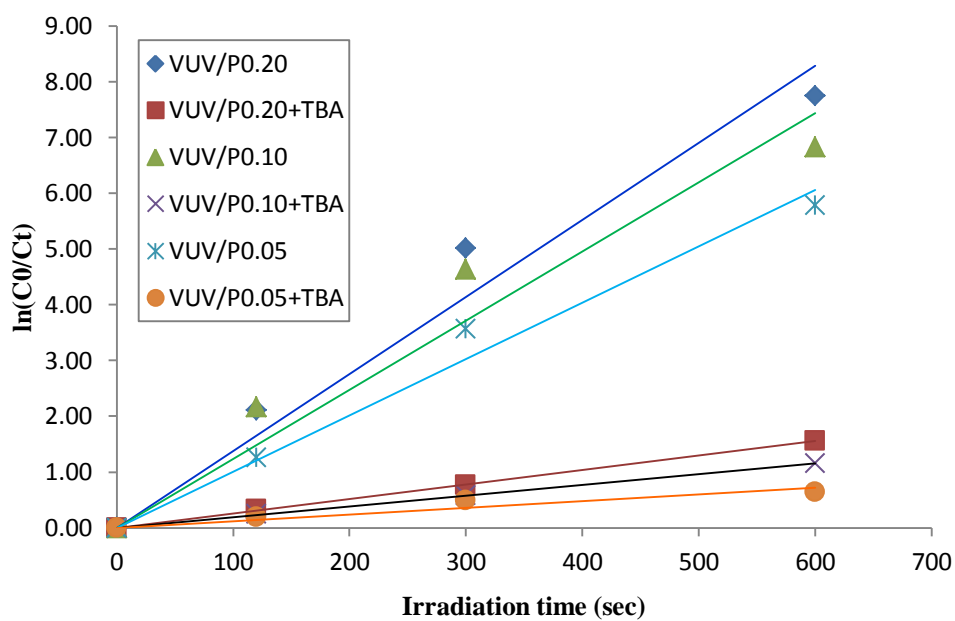
(a) P25
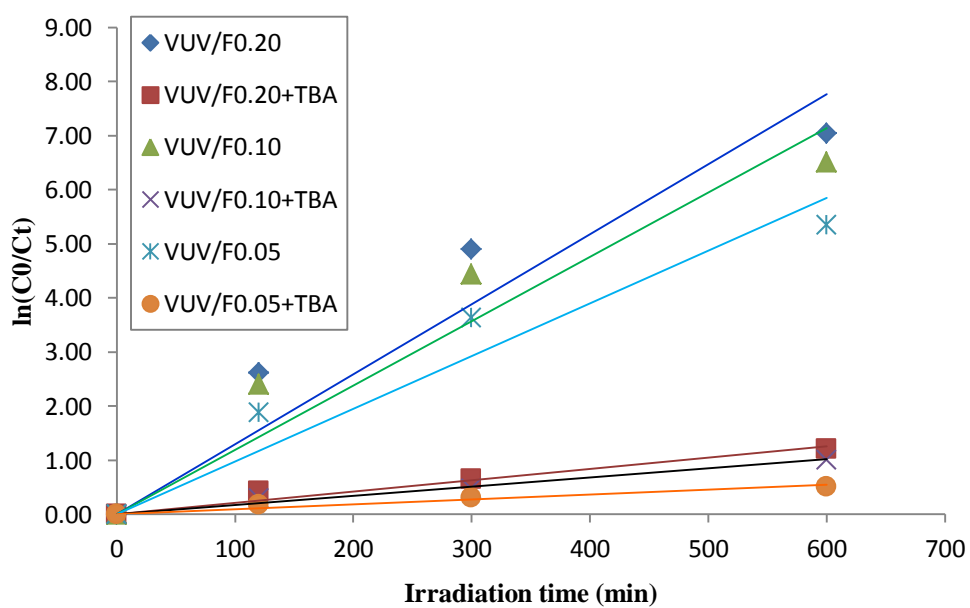
(b) Titania nanofibers

Figure 4.18 The kinetic rate on photocatalytic degradation of methylene blue under
VUV radiation with various dosage
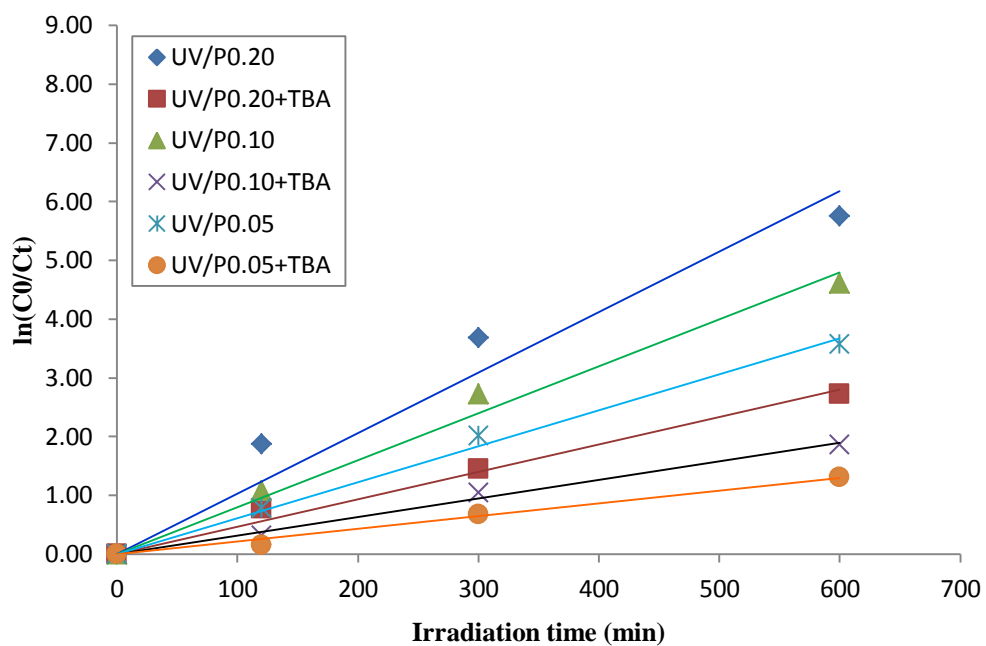
(a) P25
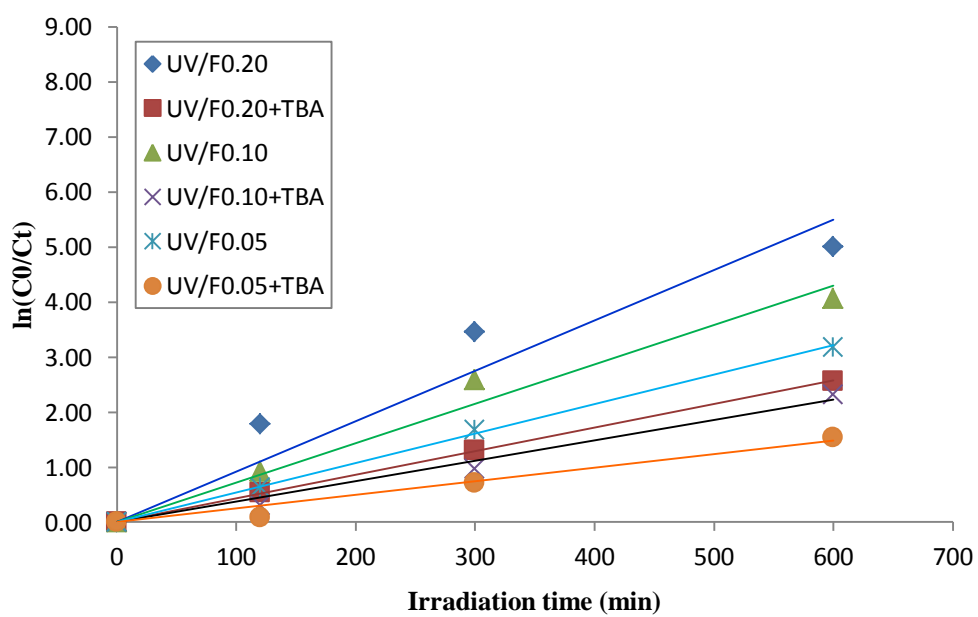
(b) Titania nanofibers

Figure 4.19 The kinetic rate on photocatalytic degradation of methylene blue under UV and UV radiation with various dosage

Table 4.4 Kinetic rate constants of probe compound degradation from each AOPs experimental condition with and without adding TBA

AOPs Condition	Kinetic Rate Constants (s^{-1})	
	Without TBA	**With TBA**
VUV alone	0.0074	0.0007
UV alone	0.0003	0.0001
UV/P25 0.20 g/L	0.0138	0.0026
UV/P25 0.10 g/L	0.0124	0.0019
UV/P25 0.05 g/L	0.0101	0.0012
VUV/P25 0.20 g/L	0.0103	0.0047
VUV/P25 0.10 g/L	0.0080	0.0032
VUV/P25 0.05 g/L	0.0061	0.0022
UV/F 0.20 g/L	0.0092	0.0043
UV/F 0.10 g/L	0.0072	0.0037
UV/F 0.05 g/L	0.0054	0.0025
VUV/F 0.20 g/L	0.0129	0.0021
VUV/F 0.10 g/L	0.0119	0.0017
VUV/F 0.05 g/L	0.0097	0.0009

*F = Titania nanofibers
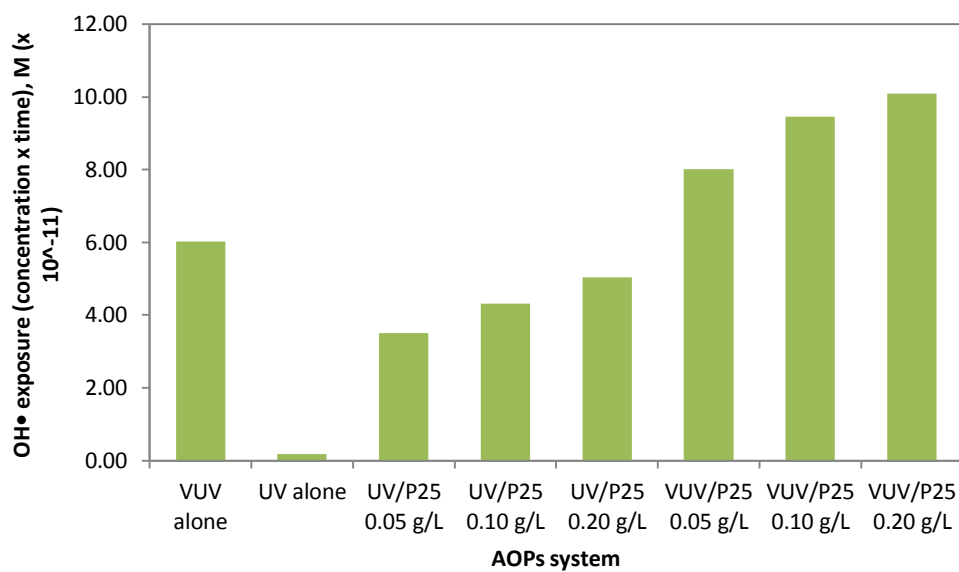
(a) P25
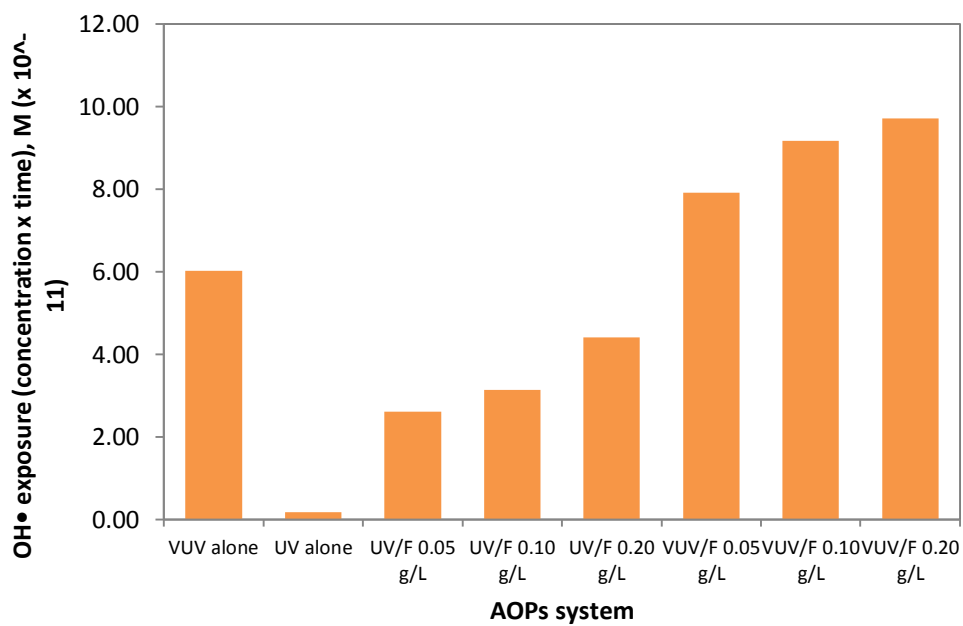
(b) Nanofibers

Figure 4.20 Hydroxyl exposure from photocatalytic processes under UV and VUV radiation

4.6 Reusability of the titania nanocatalyst

The reusability of titania nanocatalyst (both P25 nanoparticles and electrospun TiO_2/PVP nanofiber) was farther examined because the reusability of heterogeneous photocatalyst is one of the most essential for practical applications, and was a key factor for enhancing process economics. Therefore, profenofos was used as a model substrate for testing the reusability of the nanocatalyst with this selected condition ($[PF]_0$ = 10 mg/L, TiO_2 dosage = 0.20 g/L, 30 min of VUV illumination, 10 cycles). It should be noted that no treatment for reusable catalyst after ten consecutive cycles, just only separated by filtration, washing with DI water and drying at room temperature overnight. After that the catalyst was reused directly for the next experimental reaction. The photocatalyst was reused in order to investigate its stability and activity on profenofos degradation in aqueous solution of any experimental run. In this study, the percentage of reusability on catalyst could be calculated in the same procedure as the removal efficiency of profenofos, as shown more detailed in Appendix F. The removal efficiencies of profenofos in aqueous solution for VUV/P25 and VUV/nanofibers are shown in Figure 4.20 a, b.
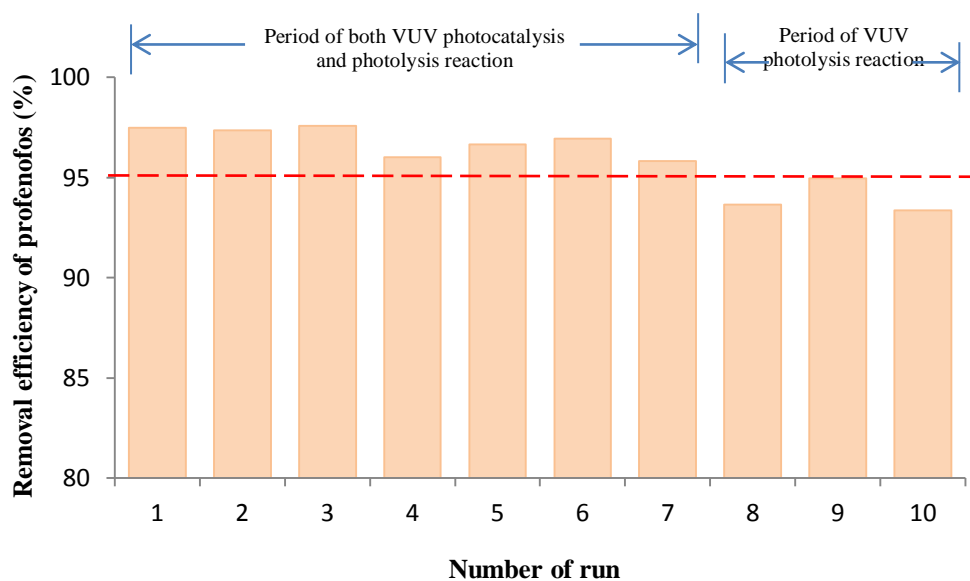
(a) P25
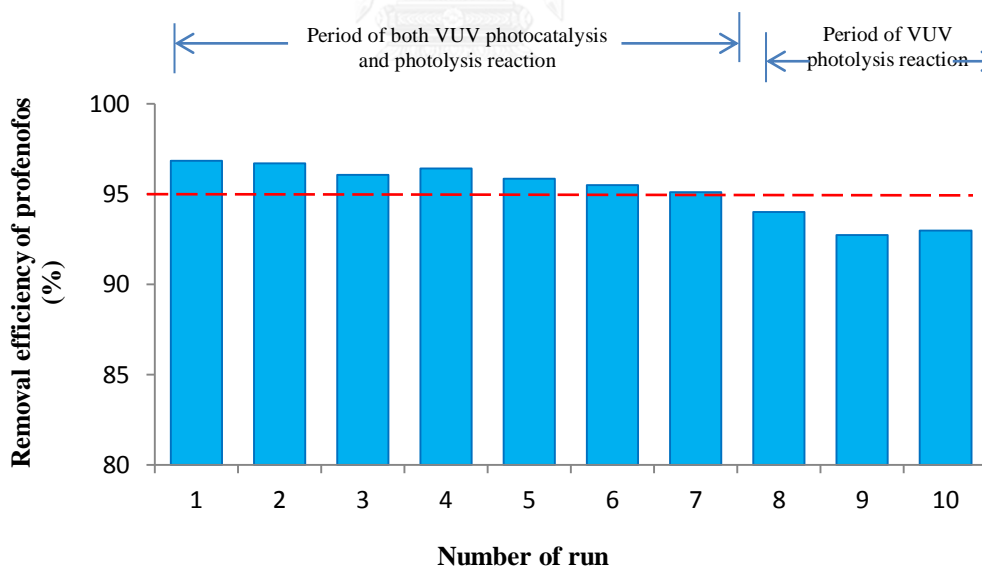
(b) TiO₂ nanofibers

Figure 4.21 Reusability of VUV/TiO$_2$ for profenofos removal as a function of the number of run

It was found that profenofos removal efficiencies of both VUV/P25 and VUV/nanofibers were between 96-97% for during 7th cycles of consecutive experimental runs. At later cycles of 8th to 10th, the removal efficiencies decreased slightly to be about 92-95% which was equal to VUV alone. Irani and coworkers (2012) also found that titania nanocatalyst could be reused for many times without considerable loss in adsorption capacity on their surface area after seven cycles. The decrease in profenofos removal efficiencies was due to accumulation of profenofos molecules and intermediates on the catalyst's surface after consecutive runs. As a result, the catalysts had no additional generation of •OH on their surface area due to catalyst deactivation. Piera and coworkers (2002) reported that the catalyst permanent deactivation was related to reactant adsorption capability on top of some of the organic deposits in the dark reaction prior to the light reaction that led to significantly decrease the kinetic rate constant for organic compound decomposition under photocatalytic system with an increasing number of runs. Moreover, Peral and coworkers (1997) had recommended that the species of carbonaceous nature were corresponding to permanent deactivation on TiO_2 surface. It was observed that titania nanocatalyst (both P25 and nanofibers) had a permanent pale yellow color, indicating that there were much more the existence of carbonaceous on their surface (Piera et al., 2002). In addition, Muggli and coworkers (1998) found that competition between the target compounds and intermediate had been happened onto the same adsorption sites hence much more reaction time was needed for complete destruction of substances in the system.

Recovery yields of the nanocatalyst P25 and electrospun nanofibers after each experimental run were shown in Table 4.5 and 4.6, respectively. The resulted presented that the loss of P25 nanoparticles during 10th cycles of experiment was more than those of electrospun nanofibers. The loss of amount of titania after ten consecutive runs was more than 30% whereas the titania recoveries from synthesized nanofibers were slightly reduced. It was 5% less than 5% after ten reusable cycles. Loss of P25 nanoparticles mass might be resulted from the separation step that these catalysts must be filtratedwith the Nylon filter membrane that some catalysts were attached on it. In addition, P25 nanoparticles also showed more darkened yellow color on the catalyst's appearance than the elctrospun nanofibers, indicating that these particles had more absorbed carbonaceous species onto P25 surface area and more catalyst deactivation activity. Hence, reusability of electrospun TiO_2/PVP composite nanofibers was better than using P25 commercial particles because of easy separation, readily easy reusable, eco – friendly solid photocatalyst, high activity, long-term stability, insignificant loss in adsorption performance, and recovery yield (Gómez et al., 1999; Irani et al., 2012; Haghighi and Nikoofar, 2014b).

Table 4.5 Isolated yield of P25 from for profenofos removal as a function of the number of run

Number of run	Titania mass in (g)	Titania mass lost (g)	Volume in (mL)	Recovery (%)
1	0.1038	0.0097	500	91
2	0.0941	0.0097	500	91
3	0.0836	0.0105	500	89
4	0.0743	0.0093	500	89
5	0.0638	0.0109	500	86
6	0.0535	0.0103	500	84
7	0.0437	0.0098	500	82
8	0.0332	0.0105	500	76
9	0.0231	0.0101	500	70
10	0.0136	0.0095	500	59

Table 4.6 Isolated yield of electrospun TiO_2 nanofibers from for profenofos removal as a function of the number of run

Number of run	Titania mass in (g)	Titania mass lost (g)	Volume in (mL)	Recovery (%)
1	0.1027	0.0032	500	97
2	0.0995	0.0032	500	97
3	0.0962	0.0033	500	97
4	0.0926	0.0036	500	96
5	0.0890	0.0039	500	96
6	0.0852	0.0038	500	96
7	0.0810	0.0042	500	95
8	0.0762	0.0048	500	94
9	0.0716	0.0046	500	94
10	0.0666	0.0050	500	93

CHAPTER V

CONCLUSIONS AND RECOMMENDATIONS

5.1 Conclusions

In this research, the electrospun TiO_2/PVP composite nanofibers had been synthesized and tested for its photocatalytic degradation on profenofos (as the target compound) in aqueous solution compared to the activity from P25 commercial nanoparticles under UV, VUV, UV/TiO_2, and VUV/TiO_2 reaction systems. The essential findings from this research can be concluded as follows:

1. The photodegradation performances (kinetic rate) of profenofos under photocatalytic and photolytic processes in both P25 nanoparticles and electrospun titania nanofibers were in the order: VUV/TiO_2> VUV > UV/TiO_2> UV. The photocatalytic degradation (with catalyst) obtains higher degradation efficiency than photolytic degradation (without catalyst).

2. The photodegradation behaviors (removal efficiency, kinetic rate, and mineralization efficiency) of profenofos under UV and VUV photocatalytic system in both P25 nanoparticles and electrospun titania nanofibers were relatively similar and increase as the function of increasing titania nanocatalyst dosage from 0 to 0.20 g/L.

3. The photodegradation performances of profenofos under UV and VUV irradiation in both P25 nanoparticles and electrospun titania nanofibers were considerably associated to hydroxyl radical formation in the system, and increasing of

titania nanocatalyst dosage can also cause much more of hydroxyl radical formation led to high removal efficiency, kinetic rate, and mineralization rate.

4. Both Degussa-P25 nanoparticles and the synthesized electrospun titania nanofibers can be reused for many consecutive reusable cycles without any treatment and still obtained high removal efficiency of profenofos. However, the electrospun nanofibers had obviously more reusability and easy separation than Degussa-P25 commercial nanoparticles.

5.2 Recommendations for Future work

1. Study of the photolytic and photocatalytic degradation activity of pesticides using the reactor with aeration should be investigated to obtain much more removal efficiency, kinetic rate, and mineralization rate.

2. The application VUV/TiO_2 for real natural water (lower concentration than this research study) should be investigated to determine the system performance and effect of organic and inorganic species in the water matrix that might interfere or scavenge the hydroxyl radicals because the application for natural water could have lower kinetic rate than the synthesized 10 mg/L of profenofos, as done in this research study.

3. Study the photocatalytic activity of synthesized electrospun TiO_2 nanofibers doped with other secondary metals should be investigated to obtain much more removal efficiency, kinetic rate, and mineralization rate.

4. Study of the intermediates products from both photolytic and photocatalytic activity under UV and VUV irradiation should be investigated by using Gas-Chromatography Mass Spectrometer.

5. Study the photocatalytic activity with other photocatalyst should be investigated to improve the removal efficiency, kinetic rate, and mineralization rate and compared the resulted to profenofos in aqueous solution case.

6. Study the other methods of photocatalysis with nanofibers for applying in the real scale such as fixing on the plate or coating on the glass tube outer of light source.

7. Study the effect of water matrix scavengers such as natural organic matter (NOM), bicarbonate, carbonate, nitrate to the degradation kinetic rate of the target pollutant.

Ahmed, S., Rasul, M. G., Brown, R., & Hashib, M. A. (2011). Influence of parameters on the heterogeneous photocatalytic degradation of pesticides and phenolic contaminants in wastewater: A short review. *Journal of Environmental Management, 92*(3), 311-330.

Akhtar, M., Hasany, S. M., Bhanger, M. I., & Iqbal, S. (2007). Low cost sorbents for the removal of methyl parathion pesticide from aqueous solutions. *Chemosphere, 66*(10), 1829-1838.

Andersen, J., Pelaez, M., Guay, L., Zhang, Z., O'Shea, K., & Dionysiou, D. D. (2013). NF-TiO2 photocatalysis of amitrole and atrazine with addition of oxidants under simulated solar light: Emerging synergies, degradation intermediates, and reusable attributes. *Journal of Hazardous Materials, 260*, 569-575.

Arany, E., Szabó, R. K., Apáti, L., Alapi, T., Ilisz, I., Mazellier, P., . . . Gajda-Schrantz, K. (2013). Degradation of naproxen by UV, VUV photolysis and theircombination. *Journal of Hazardous Materials, 262*, 151-157.

Badawy, M. I., Ghaly, M. Y., & Gad-Allah, T. A. (2006). Advanced oxidation processes for the removal of organophosphorus pesticides from wastewater. *Desalination, 194*(1–3), 166-175.

Barr, D., & Needham, L. (2002). Analytical methods for biologibal monitoring of exposure to pesticides. *J Chromatogr B Analyt Technologies in the Biomedical and Life Sciences, 778*, 5-9.

Behnajady, M. A., Modirshahla, N., & Hamzavi, R. (2006). Kinetic study on photocatalytic degradation of C. I. Acid Yellow 23 by ZnO photocatalyst. *Journal of Hazardous Materials, 133*(1-3), 226-232.

Beltran, F. J., Gonzalez, M., & Rivas, J. F. (1996). Aqueous UV irradiation and UV/H2O2 oxidation of atrazine first degradation produts: dethylatrazine and deisopropylatrazine. *Environmental Toxicology and Chemistry, 15*(6), 868-872.

Benabbou, A. K., Derriche, Z., Felix, C., Lejeune, P., & Guillard, C. (2007). Photocatalytic inactivation of Escherischia coli: Effect of concentration of TiO2 and microorganism, nature, and intensity of UV irradiation. *Applied Catalysis B: Environmental, 76*(3–4), 257-263.

Buonasera, K., D'Orazio, G., Fanali, S., Dugo, P., & Mondello, L. (2009). Separation of organophosphorus pesticides by using nano-liquid chromatography. *Journal of Chromatography A,* 1216(18), 3970-3976.

Buxton, G. V., Greenstock, C. L., Helman, W. P., & Ross, A. B. (1988). Critical review of rate constants for reactions of hydrated electrons, hydrogen atoms and hydroxyl radicals (.OH/O-) in aqueous solution. *Journal of Physical and Chemical,* 17, 513-886.

Chantam, P. (2006). *Removal of phenyl urea herbicides from water by adsolubilization on surfactant modified titania nanofibers.* (Master's Thesis), Department of Chemical Engineering, Faculty of Engineering, Chulalongkorn University.

Chen, Y., Xiong, Y., Wang, Z., Chen, Y., Chen, G., & Liu, Z. (2014). UV/ferrate(VI) oxidation of profenofos: efficiency and mechanism. *Desalination and Water Treatment,* 15(1-8).

Chin, Y. P., Miller, P. L., Zeng, L., Cawley, K., & Weavers, L. K. (2004). Photosensitized degradation of bisphenol A by dissolved organic matter. *Environmental Science and Technology,* 38, 5888–5894.

Chunhapimol, P. (2013). *Degradation of 17α-methyltestosterone by UV-C and Vacuum UV (VUV) radiation.* (Master's degree), Chulalongkorn Universit, Department of Environmental Engineering, Faculty of Engineering.

Clark, J. (2002). The effect of temperature on reaction rates. http://www.chemguide.co.uk/physical/basicrates/temperature.html

Cordeiro, G. S., Rocha, R. S., Valim, R. B., Migliorini, F. L., Baldan, M. R., Lanza, M. R. V., & Ferreira, N. G. (2013). Degradation of profenofos in an electrochemical flow reactor using boron-doped diamond anodes. *Diamond and Related Materials,* 32, 54-60.

Department of Agriculture [DOA]. (2007-2014). List of Hazardous Substances. Thailand Pesticide Alert Network.

Doh, S. J., Kim, C., Lee, S. G., Lee, S. J., & Kim, H. (2008). Development of photocatalytic TiO2 nanofibers by electrospinning and its application to degradation of dye pollutants. *Journal of Hazardous Materials,* 154, 118–127.

Doong, R., & Chang, W.-H. (1998). Photoassisted iron compound catalytic degradation of organophosphorous pesticides with hydrogen peroxide. *Chemosphere,* 37(13), 2563-2572.

Duriyasart, F. (2012). *Synthesis of polyacrylonitrile/titania co-axial nanofibers via electrospinning.* (Master's Thesis), Department of Chemical Engineering, Faculty of Engineering, Chulalongkorn University.

Einschlag, F. G., Feliz, M. R., & Cappareili, A. L. (1997). Effect of temperature on hydrogen peroxide photolysis in aqueous solutions. *JoumM of Photofhemistry and Pholobiology A; Chemistry I,* 10, 235--242.

Eskandarloo, H., Badiei, A., & Behnajady, M. A. (2014). Optimization of UV/inorganic oxidants system efficiency for photooxidative removal of an azo textile dye. *Desalination and Water Treatment.*

Farhataziz, A., & Rodgers, M. A. J. (1987). *Radiation Chemistry, Principles and Applications*: VCH Publishers, New York.

Fu, X. C., Shen, W. X., Yao, Y. Y., & Hou, W. H. (2006). *Physical Chemistry (5th edition)*. Beijing: Higher Education Press.

Gómez, F., Martínez-Toledo, M. V., Salmerón, V., Rodelas, B., & González-López, J. (1999). Influence of the insecticides profenofos and diazinon on the microbial activities of Azospirillum brasilense. *Chemosphere,* 39(6), 945-957.

Gomez, S., Marchena, C. L., Renzini, M. S., Pizzio, L., & Pierellaa, L. (2015). In situ generated TiO2over zeolitic supports as reusablephotocatalysts for the degradation of dichlorvos. *Applied Catalysis B: Environmental,* 162, 167-173.

Griffin, R. (Producer). (1999). Human Health Risk Assessment [online]. Retrieved from http://www.ncbi.nlm.nih.gov/pmc/articles/PMC13922230/

Guittonneau, S., DeLaat, J., Dore, M., Duguet, J. P., & Bonnel, C. (1988). Comparative study of the photodegradation of aromatic compounds in water by UV and H2O2/UV.Environmental Science & Technology Letters(9), 1115-1128.

Guo, J., Ge, L., Li, X., Mu, C., & Li, D. (2014). Periodate oxidation of xanthan gum and its crosslinking effects on gelatin-based edible films. *Food Hydrocolloids,* 39, 243-250.

Gupta, V. K., Gupta, B., Rastogi, A., Agarwal, S., & Nayak, A. (2011). Pesticides removal from waste water by activated carbon prepared from waste rubber tire. *Water Research,* 45(13), 4047-4055.

Haghighi, M., & Nikoofar, K. (2014a). Nano TiO2/SiO2: An efficient and reusable catalyst for the synthesis of oxindole derivatives. *Journal of Saudi Chemical Society,* 3, 1-6.

Haghighi, M., & Nikoofar, K. (2014b). Nano TiO2/SiO2: An efficient and reusable catalyst for the synthesis of oxindole derivatives. *Journal of Saudi Chemical Society,* 15, 1-6.

Halminton, D. J., Ambrus, A., Dieterle, R. M., Katyam, A., Felsot, A. S., Harris, C. A., . . . Wong, S. S. (2003). Regulatory Limits for Pesticides Residue in Water. *Pure and Applied Chemistry,* 75(8), 1123-1155.

Han, W., Zhang, P., Zhu, W., Yin, J., & Li, L. (2004). Photocatalysis of p-chlorobenzoic acid in aqueous solution under irradiation of 254 nm and 185 nm UV light. *Water Research,* 38(19), 4197-4203.

Hangzhou weiku information & Technology Co., L. (Producer). (2008). Look for Chemicals: Profenofos. Retrieved from http://www.lookchem.com/Profenofos/

Harnpicharnchai, K., Chaiear, N., & Charerntanyarak, L. (2013). Residues of organophosphate pesticides used invegetable cultivation in ambient air, surface water, and soil in Bueng Niam Subdistricy, Khon Kaen, Thailand. *The Southeast Asian Journal of Tropical Medicine and Public Health,* 44(6), 1088-1097.

Hatchard, G., & Parker, A. (1956). A new sensitive chemical actinometer. II: Potassium ferrioxalate as a standard chemical actinometer. *Proceedings of the Royal Society of London A,* 235(1203), 518-536.

He, J., Fan, M., & Liu, X. (2010). Environmental Behavior of Profenofos Under Paddy Field Conditions. *Bulletin of Environmental Contamination and Toxicology,* 84, 771-774.

Heit, G., & Braun, M. (1997). VUV-photolysis of aqueous systems: Spatial differentiation between volumes of primary and secondary reactions. *Water Science and Technology,* 35(4), 25-30.

Heit, G., Neuner, A., Saugy, P.-Y., & Braun, A. M. (1998). Vacuum-UV (172 nm) Actinometry. The Quantum Yield of the Photolysis of Water. *The journal of Physical Chemistry,* 102, 5551-5561.

Hirahara, Y., Kimura, M., Inoue, T., Uchikawa, S., Otani, S., Haganuma, A., . . . Uchida, Y. (2005). Validation of Multiresidue Screening Methods for the Determination of 186 Pesticides in 11 Agricultural Products Using Gas Chromatography (GC). *Journal of Health Science,* 51(5), 617-627.

Hoffmann, M. R., Martin, S. T., Choi, W., & Bahnemann, D. W. (1995). Environmental Applications of Semiconductor Photocatalysis. *Chemical Reviews,* 95, 69-96.

Hongling, Y., Jiali, X., YangQingliang, Chen, Y., Yan, W., & Feng, Y. (2003). Mechanism of ozone decomposition on the surface of metal oxide,. *Chemical Research and Application,* 15, 1-5.

Houas, A., Lachheb, H., Ksibi, M., Elaloui, E., Guillard, C., & Herrmann, J.-M. (2001). Photocatalytic degradation pathway of methylene blue in water. *Applied Catalysis B: Environmental,* 31(2), 145-157.

Huang, H., Leung, D. Y. C., Kwong, P. C. W., Xiong, J., & Zhang, L. (2013). Enhanced photocatalytic degradation of methylene blue under vacuum ultraviolet irradiation. *Catalysis Today,* 201, 189-194.

Imoberdorf, G., & Mohseni, M. (2011). Degradation of natural organic matter in surface water using vacuum-UV irradiation. *Journal of Hazardous Materials,* 186(1), 240-246.

Irani, M., Keshtkar, A. R., & Moosavian, M. A. (2012). Removal of cadmium from aqueous solution using mesoporous PVA/TEOS/APTES composite nanofiber prepared by sol–gel/electrospinning. *Chemical Engineering Journal,* 200, 192-201.

Jaipieam, S. (2008). *Risk assessment of multi-route exposure to organophosphate pesticide of vegetable growers (A case study at Bang Rieng sub-district, Khuan Nieng district, Songkhla province)* (Doctor of Philosophy Thesis), Chulalongkorn University, Chulalongkorn University.

Jaroensin, P. (2006). *Removal of cyanide using ultraviolet ray and Titanium dioxide in continuous flow.* (Master's degree), Chulalongkorn University, Faculty of Engineering.

Jing, C., Peng-yi, Z., & Jian, L. (2007). Photodegradation of perfluorooctanoic acid by 185 nm vacuum ultraviolet light. *Journal of Environmental Science, 19,* 387-390.

Jung, K. Y., & Park, S. B. (2003). Anatase-phase titania: preparation by embedding silica and photocatalytic activity for the decomposition of trichlororthylene. *Journal of Photochemistry and Photobiology A: Chemistry-Elsevier, 127.*

Kaewsaenee, J., Visal-athaphand, P., Supaphol, P., & Pavarajarn, V. (2010). Fabrication and characterization of neat and aluminium-doped titanium (IV) oxide fibers prepared by combined sol–gel and electrospinning techniques. *Ceramics International, 36(7),* 2055-2061.

Kaliwoh, N., Zhang, J.-Y., & Boyd, I. W. (2000). Titanium dioxide films prepared by photo-induced sol–gel processing using 172 nm excimer lamps. *Surface and Coatings Technology, 125(1–3),* 424-427.

Kang, J.-x., Lu, L., Zhan, W., Li, B., Li, D.-s., Ren, Y.-z., & Liu, D.-q. (2011). Photocatalytic pretreatment of oily wastewater from the restaurant by a vacuum ultraviolet/TiO2 system. *Journal of Hazardous Materials, 186(1),* 849-854.

Keen, O. S., Love, N. G., & Linden, K. G. (2012). The role of effluent nitrate in trace organic chemical oxidation during UV disinfection. *Water Research, 46(16),* 5224-5234.

Khemvong, S., & Choungpim, S. (2010). *Pesticide residues in agricultural products from the process of good agricultural practce (GAP) in lower southern Thailand.* Paper presented at the The Sixth National Agricultural Systems Seminar, Faculty of Agriculture, Chiangmai University. http://www.mcc.cmu.ac.th/Seminar/pdf/989629980.pdf

Khezrianjoo, S., & Revanasiddappa, H. (2012). Langmuir-Hinshelwood Kinetic Expression for the Photocatalytic Degradation of Metanil Yellow Aqueous Solutions by ZnO Catalyst. *Chemical Sciences Journal, 85,* 1-7.

Kommineni, S., Zoeckler, J., Stocking, A., Liang, S., Flores, A., Kavanaugh, M., . . . Stocking, A. (2000). Advanced Oxidation Processes (pp. 109-208). Retrieved from http://www.nwri-usa.org/pdfs/TTChapter3AOPs.pdf.

Krieger, R. (2010). *Hayes' Handbook of Pesticides Toxicology* (Vol. 1): Macmillan Publishing Solutions.

Kutschera, K., Bornick, H., & Worch, E. (2009). Photoinitiated oxidation of geosmin and 2-methylisoborneol by irradiation with 254 nm and 185 nm UV light. *Water Research,* 43(8), 2224-2232.

Lai, Y., Chen, Y., Zhuang, H., & Lin, C. (2008). A facile method for synthesis of Ag/TiO2 nanostructures. *Materials Letters,* 62, 3688–3690.

Leifer, A. (1988). *The Kinetics of Environmental Aquatic Photochemistry (ACS Professional Reference Books)*. Washington DC: American Chemical Society.

Liu, P., Zhang, H., Feng, Y., Yang, F., & Zhang, J. (2014). Removal of trace antibiotics from wastewater: A systematic study of nanofiltration combined with ozone-based advanced oxidation processes. *Chemical Engineering Journal,* 240, 211-220.

Lu, J. (2010). Multipesticides Residue Assessment of Agricultural Soil and Waterin Major Farming Areas in Benguet, Phillippines. *Archives of Environmental Contamination and Toxicology,* 59(175-181).

Macedo, L. C., Zaia, D. A. M., Moore, G. J., & Santana, H. D. (2007). Degradaion of leather dye on TiO2: A study of applied parameters on photoelectrocatalysis. *Journal of Photochemistry and Photobiology A: Chemistry,* 185, 86-93.

Mahata, S., & Kundu, D. (2009). Hydrothermal synthesis of aqeous nano-TiO2 sols. *Materials Science-Poland,* 27, 463-470.

Malghani, S., Chatterjee, N., Hu, X., & Zejiao, L. (2009a). Isolation and characterization of a profenofos degrading bacterium. *Journal of Environmental Sciences,* 21(11), 1591-1597.

Malghani, S., Chatterjee, N., Hu, X., & Zejiao, L. (2009b). Isolation and characterization of a profenofos degrading bacterium. *Journal of Environmental Sciences,* 21, 1591–1597.

Martínez-Toledo, M. V., Salmerón, V., & González-López, J. (1992). Effect of an organophosphorus insecticide, profenofos, on agricultural soil microflora. *Chemosphere,* 24(1), 71-80.

Mattisson, D. R., Nightingale, M. S., & Shiromizu, K. (1983). Effects of toxic substances on female reproduction. *Environmental Health Perspectives,* 48, 43-52.

Metcalf, & Eddy. (2003). *Wastewater Engineering*: McGraw-Hill International Edition, USA.

Meyer, A., Seidler, F. J., & Slotkin, T. A. (2004). Developmental effects onchlorpyrifos extend beyond neurotoxicity: critical periods for immediate and delayed-onset effects on cardiac and hepatic cell sihnaling. *Environmental Health Perspectives,* 112, 170-178.

Miloševic, M. D., Logar, M. M., Poharc-Logar, A. V., & JakšiT, N. L. (2013). Orientation and Optical Polarized Spectra (380–900 nm) of Methylene Blue Crystals on a Glass Surface. *Journal of Spectroscopy,* 923739(1-6).

MingMa, C., Hong, G. B., Chen, H. W., Hang, N. T., & Shen, Y. S. (2011). Photooxidation Contribution Study on the Decomposition of AzoDyes inAqueous Solutions by VUV-Based AOPs. *Hindawi Publishing Corporation International Journal of Photoenergy,* 156, 1-8.

Moussavi, G., Hossaini, H., Jafari, S. J., & Farokhi, M. (2014). Comparing the efficacy of UVC, UVC/ZnO and VUV processes for oxidation of organophosphate pesticides in water. *Journal of Photochemistry and Photobiology A: Chemistry,* 290, 86-93.

Muggli, D. S., Lowery, K. H., & Falconer, J. L. (1998). Identification of Adsorbed Species during Steady-State Photocatalytic Oxidation of Ethanol on TiO2. *Journal of Catalysis,* 111, 180.

Naeem, K., & Ouyang, F. (2013). Influence of supports on photocatalytic degradation of phenol and 4-chlorophenol in aqueous suspensions of titanium dioxide. *Journal of Environmental Sciences (China),* 25(2), 399-404.

Nakata, K., & Fujishima, A. (2012). TiO2 photocatalysis: Design and applications. *Journal of Photochemistry and Photobiology C: Photochemistry Reviews,* 13(3), 169-189.

Nakazawa, T. (1974). Chronic organophosphorus intoxication in women. *Journal of The Japanese Association of Rural Medicine, 22*, 256-261.

Nasrabadi, T., Bidhendi, G., Karbassi, A., Grathwohl, P., & Mehrdadi, N. (2011). Impact of major organophosphate pesticides used in agriculture to surface water and Sediment quality (Southern Caspian Sea basin, Haraz River). *Environmental Earth Sciences, 63*, 873-883.

National Bureau of Agricultural Commodity and Food Standards (AEFS). (2008). Maximum Residue Limit (MRL) in food, Thailand. from Agriculural Standard http://www.acfs.go.th/agri_standards.php

National Water Research Instituete (NWRI). (2013). Advanced Oxidation Process. http://www.nwri-usa.org/pdfs/TTChapter3AOPs.pdf

Neshvar, N., Salari, D., & Khataee, A. R. (2004). Photocatalytic degradation of azo dye acid red 14 in water on ZnO as an alternative catalyst to TiO2. *Journal of Photochemistry and Photobiology A: Chemistry, 162*(2-3), 317-322.

Nirmala, R., Kim, H. Y., Navamathavan, R., Yi, C., Won, J. J., Jeon, K., . . . El-Newehy, M. (2012). Photocatalytic activities of electrospun tin oxide doped titanium dioxide nanofibers. *Ceramics International, 38*(6), 4533-4540.

Ochiai, T., Masuko, K., Tago, S., Nakano, R., Niitsu, Y., Kobayashi, G., . . . Fujishima, A. (2013). Development of a hybrid environmental purification unit by using of excimer VUV lamps with TiO2 coated titanium mesh filter. *Chemical Engineering Journal, 218*(0), 327-332.

Ollis, D. F. (1985). Contaminant degradation in water. *Environmental Sciences Technology, 19*, 480-484.

Oppenlander, T., Walddorfer, C., Burqbacher, J., Kiermeier, M., Lachner, K., & Weinschott, H. (2005). Improved vacuum-UV (VUV)-initiated photomineralization of organic compounds in water with a xenon excimer flow-through photoreactor (Xe2* lamp, 172 nm) containing an axially centered ceramic oxygenator. *Chemosphere, 60*, 302-309.

Padikkaparambil, S., Narayanan, B., Yaakob, Z., Viswanathan, S., & Tasirin1, S. M. (2013). Au/TiO2 Reusable Photocatalysts for Dye Degradation. *International Journal of Photoenergy, 2013*, 1-10.

Parsons, S. (2004). *Advanced Oxidation Process for Water and Wastewater Treatment*: IWA Publishing.

Peral, J., Domènec, X., & Ollis, D. F. (1997). Heterogeneous Photocatalysis for Purification, Decontamination and Deodorization of Air. *Chemical Technology and Biotechnology,* 70, 117.

Petrick, L. M., Sabach, S., & Dubowski, Y. (2013). Degradation of VX Surrogate Profenofos on Surfaces via in Situ Photo-oxidation. *Environmental Sciences and Technology,* 47, 8751-8758.

Piera, E., Ayllón, J. A., Doménech, X., & Peral, J. (2002). TiO2 deactivation during gas-phase photocatalytic oxidation of ethanol. *Catalysis Today,* 76, 259–270.

Pingfeng, F., Pengyi, Z., & Jia, L. (2011). Photocatalytic degradation of low concentration formaldehyde and simultaneous elimination of ozone by-product using palladium modified TiO2 films under UV254+185nm irradiation. *Applied Catalysis B: Environmental,* 105(1–2), 220-228.

Prasertwongchai, A. (2011). *Profenofos Removal in Water using Vacuum Ultraviolet (VUV) Process* (Master's Thesis), Department of Environmental Engineering, Faculty of Engineering, Khon Kaen University.

Pruden, A. L., & Ollis, D. F. (1983). Photoassisted heterogeneous catalysis: the

degradation of trichloroethylene in water. *Journal of Catalysis,* 82, 404-417.

Putta, T. (2009a). *Photocatalytic Characterictics of Titanium Dioxide Doped with Various Elements and Hydrothermal Treatment Under Visible - Light Activation.* (Degree of Doctor), Chulalongkorn University.

Putta, T. (2009b). *Photocatalytic characteristis of titanium dioxide doped with various elements and hydrothermal treatment under visible-light activation.* (Degree of Doctor of Philosophy), Chulalongkorn University, Graduation School.

Ramathibodi Poison Center (Producer). (2001). Organophosphate [online]. *Poison & Drug Information Bulletin*. Retrieved from http://med.mahidol.ac.th/poisoncenter/th/bulletin/bul_01/v9n2/Op

Ratpukdi, T., Siripattanakul, S., & Khan, E. (2010). Mineralization and biodegradability enhancement of natural organic matter by ozoneeVUV in

comparison with ozone, VUV, ozoneeUV, and UV: Effects of pH and ozone dose. *Water Research,* 44, 3531-3543.

Rongchang, W., Dianjun, R., Siqing, X., Yalei, Z., & Jianfu, Z. (2009). Photocatalytic degradation of Bisphenol A (BPA) using immobilized TiO2 and UV illumination in a horizontal circulating bed photocatalytic reactor (HCBPR). *Journal of Hazardous Materials,* 169(1–3), 926-932.

Rosenfeldt, E., Linden, K. G., Canonica, S., & Gunten, U. v. (2006). Comparison of the efficiency of OH radical formation during ozonation and the advanced oxidation processes O3/H2O2 and UV/H2O2. *Water Research,* 40(20), 3695-3704.

Rosenfeldt, E. J., & Linden, K. G. (2007). The ROH,UV Concept to Characterize and the Model UV/H2O2 Process in Natural Waters. *Environmental Sciences and Technology,* 41, 2548-2553.

Sankom, A. (1999). *Application of oxidizing agents on Watching process to Reduce Organophosphate Residue on Fresh Vegetable.* (Master's Thesis), Department of Food Science and Tecnology, Faculty of Science, Kasetsart University.

Scherrer, P. (1918). Bestimmung der Grösse und der inneren Struktur von Kolloidteilchen mittels Röntgenstrahlen. *Nachrichten von der Gesellschaft der Wissenschaften zu Göttingen,* 26, 98-100.

Siriwong, W., Taneepanichskul, N., Norkaew, S., Siripattanakul, S., Chotpantarat, S., & Robson, M. (2011). Health Risk Assessment of Organophosphate Pesticides Exposure for Chilli-growing Farmers in Ubon Ratchathani Province, Northeastern, Thailand. *Epidemiology,* 22(1), S84-S85.

Space Environmental Technology. (2013). ISO Solar Irradiances Standard 21348. http://www.spacewx.com/SpaceWxPubs.html

Srisawangwong, W., Saisuphan, P., Prasopsak, J., & Paewpolsong, C. (2009). *Pesticise residues in vegetables andvfruits in upper northeast Thailand followed good agricultural practice (GAP).* Paper presented at the The Seventh Center for Agricultural Resource Systems Research Faculty of Agriculture, Chiangmai University. http://www.mcc.cmu.ac.th/Seminar/pdf/P989630056.pdf

Stefan, M. I. (2005). Study on the Photocatalytic Mechanism of Red 141 Dye Wastewater with an 185 nm Vacuum-UV lamp. *Journaol of Water Environmental and Technology,* 3, 19-27.

Torrents, A., Anderson, B. G., Bilboulian, S., Johnson, W. E., & Hapeman, C. (1997). Atrazine photolysis: mechanistic investigations of direct and nitrate-mediated hydroxyl radical processes and influence of diissolved organic carbon from Chesapeake Bay. *Environmental Science and Technology,* 31(5), 1476-1482.

Tsai, W.-T., Lee, M.-K., Su, T.-Y., & Chang, Y.-M. (2009). Photodegradation of bisphenol-A in a batch TiO2 suspension reactor. *Journal of Hazardous Materials,* 168, 269–275.

U.S.EPA. (1984). 40 CFR Part 158. Data Requirements for Pesticides Registration; Final rule (Vol. Fed. Reg, 49, pp. 42856-42905): United States Environmental Protection Agency.

U.S.EPA. (1996). EFED Risk Characterization and Recomendations for the Regeristation of Profenofos: United States Environmental Protection Agency

U.S.EPA. (2000). Interim Reregistration Eligibility Decision (IRED), Profenofos (Vol. Prevention, Pesticides And Toxic Substances (7508C)).

United States Environmental Protection Agency (U.S.EPA). (2000). Finalization of Interim Reregistration Eligibility Decisions (IREDs) and Interim Tolerance Reassessment and Risk Management Decisions (TREDs) for the Organophosphate Pesticides, and Completion of the Tolerance Reassessment and Reregistration Eligibility Process for the Organophosphate Pesticides (Vol. Prevention, Pesticides And Toxic Substances (7508C), pp. 1-100).

Wang, C. W., & Liang, C. (2014). Oxidative degradation of TMAH solution with UV persulfate activation. *Chemical Engineering Journal,* 254, 472-478.

Watanabe, N., Horikoshi, S., Kawabe, H., sufie, Y., Zhao, J., & Hidaka, H. (2003). Photodegradation mechanism for bisphenol A at the TiO2/H2O interfaces. *Chemosphere 52,* 52, 851–859.

Water Treatment Guide. (2007). Ultraviolet Systems Questions & Answers. from Applied Membranes, Inc. http://www.watertreatmentguide.com/ultraviolet_systems.htm

Watthanaarun, J. (2004). *Effects of synthesis parameters and secondary metal doping on physical and chemical properties of the electrospun titanium (IV) oxide nanofibers.* (Master's Thesis), Department of Chemical Engineering, Faculty of Engineering, Chulalongkorn University.

Watthanaarun, J., Supaphol, P., & Pavarajarn, V. (2007). Photocatalytic Activity of Neat and Silicon-Doped Titanium (IV) Oxide Nanofibers Prepared by Combined Sol-Gel and Electrospinning Tecniques. *Journal of Nanoscience and Nanotechnology,* 7, 2443-2450.

Wols, B. A., Harmsen, D. J. H., Beerendonk, E. F., & Hofman-Caris, C. H. M. (2015). Predicting pharmaceutical degradation by UV (MP)/H2O2 processes: A kinetic model. *Chemical Engineering Journal,* 263, 336-345.

Xia, D. L. a. Y. (2003). Fabrication of Titania Nanofibers by Electrospinning. *Nanoletters,* 3(4), 555-560.

Xianzhi, F. U., Clark, L. A., Yang, Q., & Anderson, M. A. (1996). Enhanced photocatalytic performance of titania-based binary metal oxides: TiO2/SiO2 and TiO2/ZrO2. *Environmental Science and Technology,* 30(2), 647-653.

Xing, R., Zheng, Z., & Wen, D. (2015). Comparison between UV and VUV photolysis for the pre- and post-treatment of coking wastewater. *Journal of Environmental Sciences.*

Xu, G.-R., Wang, J.-N., & Li, C.-J. (2013). Template directed preparation of TiO2 nanomaterials with tunable morphologies and their photocatalytic activity research. *Applied Surface Science,* 279(0), 103-108.

Yixin, Y., Hongbinb, C., Paic, P., & Hongmiao, B. (2014). Degradation and transformation of atrazine under catalyzedozonation process with TiO2as catalyst. *Journal of Hazardous Materials,* 279, 444-451.

Yoon, S. H., Lee, J. H., Oh, S., & Yang, J. E. (2008). Photochemical oxidation of AS (III) by vcuum-UV lamp irradiation. *Water Research,* 42(3455-3463).

Zamy, C., Mazellier, P., & Legube, B. (2004). Phototransformation of selected organophosphorus pesticides in dilute aqueous solutions. *Water Resource,* 38(9), 2304-2313.

Zoschke, K., Börnick, H., & Worch, E. (2014). Vacuum-UV radiation at 185 nm in water treatment – A review. *Water Research,* 52(0), 131-145.

REFERENCES

APPENDIX

APPENDIX A

Analytical Method of Profenofos solutions

Analytical Method of Profenofos

1. Analytical method

1.1 Sample preparation

The obtained samples should be periodically extracted before GC-µECD analysis by using 0.1% by volume of n-hexane: acetic acid solvent (1:1 ratio) in a total volume of 1.2 ml, after that the samples were well shaken using a Thermomixer at 1,700 rpm for 20 min, and then the solid suspensions were separated by centrifugation at 14,000 rpm for 5 min. The supernatant liquid in microcentrifuge tube was sucked with a plastic syringe and immediately filtered through a 0.2-µm Nylon filter in order to remove the electrospun TiO_2 nanofibers and solid particles from the collected solution. The filtered samples were stored at 4 $^\circ$C in the amber glass prior to analysis.

1.2 Sample analysis

The samples from 1.1 were examined by using gas chromatography – electron capture detection (GC – µECD, 6890N, Agilent Technologies, USA) equipped with a Ni^{63} electron capture detector with a column (HP-5, 19091J-413, 0.25 µm film, 0.32 mm x 30 m, Agilent Technologies, USA). The GC-ECD method for profenofos analysis was used with some minor modifications proposed by (Malghani et al., 2009b). The operating conditions included 1.0 µL of injection volume, splitless mode, 240 ℃ of injection temperature, 300 ℃ of detector temperature, 170 ℃ of initial temperature (3 min), 40 ℃/min to 230 ℃ (5 min), 50 ℃ of post temperature (0 min), and 9.5 min of total run time. The carrier gas is helium with 27 cm/sec of flow rate, and profenofos peak was showed at 8.85 min of retention time. The chromatogram diagram of profenofos was shown in Figure A.1.
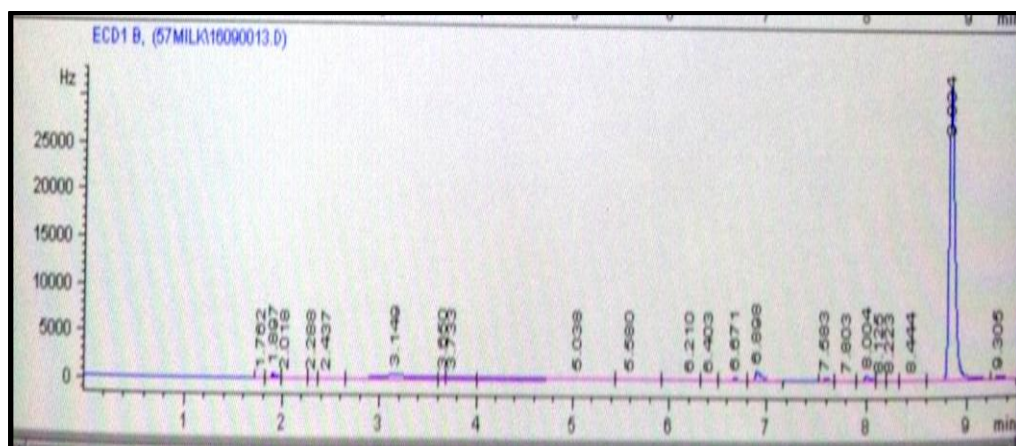
Figure A.1 The chromatogram diagram of profenofos

1.3 Standard curve of profenofos

The commercial grade of profenofos from Nonkasate Co., Ltd, Thailand with 50% W/V was used to prepare a standard curve. All standard solution concentrations of profenofos were diluted in hexane including 0.2, 0.4, 0.6, 2, 4, and 10 mg/L by serial dilution. Prior to GC analysis, these solutions must be filtered through a 0.2-µm Nylon filter in order to remove the solid particles from the solution. The concentration of profenofos was analyzed by using GC-ECD, and the result was plotted to obtain a standard curve as seen in Table A.2 and Figure A.1.

Table A.1 Area data from GC-µECD analysis

Concentration (mg/L)	Area		Average Area
	No.1	No.2	
0.2	253	255	254.00
0.4	318.7	334.6	326.70
0.8	1,153.8	1,163.9	1,158.90
2	2,540.9	2,546.4	2,543.60
4	5,847.8	5,859.9	5,853.80
10	14,659.4	14,659.1	14,659.30
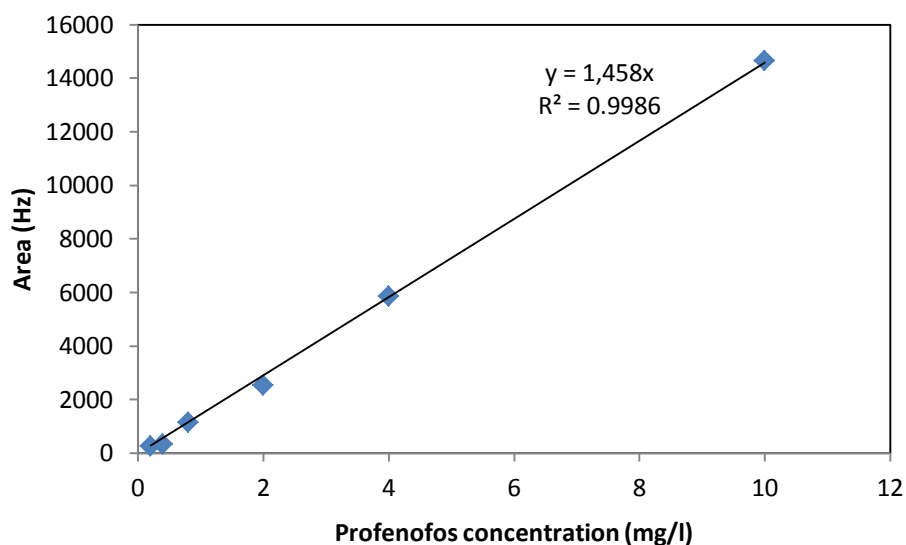
Figure A.2 The standard curve of profenofos plotted between PF concentrations and Area

The slope of standard curve was 1,458 Hz./mg/L

The concentrations of PF at specific time interval were calculated according to equation A.1

$$PF\ concentration\ (\mu M) = \frac{(Area)}{1,458} \qquad (A.1)$$

1.4 The recovery percentage of profenofos solution

For checking the obtain recovery percentage of profenofos, 1,000 mg/L of profenofos stock solution was utilized to prepare these concentration including 0.1, 0.2, 0.4, 0.8, 2, and 10 mg/L in DI water, and then each concentration was immediately extracted by using 0.1% by volume of n-hexane: acetic acid solvent (1:1 ratio) in a total volume of 1.2 ml, shaking with a Thermomixer at 1,700 rpm for 20 min and centrifugation at 14,000 rpm for 5 min. The supernatant liquid was sucked to filter through a 0.2-µm Nylon filter for GC-µECD analysis. The recovery percentage

of profenofos solutions were revealed in Table A.2. The results were in the range of 70 – 120% that could be accepted in this research study.

Table A.2 The recovery percentage of profenofos solutions

Concentration (mg/L)	Recovery Percentage (%)			Average Recovery Percentage (%)	SD	% RSD
	No.1	No.2	No.3			
0.1*	-	-	-	-	-	-
0.2	93.74	92.93	94.51	93.73	0.79	0.84
0.4	93.44	93.23	92.76	93.14	0.35	0.37
0.8	90.45	92.89	92.75	92.03	1.37	1.49
2	92.22	92.05	90.63	91.63	0.87	0.95
10	93.56	94.37	94.72	94.22	0.60	0.63

*Detection limit of profenofos is 0.1 mg/L

When % RSD is the precision value that can express the concordance of the experimental data more than duplicate experiment. Some data might be nearly or equally, indicating that the experimental measurement has high certainty. Percent of RSD can be calculated from equation A.2.

$$\% \, RSD \;\; = \;\; \frac{SD}{X} \; x \; 100 \tag{A.2}$$

where SD is standard deviation and X is average. It should be noted that too less value of % RSD is meant to having high precision.

APPENDIX B

Analytical Method of Methylene Blue

Analytical Method of Methylene Blue

1. Standard curve of methylene blue, a probe compound

The solids of methylene blue from Sigma Aldrich, Germany were used to prepare a standard curve with various concentrations including 0.1, 0.5, 1, 5, 10 μM dissolved in DI water by serial dilution. The concentration of methylene blue was examined by using a UV-Visible spectrophotometer, and the result was plotted to generate a standard curve as seen in Table B.1 and Figure B.1.

Table B.1 Absorbance data from UV-spectrometer analysis

Concentration (mg/L)	Absorbance		Average Absorbance
	No. 1	No. 2	
0.1	0.005	0.005	0.005
0.5	0.036	0.041	0.039
1	0.050	0.062	0.056
5	0.279	0.286	0.283
10	0.568	0.576	0.569
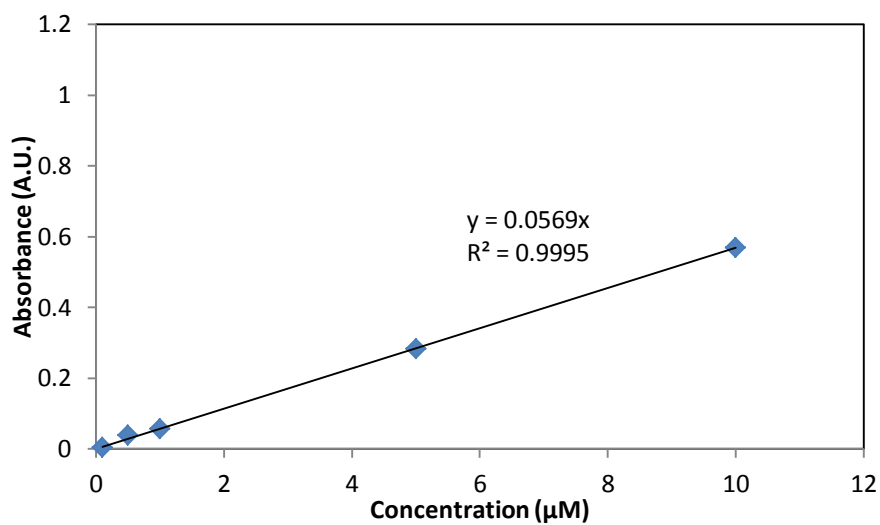
Figure B.1 The standard curve of Methylene blue plotted between MB concentrations and absorbance

The slope of standard curve was 0.0565 AU./μM

The concentrations of MB at specific time interval were calculated according to equation B.1

$$MB\ concentration\ (\mu M) = \frac{(Absorbance)}{0.0569} \tag{B.1}$$

APPENDIX C

Study of Profenofos Concentration Degradation

Table C.1 Profenofos concentration from the control experiment

Irradiation time (min)	Concentration of profenofos (mg/L)			
	No.1	**No.2**	**No.3**	**No.1**
0	10.21	10.31	10.25	10.26
2	10.25	10.23	10.08	10.19
5	10.15	10.26	10.18	10.20
10	9.88	10.02	10.31	10.07
15	9.90	9.76	10.07	9.91
20	9.75	9.66	9.90	9.77
25	9.90	9.95	10.02	9.96
30	10.21	10.31	10.25	10.01

จุฬาลงกรณ์มหาวิทยาลัย
CHULALONGKORN UNIVERSITY

Table C.2 Profenofos concentration from each photolytic experiment

Irradiation time (min)	Concentration of profenofos (mg/L)					
	UV			VUV		
	No.1	No.2	Avg.	No.1	No.2	Avg.
0	9.86	9.78	9.86	9.80	9.60	9.70
2	8.79	8.78	8.79	7.10	6.91	7.01
5	7.88	7.88	7.88	5.31	5.56	5.43
10	6.71	6.70	6.71	3.07	3.11	3.09
15	5.75	5.51	5.75	1.90	1.96	1.93
20	4.63	4.63	4.63	1.20	1.16	1.18
25	3.89	3.75	3.89	0.65	0.65	0.65
30	3.49	3.24	3.49	0.47	0.47	0.47

Table C.3 Profenofos concentration from the UV process with various dosages of P25 nanopowder

Irradiation time (min)	Concentration of profenofos (mg/L)											
	0 g/L			0.05 g/L			0.10 g/L			0.20 g/L		
	No.1	No.2	Avg.	No.1	No.2	Avg.	No.1	No.2	Avg.	No.1	No.2	Avg.
0[b]	9.86	9.78	9.86	9.82	9.71	9.77	9.82	9.71	9.77	9.68	9.68	9.68
0[a]	9.86	9.78	9.86	8.85	8.85	8.85	8.13	8.13	8.13	7.87	7.87	7.87
2	8.79	8.78	8.79	6.77	6.77	6.77	5.24	5.24	5.24	4.53	4.53	4.53
5	7.88	7.88	7.88	6.19	6.18	6.19	4.56	4.56	4.56	4.02	4.02	4.02
10	6.71	6.70	6.71	5.17	5.17	5.17	3.92	3.91	3.92	3.36	3.35	3.36
15	5.75	5.51	5.75	4.31	4.32	4.31	3.10	3.26	3.18	2.86	2.86	2.86
20	4.63	4.63	4.63	3.60	3.62	3.61	2.71	2.71	2.71	2.34	2.33	2.34
25	3.89	3.75	3.89	2.81	3.28	3.05	2.26	2.27	2.26	1.94	1.95	1.94
30	3.49	3.24	3.49	2.76	2.80	2.78	1.95	1.94	1.95	1.67	1.67	1.67

[b] Catalyst before absorbed in profenofos solution in the absence of light 30 min

[a] Catalyst after absorbed in profenofos solution in the absence of light 30 m

Table C.4 Profenofos concentration from the VUV process with various dosages of P25 nanopowder

Irradiation time (min)	Concentration of profenofos (mg/L)											
	0 g/L			0.05 g/L			0.10 g/L			0.20 g/L		
	No.1	No.2	Avg.	No.1	No.2	Avg.	No.1	No.2	Avg.	No.1	No.2	Avg.
0[b]	9.80	9.60	9.70	9.81	9.80	9.81	9.83	9.70	9.77	9.73	9.81	9.77
0[a]	9.80	9.60	9.70	8.89	8.89	8.89	8.09	8.10	8.78	7.93	7.94	7.93
2	7.10	6.91	7.01	6.06	6.07	6.06	5.15	5.15	5.15	4.17	4.17	4.17
5	5.31	5.56	5.43	4.27	4.28	4.27	3.63	3.63	3.63	3.00	3.00	3.00
10	3.07	3.11	3.09	2.54	2.54	2.54	2.03	2.03	2.03	1.63	1.63	1.63
15	1.90	1.96	1.93	1.50	1.50	1.50	1.14	1.14	1.14	0.88	0.87	0.88
20	1.20	1.16	1.18	0.94	0.94	0.94	0.68	0.67	0.68	0.53	0.53	0.53
25	0.65	0.65	0.65	0.52	0.52	0.52	0.41	0.41	0.41	0.32	0.33	0.32
30	0.47	0.47	0.47	0.36	0.37	0.36	0.26	0.26	0.26	0.24	0.23	0.24

[b] Catalyst before absorbed in profenofos solution in the absence of light 30 min

[a] Catalyst after absorbed in profenofos solution in the absence of light 30 m

Table C.5 Profenofos concentration from the UV process with various dosages of TiO$_2$ nanofibers photocatalyst

Irradiation time (min)	Concentration of profenofos (mg/L)											
	0 g/L			0.05 g/L			0.10 g/L			0.20 g/L		
	No.1	No.2	Avg.	No.1	No.2	Avg.	No.1	No.2	Avg.	No.1	No.2	Avg.
0[b]	9.86	9.78	9.86	11.01	10.72	10.86	10.17	9.92	10.05	10.49	9.92	10.20
0[a]	9.86	9.78	9.86	10.06	10.08	10.07	9.14	8.82	8.98	8.43	8.66	8.54
2	8.79	8.78	8.79	8.56	8.92	8.74	8.07	7.88	7.97	7.02	7.00	7.01
5	7.88	7.88	7.88	7.60	7.01	7.30	6.59	6.70	6.64	6.39	6.64	6.51
10	6.71	6.70	6.71	6.31	6.47	6.39	5.44	5.37	5.41	5.02	5.31	5.16
15	5.75	5.51	5.75	4.93	5.22	5.08	4.45	4.61	4.53	4.16	4.16	4.16
20	4.63	4.63	4.63	4.45	4.73	4.59	3.80	3.73	3.77	3.59	3.36	3.48
25	3.89	3.75	3.89	3.61	3.88	3.74	3.27	3.22	3.24	3.20	3.22	3.21
30	3.49	3.24	3.49	3.64	3.43	3.54	3.05	2.80	2.92	2.53	2.16	2.34

[b] Catalyst before absorbed in profenofos solution in the absence of light 30 min

[a] Catalyst after absorbed in profenofos solution in the absence of light 30 m

Table C.6 Profenofos concentration from the VUV process with various dosages of TiO$_2$ nanofibers photocatalyst

Irradiation time (min)	Concentration of profenofos (mg/L)											
	0 g/L			0.05 g/L			0.10 g/L			0.20 g/L		
	No.1	No.2	Avg.	No.1	No.2	Avg.	No.1	No.2	Avg.	No.1	No.2	Avg.
0[b]	9.80	9.60	9.70	9.80	10.02	9.91	11.12	9.95	10.53	10.20	10.14	10.17
0[a]	9.80	9.60	9.70	9.52	8.88	9.20	8.80	8.98	8.89	8.40	8.90	8.65
2	7.10	6.91	7.01	6.39	6.67	6.53	5.59	5.61	5.60	4.01	4.56	4.29
5	5.31	5.56	5.43	4.94	4.61	4.77	3.79	4.25	4.02	3.23	3.11	3.17
10	3.07	3.11	3.09	2.26	2.57	2.41	2.70	2.15	2.43	1.67	1.87	1.77
15	1.90	1.96	1.93	2.09	1.93	2.01	1.20	1.08	1.14	0.92	0.98	0.95
20	1.20	1.16	1.18	0.94	0.88	0.91	0.98	0.86	0.92	0.61	0.41	0.51
25	0.65	0.65	0.65	0.56	0.57	0.57	0.45	0.43	0.44	0.38	0.32	0.35
30	0.47	0.47	0.47	0.44	0.42	0.43	0.41	0.38	0.40	0.36	0.31	0.33

[b] Catalyst before absorbed in profenofos solution in the absence of light 30 min

[a] Catalyst after absorbed in profenofos solution in the absence of light 30 m

APPENDIX D

Study of Profenofos Degradation Efficiency

Table D.1 Profenofos efficiency from each photolytic experiment

Irradiation time (min)	Degradation Efficiency (%)	
	UV	VUV
0	0.00	0.00
2	10.54	27.78
5	19.75	43.97
10	31.71	68.15
15	42.70	80.12
20	52.87	87.85
25	61.10	93.31
30	65.73	95.14

Table D.2 Profenofos efficiency from the UV process with various dosages of P25 nanopowder

Irradiation time (min)	Degradation Efficiency (%)			
	0 g/L	0.05 g/L	0.10 g/L	0.20 g/L
0^b	0.00	0.00	0.00	0.00
0^a	0.00	9.44	16.78	17.53
2	10.54	30.70	46.38	52.53
5	19.75	36.67	53.34	57.85
10	31.71	47.09	59.92	64.82
15	42.70	55.85	67.47	70.03
20	52.87	63.03	72.27	75.50
25	61.10	68.82	76.84	79.63
30	65.73	71.56	80.07	82.49

[b] Catalyst before absorbed in profenofos solution in the absence of light 30 min

[a] Catalyst after absorbed in profenofos solution in the absence of light 30 min

Table D.3 Profenofos efficiency from the VUV process with various dosages of P25 nanopowder

Irradiation time (min)	Degradation Efficiency (%)			
	0 g/L	0.05 g/L	0.10 g/L	0.20 g/L
0[b]	0.00	0.00	0.00	0.00
0[a]	0.00	10.18	17.14	18.79
2	27.78	38.74	47.27	57.33
5	43.97	56.84	62.86	69.29
10	68.15	74.32	79.20	83.30
15	80.12	84.83	88.32	91.02
20	87.85	90.52	93.08	94.59
25	93.31	94.77	95.80	96.68
30	95.14	96.33	97.36	97.58

[b] Catalyst before absorbed in profenofos solution in the absence of light 30 min

[a] Catalyst after absorbed in profenofos solution in the absence of light 30 min

Table D.4 Profenofos efficiency from the UV process with various dosages of TiO_2 nanofibers photocatalyst

Irradiation time (min)	Degradation Efficiency (%)			
	0 g/L	0.05 g/L	0.10 g/L	0.20 g/L
0[b]	0.00	0.00	0.00	0.00
0[a]	0.00	7.29	10.65	16.24
2	10.54	19.50	20.67	31.29
5	19.75	32.75	33.89	36.16
10	31.71	41.19	46.19	49.38
15	42.70	53.26	54.93	59.22
20	52.87	57.74	62.51	65.93
25	61.10	65.53	67.74	68.49
30	65.73	67.43	70.90	77.05

[b] Catalyst before absorbed in profenofos solution in the absence of light 30 min

[a] Catalyst after absorbed in profenofos solution in the absence of light 30 min

Table D.5 Profenofos efficiency from the VUV process with various dosages of TiO_2 nanofibers photocatalyst

Irradiation time (min)	Degradation Efficiency (%)			
	0 g/L	0.05 g/L	0.10 g/L	0.20 g/L
0[b]	0.00	0.00	0.00	0.00
0[a]	0.00	7.17	15.57	14.93
2	27.78	34.12	46.83	57.85
5	43.97	51.84	61.79	68.83
10	68.15	75.64	76.96	82.60
15	80.12	79.73	89.14	90.68
20	87.85	90.81	91.25	94.99
25	93.31	94.28	95.80	96.59
30	95.14	95.65	96.24	96.88

[b] Catalyst before absorbed in profenofos solution in the absence of light 30 min

[a] Catalyst after absorbed in profenofos solution in the absence of light 30 min

APPENDIX E

Study of Profenofos Mineralization

Table E.1 Profenofos mineralization from each photolytic experiment

Irradiation time (min)	UV		VUV	
	TOC (mg/L)	Mineralization (%)	TOC (mg/L)	Mineralization (%)
0	4.80	0.00	4.98	0.00
30	4.62	3.75	4.59	7.83
60	4.45	7.29	2.49	50.00
90	3.92	18.33	1.65	66.87
120	3.78	21.25	1.34	73.09

Table E.2 Profenofos mineralization from the UV process with various dosages of P25 nanopowder

Irradiation time (min)	0 g/L		0.05 g/L		0.10 g/L		0.20 g/L	
	TOC (mg/L)	Mineralization (%)	TOC (mg/L)	Mineralization (%)	TOC (mg/L)	Mineralization (%)	TOC (mg/L)	Mineralization (%)
0^b	4.80	0.00	4.66	0.00	5.48	0.00	4.94	0.00
30	4.62	3.75	4.14	11.16	3.54	35.40	3.08	37.65
60	4.45	7.29	3.33	28.54	3.05	44.34	2.99	39.47
90	3.92	18.33	3.03	34.98	3.20	41.61	2.51	49.19
120	3.78	21.25	3.15	32.40	2.92	46.72	2.11	57.29

[b] Catalyst before absorbed in profenofos solution in the absence of light 30 min

Table E.3 Profenofos mineralization from the VUV process with various dosages of P25 nanopowder

Irradiation time (min)	0 g/L		0.05 g/L		0.10 g/L		0.20 g/L	
	TOC (mg/L)	Mineralization (%)	TOC (mg/L)	Mineralization (%)	TOC (mg/L)	Mineralization (%)	TOC (mg/L)	Mineralization (%)
0[b]	4.98	0.00	3.72	0.00	4.66	0.00	4.67	0.00
30	4.59	7.83	3.19	14.25	3.74	19.74	3.09	33.83
60	2.49	50.00	1.86	50.00	1.82	60.94	1.64	64.88
90	1.65	66.87	1.53	58.87	1.39	70.17	0.76	83.73
120	1.34	73.09	0.87	76.61	0.75	83.91	0.57	87.79

[b] Catalyst before absorbed in profenofos solution in the absence of light 30 min

Table E.4 Profenofos mineralization from the UV process with various dosages of TiO_2 nanofibers photocatalyst

Irradiation time (min)	0 g/L		0.05 g/L		0.10 g/L		0.20 g/L	
	TOC (mg/L)	Mineralization (%)	TOC (mg/L)	Mineralization (%)	TOC (mg/L)	Mineralization (%)	TOC (mg/L)	Mineralization (%)
0[b]	4.80	0.00	4.65	0.00	5.03	0.00	4.99	0.00
30	4.62	3.75	4.08	12.26	4.35	13.52	3.57	28.46
60	4.45	7.29	3.74	19.57	3.25	35.39	3.31	33.67
90	3.92	18.33	3.28	29.46	3.14	37.57	2.77	44.49
120	3.78	21.25	3.37	27.53	3.11	38.17	2.52	49.50

[b] Catalyst before absorbed in profenofos solution in the absence of light 30 min

Table E.5 Profenofos mineralization from the VUV process with various dosages of TiO$_2$ nanofibers photocatalyst

Irradiation time (min)	0 g/L		0.05 g/L		0.10 g/L		0.20 g/L	
	TOC (mg/L)	Mineralization (%)	TOC (mg/L)	Mineralization (%)	TOC (mg/L)	Mineralization (%)	TOC (mg/L)	Mineralization (%)
0[b]	4.98	0.00	4.38	0.00	5.06	0.00	0.96	0.00
30	4.59	7.83	3.72	15.07	4.21	16.80	0.96	28.48
60	2.49	50.00	2.33	46.80	2.85	43.68	0.96	58.46
90	1.65	66.87	1.66	62.10	1.75	65.42	0.96	79.44
120	1.34	73.09	1.25	71.46	1.14	77.47	0.96	81.37

[b] Catalyst before absorbed in profenofos solution in the absence of light 30 min

APPENDIX F

Study of Reusability of the PVP/Composite Titania Nanofibers

Table F.1 Reusability of P25 nanoparticle (VUV/TiO$_2$, C$_0$ = 10 mg/L, TiO$_2$ = 0.20 g/L, Treatment numbers = 10)

Irradiation time (min)	Removal efficiency of profenofos (%)									
	No.1	No.2	No.3	No.4	No.5	No.6	No.7	No.8	No.9	No.10
0[b]	0.00	0.00	0.00	0.00	0.00	0.00	0.00	0.00	0.00	0.00
0[a]	18.44	17.25	16.62	10.30	11.66	7.74	8.63	3.09	3.40	1.18
30	97.49	97.37	97.59	96.00	96.64	96.93	96.11	93.66	94.95	93.35

Table F.2 Reusability of Titania/PVP nanofibers (VUV/TiO$_2$, C$_0$ = 10 mg/L, TiO$_2$ = 0.20 g/L, Treatment numbers = 10)

Irradiation time (min)	Removal efficiency of profenofos (%)									
	No.1	No.2	No.3	No.4	No.5	No.6	No.7	No.8	No.9	No.10
0[b]	0.00	0.00	0.00	0.00	0.00	0.00	0.00	0.00	0.00	0.00
0[a]	14.37	14.50	12.37	13.18	10.78	8.94	6.64	2.91	1.36	0.58
30	96.85	96.73	96.08	96.42	95.87	95.92	95.80	94.03	92.73	92.99

จุฬาลงกรณ์มหาวิทยาลัย
CHULALONGKORN UNIVERSITY

APPENDIX G

Study of Probe compound

Table G.1 Methylene blue concentration from the control experiment

Irradiation time (min)	Concentration of methylene blue (mM)			
	No.1	No.2	No.3	Average
0	10.11	10.06	9.93	10.03
2	10.28	10.47	10.02	10.26
5	9.83	10.27	10.09	10.06
10	9.91	9.92	9.98	9.94
15	9.86	10.10	9.81	9.92
20	10.31	9.84	10.05	10.07
25	9.91	9.85	9.89	9.88
30	10.02	9.85	9.83	9.90

Table G.2 Methylene Blue concentration of each AOPs experimental condition using P25 nanopowder without adding TBA

Irradiation time (min)	Methylene Blue concentration (mM)							
	UV process				VUV process			
	0 g/L	0.05 g/L	0.10 g/L	0.20 g/L	0 g/L	0.05 g/L	0.10 g/L	0.20 g/L
0[b]	10.65	9.86	10.17	9.58	10.25	9.40	10.26	9.24
0[a]	10.65	9.42	9.16	9.04	10.25	8.85	9.30	7.91
2	10.13	4.52	3.45	1.40	2.74	2.68	1.17	1.12
5	9.72	1.32	0.67	0.23	0.55	0.10	0.10	0.06
10	9.12	0.12	0.17	0.05	0.39	0.04	0.09	0.02
15	10.57	0.04	0.11	0.04	0.05	0.02	0.03	0.02
20	10.24	0.04	0.04	0.04	0.07	0.02	0.03	0.02
25	9.28	0.03	0.05	0.03	0.07	0.02	0.02	0.02
30	9.26	0.04	0.05	0.04	0.03	0.02	0.04	0.02

[b] Catalyst before absorbed in profenofos solution in the absence of light 30 min

[a] Catalyst after absorbed in profenofos solution in the absence of light 30 min

Table G.3 Methylene Blue concentration of each AOPs experimental condition using P25 nanopowder with adding TBA

Irradiation time (min)	Methylene Blue concentration (mM)							
	UV process				VUV process			
	0 g/L	0.05 g/L	0.10 g/L	0.20 g/L	0 g/L	0.05 g/L	0.10 g/L	0.20 g/L
0[b]	10.91	9.92	10.11	9.98	9.96	10.03	9.40	10.25
0[a]	10.91	9.60	9.10	9.67	9.96	9.49	8.61	9.08
2	10.69	8.51	7.37	4.59	9.37	8.29	7.33	7.42
5	10.49	5.08	3.57	2.33	8.29	6.15	5.27	4.79
10	10.81	0.54	0.70	0.48	6.29	0.87	0.33	0.33
15	10.40	0.15	0.18	0.13	1.07	0.18	0.07	0.03
20	9.47	0.14	0.12	0.08	0.03	0.18	0.07	0.03
25	9.59	0.10	0.13	0.07	0.04	0.18	0.05	0.02
30	9.38	0.10	0.12	0.07	0.03	0.17	0.05	0.02

[b] Catalyst before absorbed in profenofos solution in the absence of light 30 min

[a] Catalyst after absorbed in profenofos solution in the absence of light 30 min

Table G.4 Methylene Blue concentration of each AOPs experimental condition using TiO_2 nanofibers without adding TBA

Irradiation time (min)	Methylene Blue concentration (mM)							
	UV process				VUV process			
	0 g/L	0.05 g/L	0.10 g/L	0.20 g/L	0 g/L	0.05 g/L	0.10 g/L	0.20 g/L
0[b]	10.65	10.52	10.21	10.72	10.25	10.86	10.10	9.22
0[a]	10.65	9.22	8.73	8.78	10.25	7.26	8.73	7.57
2	10.13	5.60	4.07	1.81	2.74	1.66	0.11	0.67
5	9.72	1.96	0.77	0.34	0.55	0.29	0.12	0.07
10	9.12	0.17	0.19	0.07	0.39	0.14	0.05	0.04
15	10.57	0.08	0.11	0.05	0.05	0.08	0.12	0.04
20	10.24	0.06	0.06	0.05	0.07	0.07	0.05	0.03
25	9.28	0.05	0.05	0.04	0.07	0.05	0.06	0.03
30	9.26	0.04	0.06	0.06	0.03	0.06	0.05	0.02

[b] Catalyst before absorbed in profenofos solution in the absence of light 30 min

[a] Catalyst after absorbed in profenofos solution in the absence of light 30 min

Table G.5 Methylene Blue concentration of each AOPs experimental condition using TiO$_2$ nanofibers with adding TBA

Irradiation time (min)	Methylene Blue concentration (mM)							
	UV process				VUV process			
	0 g/L	0.05 g/L	0.10 g/L	0.20 g/L	0 g/L	0.05 g/L	0.10 g/L	0.20 g/L
0[b]	10.91	10.17	10.03	10.76	9.96	10.67	10.13	9.24
0[a]	10.91	9.14	8.59	8.57	9.96	7.68	8.43	8.01
2	10.69	9.29	7.36	6.29	9.37	8.90	7.52	6.02
5	10.49	6.75	3.80	2.92	8.29	7.83	6.28	4.83
10	10.81	0.66	0.66	0.56	6.29	0.38	0.20	0.37
15	10.40	0.15	0.29	0.18	1.07	0.18	0.14	0.10
20	9.47	0.13	0.14	0.13	0.03	0.14	0.11	0.10
25	9.59	0.10	0.14	0.14	0.04	0.11	0.13	0.08
30	9.38	0.12	0.13	0.12	0.03	0.12	0.12	0.08

[b] Catalyst before absorbed in profenofos solution in the absence of light 30 min

[a] Catalyst after absorbed in profenofos solution in the absence of light 30 min
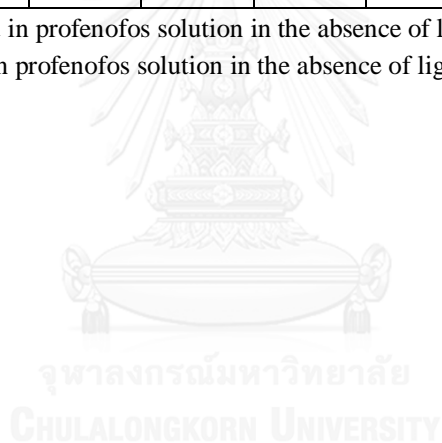
Table G.6 Kinetic rate constants of probe compound degradation from each AOPs experimental condition with and without adding TBA

AOPs Condition	Kinetic Rate Constants (s-1)	
	Without TBA	**With TBA**
UV alone	0.0097	0.0006
VUV alone	0.0003	0.0001
UV/P25 0.20 g/L	0.0120	0.0048
UV/P25 0.10 g/L	0.0091	0.0035
UV/P25 0.05 g/L	0.0067	0.0023
VUV/P25 0.20 g/L	0.0167	0.0025
VUV/P25 0.10 g/L	0.0153	0.0019
VUV/P25 0.05 g/L	0.0127	0.0011
UV/NF 0.20 g/L	0.0114	0.0043
UV/ NF 0.10 g/L	0.0087	0.0033
UV/ NF 0.05 g/L	0.0056	0.0014
VUV/ NF 0.20 g/L	0.0161	0.0021
VUV/ NF 0.10 g/L	0.0147	0.0015
VUV/ NF 0.05 g/L	0.0119	0.0010

*NF = Titania Nanofibers

APPENDIX H

Study of the TiO$_2$/PVP composite nanofibers diameters

Label H.1 The diameters of the as-spun TiO$_2$/PVP composite nanofibers before calcination at 500 ºC

No.	Nanofibers diameter (nm)	No.	Nanofibers diameter (nm)
1	161	29	253
2	160	30	122
3	220	31	402
4	213	32	400
5	303	33	247
6	267	34	160
7	278	35	126
8	253	36	530
9	200	37	179
10	85	38	362
11	140	39	362
12	141	40	241
13	301	41	141
14	108	42	384
15	120	43	161
16	376	44	144
17	428	45	253
18	261	46	279
19	328	47	310
20	146	48	144
21	224	49	422
22	316	50	140
23	322	51	144
24	141	52	405
25	180	53	181
26	286	54	200
27	197	55	228
28	120	**Average**	233

Label H.2 The diameters of the as-calcined TiO$_2$/PVP composite nanofibers after calcination at 500 ℃

No.	Nanofibers diameter (nm)	No.	Nanofibers diameter (nm)
1	129	29	60
2	108	30	262
3	172	31	80
4	100	32	162
5	166	33	261
6	207	34	261
7	146	35	244
8	210	36	120
9	162	37	145
10	100	38	83
11	257	39	600
12	161	40	216
13	63	41	142
14	72	42	108
15	60	43	102
16	261	44	114
17	129	45	108
18	312	46	85
19	114	47	127
20	241	48	80
21	181	49	257
22	161	50	161
23	129	51	45
24	312	52	63
25	241	53	144
26	181	54	90
27	161	55	162
28	129	**Average**	141

Figure H.1 The actual photo of electrospun TiO2/PVP nanofibers

VITA

Miss Pacharaporn Wangwinyoo was born on January 13th, 1990 in Bangkok, Thailand. She was completely studied in the secondary education from Surasakmontree School major in science – math class in 2002 – 2008. After that she was graduated from Chulalongkorn University, Faculty of Science major in Environmental Science for the Bachelor's degree in Thailand in 2012. She pursued her Master's degree in Hazardous Waste Management (International Program) from the Faculty of Graduation, Chulalongkorn University, Thailand on July, 2015. She finished her Master of Science Degree in August, 2015. Moreover, she was given the scholarship for research from Research Cluster, Faculty of Graduation, Chulalongkorn University.